Check for updates

View Article Online
View Journal

Sensors & Diagnostics

Accepted Manuscript

This article can be cited before page numbers have been issued, to do this please use: J. Annaraj, T. Nagendraraj and S. Sagadevan, *Sens. Diagn.*, 2026, DOI: 10.1039/D6SD00010J.

This is an Accepted Manuscript, which has been through the Royal Society of Chemistry peer review process and has been accepted for publication.

Accepted Manuscripts are published online shortly after acceptance, before technical editing, formatting and proof reading. Using this free service, authors can make their results available to the community, in citable form, before we publish the edited article. We will replace this Accepted Manuscript with the edited and formatted Advance Article as soon as it is available.

You can find more information about Accepted Manuscripts in the Information for Authors.

Please note that technical editing may introduce minor changes to the text and/or graphics, which may alter content. The journal's standard Terms & Conditions and the Ethical guidelines still apply. In no event shall the Royal Society of Chemistry be held responsible for any errors or omissions in this Accepted Manuscript or any consequences arising from the use of any information it contains.

ROYAL SOCIETY OF CHEMISTRY

rsc.li/sensors

View Article Online
DOI: 10.1039/D6SD00010J

Fluorescent Zn(II) Coordination Complexes as Advanced Bioimaging Probes for Sensitive Detection of Small Biomolecules

Jamespandi Annaraj[a]*, Thavasilingam Nagendraraj[a] and Suresh Sagadevan[b,c]*

[a]Department of Materials Science, School of Chemistry, Madurai Kamaraj University, Madurai 625021, India.

[b]Nanotechnology& Catalysis Research Centre, University of Malaya, Kuala Lumpur 50603, Malaysia

[c]Centre for Herbal Pharmacology and Environmental Sustainability, Chettinad Hospital and Research Institute, Chettinad Academy of Research and Education, Kelambakkam, Tamil Nadu 603103, India

E-mail : annaraj.chem@mkuniversity.ac.in; drsureshsagadevan@um.edu.my

Open Access Article. Published on 10 June 2026. Downloaded on 6/10/2026 10:50:53 PM.
This article is licensed under a Creative Commons Attribution 3.0 Unported Licence.

Sensors & Diagnostics Accepted Manuscript

Abstract

Advancements in diagnostic imaging have significantly improved early disease detection. Techniques such as computed tomography (CT), positron emission tomography (PET), magnetic resonance imaging (MRI), and ultrasound are widely used in clinical settings, each offering distinct advantages and limitations. These modalities are essential for monitoring disease progression and guiding therapeutic decisions. Recently, fluorescence imaging has gained considerable attention due to its high sensitivity, cost-effectiveness, and relative safety. FDA-approved fluorescent organic dyes are currently employed in limited clinical applications, including image-guided tumor surgery and retinal angiography. Emerging developments in fluorescence technology are driving the next generation of imaging agents. This review highlights the potential of mono- and binuclear Zn(II)-based coordination complexes as selective fluorescent probes for detecting small biomolecules such as phosphate, pyrophosphate, nucleotides, amino acids, sulfide, nitric oxide, and nitrate. We discuss the structural features and binding mechanisms that govern the fluorescence properties of these Zn (II) complexes, providing insights into their design principles. These findings lay the groundwork for developing innovative biosensors aimed at the early diagnosis of diseases through precise molecular recognition.

Keywords: Zn(II) complexes, biological species, fluorescent, bioimaging agents and biomolecules

View Article Online
DOI: 10.1039/D6SD00010J

Open Access Article. Published on 10 June 2026. Downloaded on 6/10/2026 10:50:53 PM.
This article is licensed under a Creative Commons Attribution 3.0 Unported Licence.

Sensors & Diagnostics Accepted Manuscript

1.Introduction

Small biomolecules and ions are key components of all biological functions, including enzymatic reactions, metabolism, growth, adaptability, and onset and progression of numerous diseases. Understanding their biological roles in biomedical systems is crucial for the early diagnosis of diseases and treatment evaluation. This can be achieved by measuring and tracking the amount of biomolecules and ions *in situ*.[1] Existing characteristic methods for the determination of such small biomolecules *in vitro* and *in vivo* may not be successful because of the hectic sample preparation methods.[2] Along these lines, although many imaging technologies such as computerized tomography, magnetic resonance imaging, and positron emission tomography are widely used in medical diagnosis, they do not provide direct information on the analysis of small biomolecules detection.[3] To overcome this problem, advanced optical spectroscopic imaging techniques can be helpful in the detection of biomolecules due to their many advantages such as high sensitivity and selectivity, fast response time, and relatively low cost.[4] Over the past few decades, there have been significant advances in the design and development of fluorescent sensors for the detection of small biomolecules and ions in biological systems, due to their excellent selectivity and sensitivity, as well as unique features such as less cost, excellent sensitivity, rapid sensing response, ease of use, and non-invasive detection processes.[5,6] Transition metal complex-based probe have proven advantageous, as fluorescence-responsive compounds have become increasingly necessary for many technological applications, such as bio-imaging, analytical probes, lighting, and switch devices. Abundant, less expensive, and environmentally Zn^{2+} metal cations are becoming progressively more popular in this field. The emission maxima of Zn^{2+} complexes can be tuned in terms of fluorescence depending on the type of ligand used in the coordination pattern. Specifically, coordination between the ligands and Zn^{2+} led to improved fluorescence amplification or metal-binding-triggered fluorescence quenching. Furthermore, qualitative fluorescence tuning could be considered a result of the excited state of the bound ligand being lower upon coordination. Thus, the objective of this review has been to incorporate mono/binuclear Zn^{2+} complexes as useful small-molecule bioimaging and detection techniques in biological systems for a few decades.

2. Biomolecules and their impact on health

Biological anions are important for biology, medicine and environmental research. Therefore, there is a lot of interest in developing molecules as sensor tools for efficient detection.[7-10] Nevertheless, anion detection remains a significant barrier in this field. Although hydrogen bonding interactions have been used to construct selective anion receptors, relatively

View Article Online
DOI: 10.1039/D6SD00010J

few receptors that rely only on these relationships can distinguish between different types of anions in water.[11] Phosphate-containing biomolecules such as phosphate (Pi), pyrophosphate (PPi), adenosine monophosphate (AMP), adenosine diphosphate (ADP), and adenosine triphosphate (ATP) are essential for several organellar biological processes (Fig. 1).[12-14] These phosphate-containing substances are not only vital for the survival of organisms, but also for the synthesis of phospholipids, energy transfer, protein activation, amino acid metabolism, and nucleic acids.[15-17] Phosphates tend to exist in biological systems, such as adenosine phosphates (AMP, ADP, and ATP), deoxyribonucleic acid (DNA), and ribonucleic acid (RNA), and are essential components of the inorganic portion of hard tissues in animals.[18-24] Additionally, ATP is an essential precursor for the production of DNA and RNA, which allows for survival, growth, and reproduction, while providing a genetic marker that maintains it intact.[25] Moreover, it is involved in a wide range of biological activities, including glycolysis, neurotransmission, ion transport in cells, and cell division.[26-28] A high level of ATP metabolism has been linked to several illnesses, including malignant tumors, ischemia, Parkinson's disease, and cardiovascular disease.[29-31] In particular, concentrations above 1.62 mM have the potential to cause PPi-induced diseases such as arthritis, cartilage fractures, excruciating arthritis, chondrocalcinosis, and cancer; conversely, concentrations below 0.85 mM have the potential to cause diseases like vascular calcification, which is caused by the production of vascular calcification inhibitors.[32-38]

Amino acids serve as basic building blocks and complexes of proteins that make up biological machinery systems. In addition, they generate a variety of significant metabolites, including neurotransmitters, purines, and pyrimidines, involved in cellular metabolism processes.[39-41] They originated from early studies on human nutrition and have been divided into essential and non-essential amino acids. This demonstrates that even in the presence of sufficient quantities of various naturally existing amino acids, certain other amino acids are essential for the proper growth of organs and nitrogen balance.[42] They might only be acquired through an external diet because internal organs in the human body might not be able to produce them spontaneously.[43,44] Especially, cysteine (Cys), histidine (His), leucine (Leu), methionine (Met), phenylalanine (Phe), serine (Ser), threonine (Thr), tyrosine (Tyr), and valine (Val) are important in role biological processes, but variations may occur based on individual metabolism (Fig. 1). Cys participates in crosslinking through the formation of disulfide bonds or Cys–Cys crosslinkers, predicting secondary protein synthesis and detoxification in living things. However, excess Cys may lead to Parkinson's disease, Alzheimer's disease, cardiovascular disease, slow growth in children, rheumatoid arthritis, and deficiency caused by

Open Access Article. Published on 10 June 2026. Downloaded on 6/10/2026 10:50:53 PM.
This article is licensed under a Creative Commons Attribution 3.0 Unported Licence.

Sensors & Diagnostics Accepted Manuscript

View Article Online
DOI: 10.1039/D6SD00010J

fat loss, edema, liver damage, and hematopoiesis.[45-52] His is essential for many biological processes, human development, and functions as a neurotransmitter in the mammalian central nervous system. Its deficiency may result in an altered nutritional status in people with chronic renal disease, whereas its rich proteins may lead to several disorders.[53-55] Leu is another essential amino acid for protein synthesis, which can control various biological functions, including tissue regeneration, metabolism, and protein synthesis. Thus, Leu supplementation has been investigated in a range of conditions, including diabetes mellitus, aging, muscle injuries, and protein deficits.[56,57] Met is a precursor of homocysteine, Cys, creatine, and carnitine and controls the innate immune system, metabolism, and digestive functions in animals.[58] The elevated levels of Phe in blood is an indication of the rare inherited disorder phenylketonuria, a metabolic illness.[59] Ser is crucial for many different cellular processes as well as for the metabolism of all nutrients. Phosphatidylserine, sphingolipids, ceramides, phosphosphingolipids, and glycosphingolipids, which are highly concentrated in all cell membranes, are substrates for glucose and protein synthesis.[60] A significant bioactive building unit of Thr plays a key role in energy metabolism, protein synthesis, and food absorption.[61,62] The ideal diet has been demonstrated to promote animal growth, enhance immune response, and maintain intestinal health.[63,64] Among the amino acids found in nature, Tyr is a special amino acid because, it can donate both an electron and a proton to enzymatic processes in biological systems. Tyr is a cofactor that can be found in the active sites of numerous enzymes, such as galactose oxidases, cytochrome c oxidase, and ribonucleotide reductase.[65-69] .Val is necessary for the biosynthesis of proteins, which enhances reproductive and developmental activities on farms. It is also essential for growth regulation, gut microbiome, and immune responses. Furthermore, neurological deficits and mental retardation are caused by Val deficiency in the human brain.[70]

Most human organs may be intoxicated by gaseous hydrogen sulfide (H_2S) (Fig. 1). It functions as a gaseous signaling molecule and chemical reagent in numerous physiological processes, including the pathogenesis of numerous illnesses, such as diabetes, heart failure, and neurodegenerative diseases. Unusual levels of H_2S in humans have been associated with hypertension, Alzheimer's disease, and Down syndrome.[71,72] Cardioprotection, neuroprotection, wound healing, reduced oxidative stress, and related damage are all facilitated by this toxic substance.[73] In the cardiovascular system, H_2S inhibits the development of smooth muscle cells and relaxes the vascular smooth muscle. Therefore, it aids in blood pressure management and, in particular, is important in the development of several vascular diseases.[74]

Open Access Article. Published on 10 June 2026. Downloaded on 6/10/2026 10:50:53 PM.
This article is licensed under a Creative Commons Attribution 3.0 Unported Licence.

Sensors & Diagnostics Accepted Manuscript

View Article Online
DOI: 10.1039/D6SD00010J

Open Access Article. Published on 10 June 2026. Downloaded on 6/10/2026 10:50:53 PM.
This article is licensed under a Creative Commons Attribution 3.0 Unported Licence.

Sensors & Diagnostics Accepted Manuscript

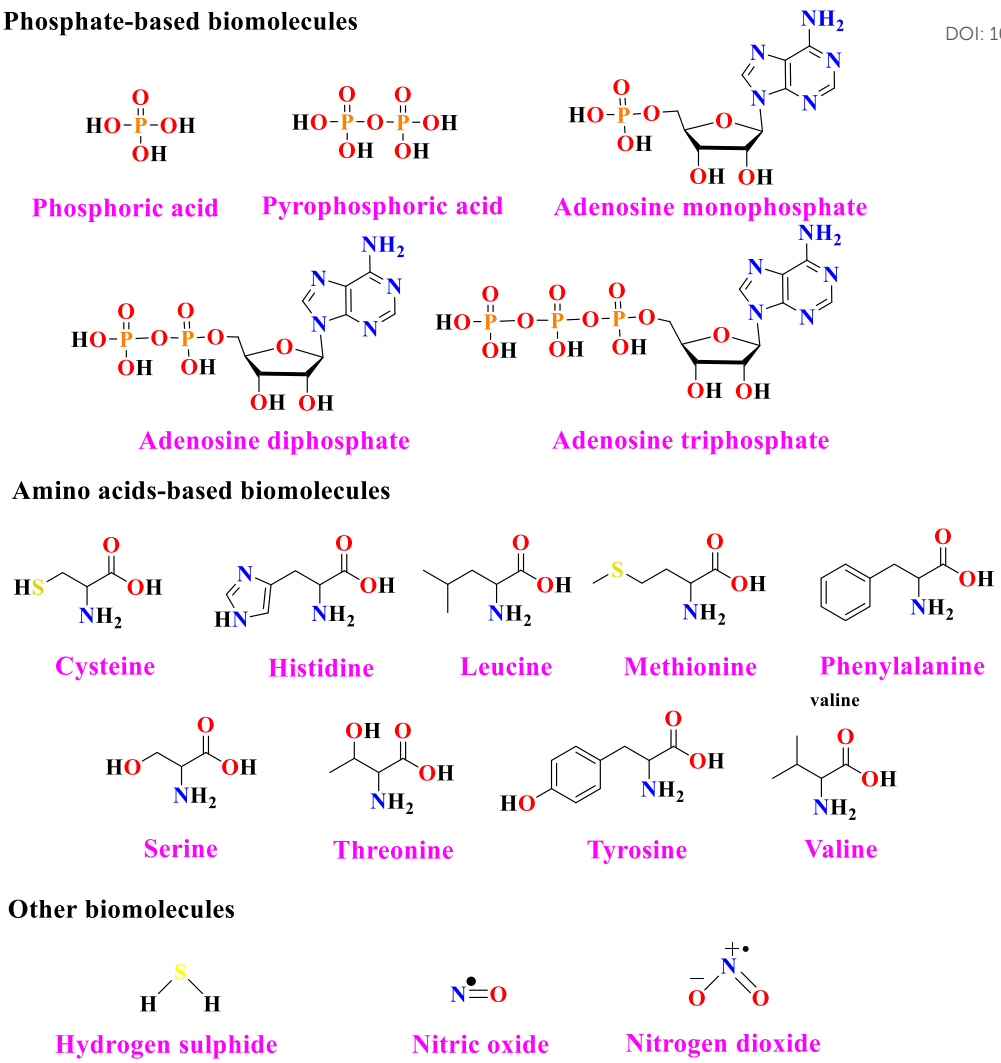

Fig. 1. Structure of biomolecules fluorescence responsive towards Zn^{2+} complexes.

Nitric oxide is another tiny gaseous signaling molecule that boosts antioxidant activity, lowers oxidative stress, and aids in plant survival in response to environmental stimuli (NO) (Fig. 1).[75] Numerous studies have demonstrated the defensive role of NO in plant responses to various abiotic stressors. Supplementing chickpeas with NO may controls the activity of superoxide dismutase and osmolytes in response to salt stress.[76] A recent report revealed that the exogenous application of NO can increase plant tolerance to heavy metal toxicity.[77] It is well known that NO can do this through several important mechanisms, including boosting antioxidant activities, limiting metal translocation from roots to shoots, and reducing metal accumulation in the roots, shoots, and stems of bamboo species under heavy metal toxicity due to excess levels of Pb^{2+} and Cd^{2+} ions. Apart from its role as a signaling agent in mitigating the toxicity of heavy metals, NO can also reduce the buildup of metalloids and trigger the antioxidant response of reactive oxygen species (ROS) in plants exposed to metal stress. Nitrite is frequently used to preserve meat,[78] however, its excess (recommended level is ~300 mg/kg

View Article Online
DOI: 10.1039/D6SD00010J

to bodyweight) intake, may lead it to interact with proteins and amines, consequently to generate N-nitrosamines, which can cause cancer and impair the ability of the living human body to transport oxygen, the common example is infant methemoglobinemia.[79,80] It is caused by nitrite entering in to the bloodstream, leading to occur an irreversible conversion of hemoglobin to methemoglobin, which obstructs oxygen intake and transportation.[81] The World Health Organization (WHO) recommends that only 65 μM is the maximum level of NO_2 concentration in drinking water; therefore, recognizing the existing level of NO_2 in food, water, and agricultural goods is crucial before they are consumed by the living system.[82] These biomolecules control biological processes in this way, and variations in their concentration can result in a variety of illnesses.

This review highlights the critical roles of key biomolecules and signaling species in living systems, with particularly emphasis on the phosphate-containing compounds, amino acids, and gaseous signaling molecules, all of which are essential for cellular function and physiological homeostasis. It also discusses the health risks associated with their imbalance, which may lead to various pathological conditions. Furthermore, the review underscores the growing importance of noninvasive fluorescence sensors for the sensitive and selective in vivo detection of these biomolecules, emphasizing their potential in biomedical diagnosis and therapeutic monitoring. Finally, it outlines the significant role of Zn^{2+} ions in biological systems and their impact on cellular health and function.

3. Biomolecule interactions: A mechanistic exploration of Zn (II) complex-based probes

Recently, noninvasive fluorescence sensors have been extensively employed in biomedical diagnosis and treatment methodologies, and they are expected to be supportive tools for radiology, imaging, and medical practice. The second most common trace element in this competition is Zn^{2+}, which has a daily requirement of 8–11 mg. On average, it gives adults about 3 g of Zn^{2+}, the majority of which is located in the brain, liver, muscles, and testicles.[83] It stimulates cell survival and protects tissues from destruction at physiological concentrations. Zn^{2+} shortage can lead to complications in nutrition, cell division, and the synthesis of RNA and DNA.[84,85] Moreover, it is an important element in biological systems because of its peculiar chemical properties including, diamagnetism, redox inertness, ligand exchange-susceptibility, and its strong Lewis acid character with a d^{10} configuration, that may support an array of coordination geometries. Its diamagnetism and white colour may limit of spectroscopic investigation and the consequent lack of d-d transitions. Since only the ligand charge and steric hindrance may change the coordination geometry, it can be incredibly flexible in the absence of ligand field stabilization.[86, 87] Zn^{2+} ions are coordinated to His, glutamate, aspartate, and Cys

Open Access Article. Published on 10 June 2026. Downloaded on 6/10/2026 10:50:53 PM.
This article is licensed under a Creative Commons Attribution 3.0 Unported Licence.

Sensors & Diagnostics Accepted Manuscript

View Article Online
DOI: 10.1039/D6SD00010J

residues in biological systems using their N, O, or S donor atoms and water molecules. This results in a variety of potential geometries, including tetrahedral, pyramidal, and octahedral coordination geometries, all of which are essential for the regular functioning of the cellular system. The most prevalent geometry found in proteins is tetrahedral, but distorted trigonal bipyramidal geometry is less common.[88] The active sites of some enzymes, Zn^{2+} ions as cofactor may reversibly coordinate with O donor atoms from phosphate-type substrates or inhibitors.[89-91] These specific characteristic of Zn^{2+} enables a quick interchange of ligands, coordination numbers and has been identified as a model for zinc enzymes, such as alkaline phosphatase and carbonic anhydrase, which generate this interaction.[92-94] However, the situation has changed owing to the progressive advancement in the development of fluorescent probes as devices or tools for efficient detection and bioimaging of ions, molecules, or other targets. Indeed, the possible interactions between Zn^{2+} complexes and various biomolecules can be signaled by different mechanistic pathways, such as internal charge transfer (ICT), photoinduced electron transfer (PET), excited-state intramolecular proton transfer (ESIPT), chelation-enhanced fluorescence (CHEF), chelation-quenched fluorescence (CHQF), C=N isomerism, and on-covalent interactions (e.g., H-bonding, π–π stacking, electrostatic interactions, etc.). The anticipated colorimetric changes and fluorescence "turn on" and "turn off" systems in response to biomolecules may be caused by these mechanisms.

In intramolecular charge transfer (ICT)-based systems, binding of an analyte to a fluorescent probe modulates the energy gap between the HOMO and LUMO orbitals (Fig. 2A), resulting in shifts in emission wavelength. Donor–acceptor interactions can induce a blue shift through electron transfer from donor-associated HOMO to acceptor-associated LUMO, while reverse electronic effects may produce a red shift.[95] Another widely employed strategy involves photoinduced electron transfer (PeT), which enables “off–on” or “on–off” fluorescence switching. Upon analyte binding, the PeT process is either inhibited or activated, thereby modulating the fluorescence signal (Fig. 2B). Typically, excitation promotes an electron to the LUMO, followed by electron transfer and charge recombination back to the ground state, governing the observed fluorescence response.[96] In ESIPT processes, a fluorescence probe can reveal fluorescence changes when intramolecular hydrogen bonding interactions occur between a hydrogen bond donor (–OH and NH_2) and a hydrogen bond acceptor; this phenomenon is commonly experienced by the keto-enol tautomer (Fig. 2C). The tautomeric forms present in the ground and excited states are not identical. In the ground state, hydrogen bonding often stabilizes the enol form. Upon excitation, a rapid proton transfer from the excited enol to the keto form occurs, resulting in emission at a longer wavelength than would be

Open Access Article. Published on 10 June 2026. Downloaded on 6/10/2026 10:50:53 PM.
This article is licensed under a Creative Commons Attribution 3.0 Unported Licence.

Sensors & Diagnostics Accepted Manuscript

View Article Online
DOI: 10.1039/D6SD00010J

observed in the absence of this process.[97,98] It is a rapid process than electron transfer, with reported durations ranging from picoseconds to tens of picoseconds.[99] Coordination of metal ions with Schiff base–based sensors can lead to either enhanced or quenched fluorescence, commonly referred to as CHEF (chelation-enhanced fluorescence) or CHEQ (chelation-enhanced quenching) (Fig. 2D). In some cases, ratiometric fluorescence responses are also observed. Paramagnetic metal ions such as Cu^{2+} and Fe^{3+} typically induce fluorescence quenching (CHEQ) upon binding to chemosensors, although fluorescence enhancement may occur in certain systems. These interactions influence the excited-state properties of the fluorophore, resulting in changes in fluorescence intensity, emission wavelength, or lifetime.[100-102] The C=N isomerization process occurred from the unique photophysical characteristics restricted compounds (Fig. 2E). This was observed in non-fluorescent probes with unbridged C=N structural constructions through decayed excited states. Conversely, in the C=N isomerization probe analogs, a notable increase in the covalent bridge structures was caused by the suppression of C=N isomerization in the excited states. This led to an emission spectral shift in the inhibition of C=N isomerization brought on by guest molecule complexation.[103,104] Resonance energy transfer is a photophysical process in which an excited donor moiety transfers its excitation energy to a nearby acceptor in a non-radiative manner, followed by radiative emission from the acceptor. (Fig. 2F).[105,106] Fluorescence amplification in dimeric systems is strongly influenced by the π-overlap, intermolecular distance, and relative orientation of π-conjugated fluorophores (Fig. 2G). Increasing the separation between π-stacked units and reducing π-overlap can suppress excimer formation in the excited state typically associated with dynamic quenching thereby enhancing fluorescence emission.[107,108]

Open Access Article. Published on 10 June 2026. Downloaded on 6/10/2026 10:50:53 PM.
This article is licensed under a Creative Commons Attribution 3.0 Unported Licence.

Sensors & Diagnostics Accepted Manuscript

View Article Online
DOI: 10.1039/D6SD00010J

Open Access Article. Published on 10 June 2026. Downloaded on 6/10/2026 10:50:53 PM.
This article is licensed under a Creative Commons Attribution 3.0 Unported Licence.

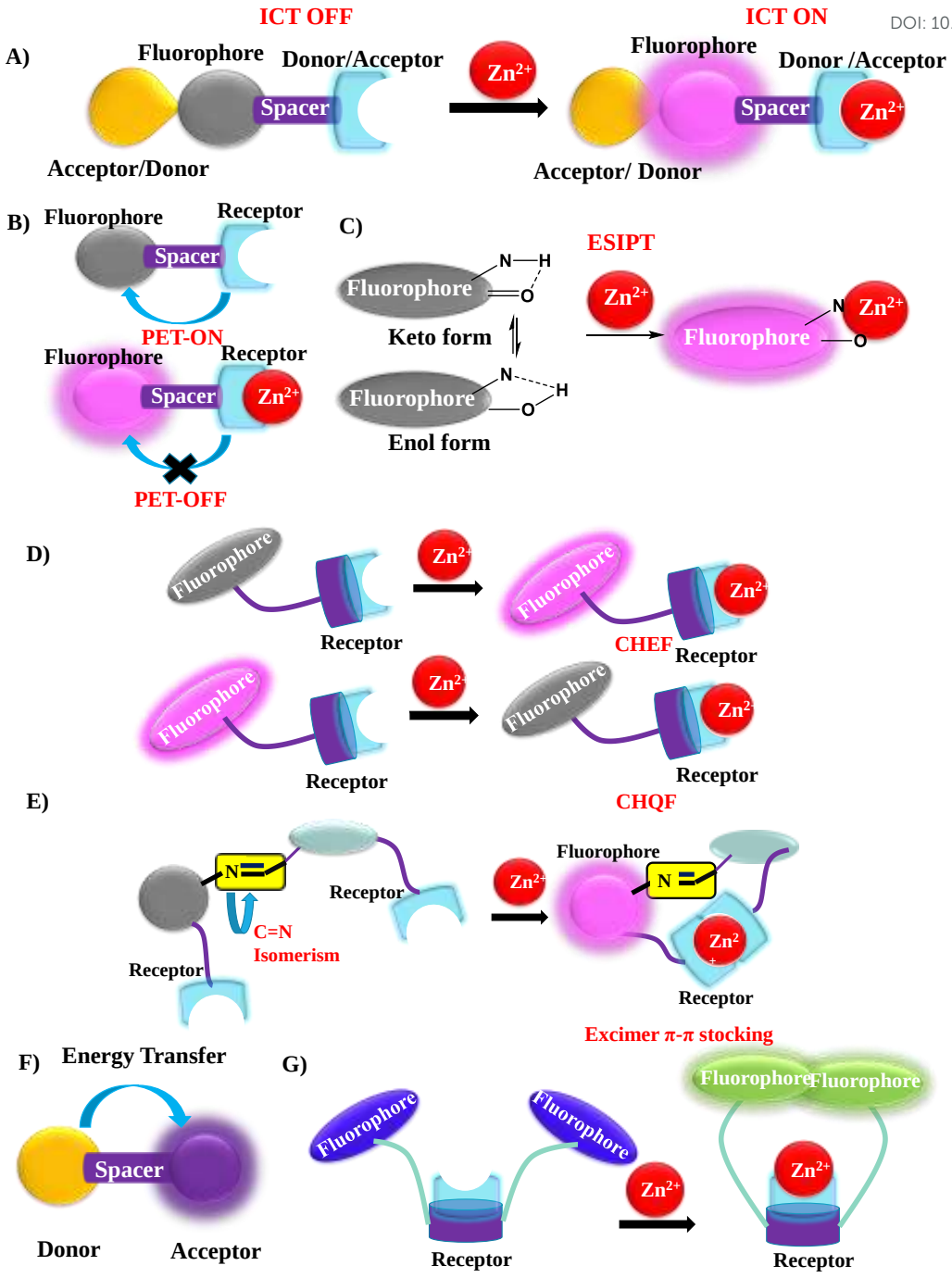

Fig. 2. Basic mechanistic fluorescence responses for the probes.

4. Mechanism of sensing biomolecules with Zn(II)-based complex probes

Biomolecules and Zn^{2+} complex probes interact by two distinct processes, namely dissociative and associative pathways.

Sensors & Diagnostics Accepted Manuscript

View Article Online
DOI: 10.1039/D6SD00010J

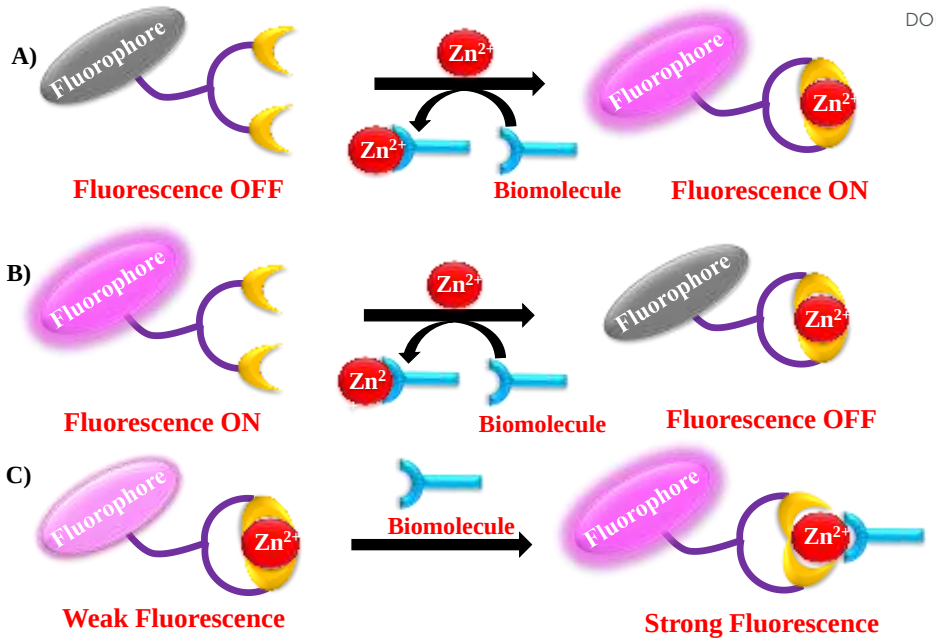

Fig.3.Proposed mechanistic sensing methodologies of biomolecules by Zn^{2+} based fluorescence probes.

Non-fluorescent probes bound to the Zn^{2+} ion displayed intense fluorescence in the dissociation pathways; nevertheless, the presence of bio-analytes caused regeneration of the non-fluorescent probe (Fig 3A). In contrast, the Zn^{2+} ion-linked fluorescence probe quenched the fluorescence, which was subsequently recovered by the incorporation of bio-analytes (Fig. 3B). The interaction between the probe and Zn^{2+} revealed the anticipated turn-on fluorescence when activated by the presence of the bio-analyte *via* the associative process (Fig. 3C). The above-mentioned fluorescence behavior of Zn^{2+} complexes as probes for biomolecules has been investigated using different methodologies. The chemical structures of numerous probes, their fluorescence nature, binding studies, operating mechanisms, and detection limits are addressed in this review. The prospects of optical imaging and the foundation of bio-analyte detection are explored in the subsequent sections.

5. Detection of biomolecules based on phosphate ions using Zn(II) complexes

5. 1. Schiff base-based family receptor probes

5.1. 1. Benzothiazole, benzoxazole, imidazole and thiazole-based fluorescence probes

Benzothiazole-based fluorescent probes has constructed by the reaction between benzothiazole and different receptors of tris(hydroxymethyl)aminomethane, 2-amino-1,3-dihydroxypropane, and ethanolamine, for the detection of Zn^{2+} and PPi ions (Fig.4A).[109] Amongst, tris(hydroxymethyl)aminomethane-based probe **1** showed weak yellowish-green

Open Access Article. Published on 10 June 2026. Downloaded on 6/10/2026 10:50:53 PM.
This article is licensed under a Creative Commons Attribution 3.0 Unported Licence.

Sensors & Diagnostics Accepted Manuscript

View Article Online
DOI: 10.1039/D6SD00010J

fluorescence (543 nm), which was shifted to 475 nm by the addition of Zn^{2+} and showed blue fluorescence. Furthermore, the addition of PPi with **1-Zn** results in the formation of the Zn-PPi complex, lead to restore **1** by the showing the yellowish-green fluorescence. Similarly, benzothiazoles and phenol were connected with spacer by Schiff base formation to create probe **2** (Fig. 4B).[110] The addition of Zn^{2+} with **2** exhibited a strong fluorescence due to the inhibition of the rotation of azomethine moiety, which led to the process of chelation-enhanced fluorescence. Subsequent addition of PPi with **2-Zn** caused for the suppression of showed suppressed fluorescence, which led to the formation of the Zn-PPi complex. In addition, a bis-receptor, probe **3** has been developed by benzothiazole coupled with bisphenol, which showed an enhanced fluorescence at 515 nm upon the addition of Zn^{2+} ion due to the formation of **3-Zn_2** complex (Fig. 4C), which was suppressed when PPi was added.[111] It remains stable after their saturation by forming Zn-PPi complex, and consequently leached out probe **3** alone. Recently, Schiff-base between benzothiazole and coumarin has been used to prepare **4** and it exhibited a significant fluorescence enhancement due to the formation of **4-Mg**/**4-Zn** complexes with the additions of Mg^{2+} and Zn^{2+} ions (Fig. 4D).[112] Among these, **4-Zn** coupled with ATP and formed Zn-ATP complex, which restored the probe, **4** by displacing Zn^{2+} from **4-Zn**.

Open Access Article. Published on 10 June 2026. Downloaded on 6/10/2026 10:50:53 PM.
This article is licensed under a Creative Commons Attribution 3.0 Unported Licence.

Sensors & Diagnostics Accepted Manuscript

View Article Online
DOI: 10.1039/D6SD00010J

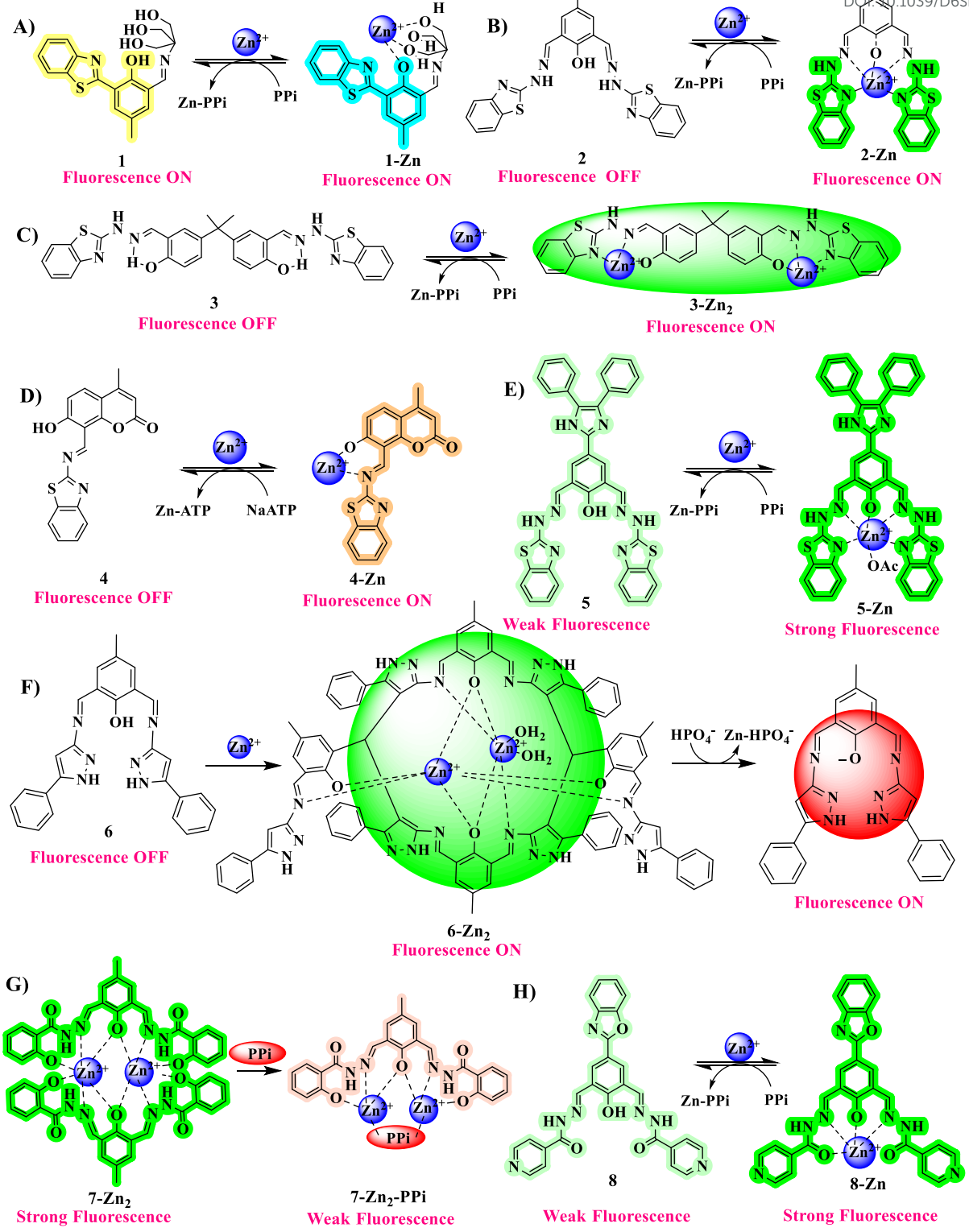

Fig. 4. Schematic representation of probes **1-8** with phosphate-based biomolecules.

Probe **5** was constructed with benzothiazole coupled diformyl phenol moiety and generated a Schiff base system (Fig. 4E).[113] It showed a weak fluorescence around 525 nm, while an enhanced fluorescence spectra was observed by the addition of Zn^{2+} *via* CHEF effects. This observation demonstrated their prospective application of molecular recognition system

Open Access Article. Published on 10 June 2026. Downloaded on 6/10/2026 10:50:53 PM.
This article is licensed under a Creative Commons Attribution 3.0 Unported Licence.

Sensors & Diagnostics Accepted Manuscript

View Article Online
DOI: 10.1039/D5SD00010J

for the Zn^{2+} and PPi ions through the possible off-on-off displacement mechanism in biological systems. Employing an imidazole derivative receptor in replace of the pyridine groups of **5**, probe **6** displayed weak green fluorescence at 520 nm and strong green fluorescence *via* CHEF upon contact with Zn^{2+} (Fig. 4F).[114] Upon the addition of HPO_4^{2-} ions, this emission band at 520 nm was completely quenched, and a new intense band appeared at 595 nm with red fluorescence, which led to the deprotonation of **6**. Similarly, probe **7** formed by the incorporation of hydroxy benzohydrazide instead of imidazole groups in **6**, and it showed a strong fluorescence at 500 nm after it is treated with Zn^{2+} ion, which was diminished by the addition of PPi (Fig. 4G).[115] The interaction of one equivalent PPi with **7-Zn$_2$** led to form an adduct as **7-Zn$_2$-PPi**, however, addition of increasing concentrations of PPi caused to a complete elimination of **7** from the earlier adduct due to the occurred strong interaction between Zn^{2+} and PPi. In the same way, probe **8** was modified with benzoxazole instead of methyl group and showed an enhanced fluorescence after it is treated with Zn^{2+} *via* CHEF effects (Fig. 4H).[116] This fluorescence enhancement was suppressed by adding PPi. When the guest interacts with the Zn^{2+} ion, the 2-(1-phenyl hydrazinyl) pyridine-based non-fluorescent **9** exhibits a turn-on fluorescence at 521 nm, which inhibits the C=N isomerization, and influenced the PET and ESIPT processes (Fig. 5A).[117] The experimental and theoretical evaluation of the interaction between PPi with **9-Zn$_2$** were studied, and the results showed that the impact of PET and CHEF processes following the binding of Zn^{2+} and PPi ions to **9** could be the cause of the fluorescence turn-off-on behavior. Besides these findings, non-fluorescent probe **10** was prepared from 2-hydroxy-1-naphthaldehyde and imidazo[2,1-b]thiazole, which showed an enhanced fluorescence with Al^{3+} and Zn^{2+} in the MeOH-H_2O and EtOH-H_2O mixture of solvents respectively (Fig. 5B).[118]. Even after six cycles of gradual and alternating additions of metal ions (Al^{3+} and Zn^{2+}) and PPi, its fluorescence intensity was reversible and exhibited a promising "off-on-off" fluorescence pattern. In a different way, selective and reversible detection of dihydrogen phosphate ($H_2PO_4^-$) in the presence of Zn^{2+} using the dipodal N-acyl hydrazone backbone of probe **11** (Fig. 5C) displayed a strong fluorescence enhancement with two maxima at 502 and 534 nm, only in the presence of Zn^{2+} ions rather than other metal ions due to the inhibition of existing ICT and dominating of CHEF effect.[119] Interestingly, appeared fluorescence bands of **11-Zn$_2$** complex were rapidly quenched by adding $H_2PO_4^-$, which leads to a remarkable color change from yellow to colorless, indicating the revival of the ICT effect and the formation of $Zn(H_2PO_4)_2$ complex. Likewise, chiral thiourea derivative coupled with various substituted salicylaldehyde moieties to afford fluorescent probes **12** (**a-f**), and are employed for the sequential detection of Zn^{2+} and $H_2PO_4^-$ (Fig. 5D).[120] Generally,

Open Access Article. Published on 10 June 2026. Downloaded on 6/10/2026 10:50:53 PM.
This article is licensed under a Creative Commons Attribution 3.0 Unported Licence.

Sensors & Diagnostics Accepted Manuscript

View Article Online
DOI: 10.1039/D6SD00010J

probe **12a-e** has shown weak fluorescence response at 447 nm, while the addition of Zn^{2+} led to enhanced fluorescence for all the derivatives. The substituents of the salicylaldehyde that are present in the ligand (probe) structures determine the variations in their fluorescence intensity. The fluorescence intensity of **12e** was better and stronger than that of **12c**, **12b**, and **12d**, which showed weak fluorescence. Surprisingly, electron-donating groups such as, –OH, $–CH_3$, and $–OCH_3$ were induced the density of the electron cloud on the benzene ring, while electron-withdrawing character of **12e** lead to obtain a strong interaction with Zn^{2+} due to the mesomeric and inductive effects. The results indicated that these probes have promising applications and offer an innovative approach to recognize Zn^{2+} and $H_2PO_4^-$ ions in real samples.

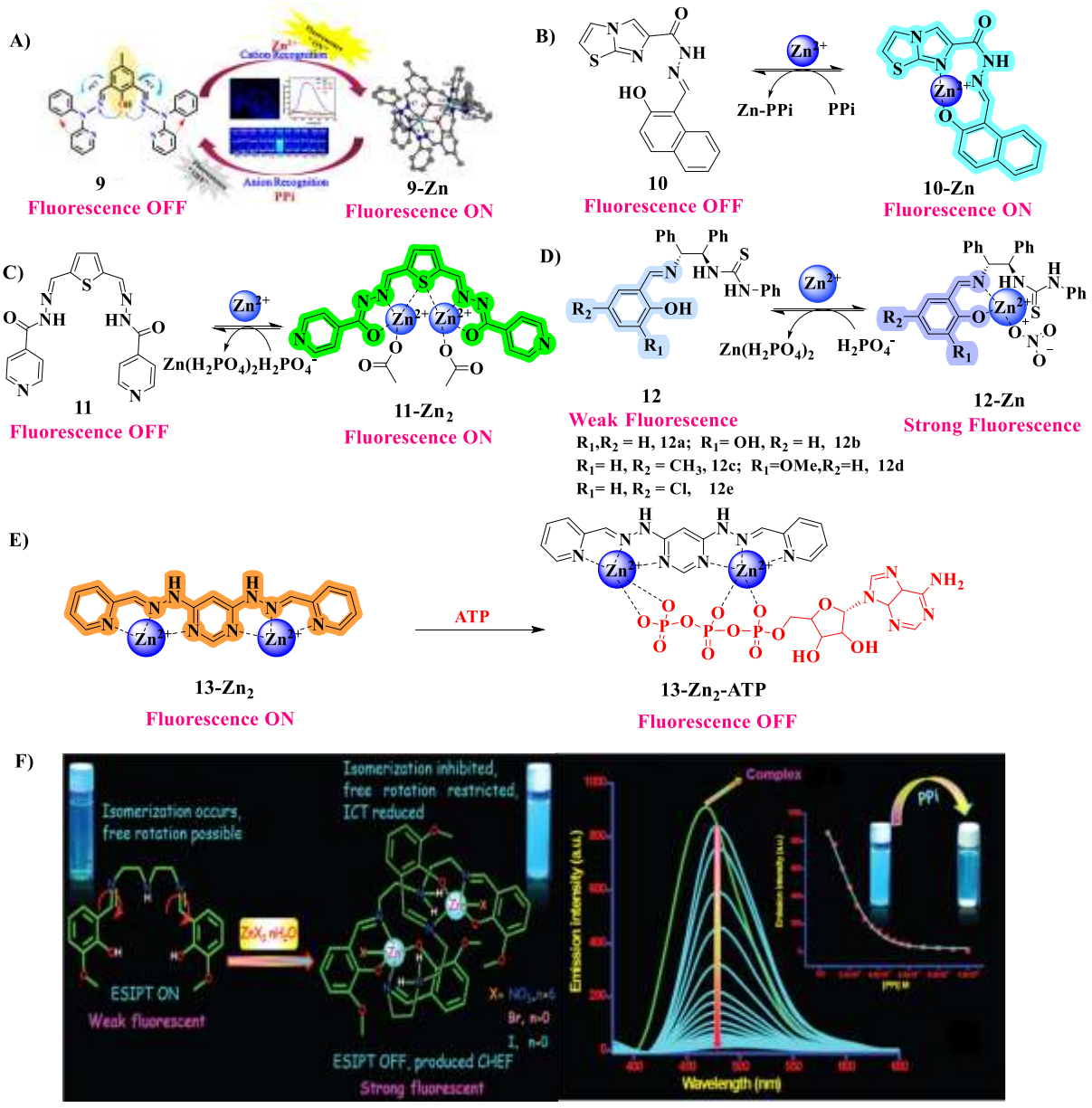

Open Access Article. Published on 10 June 2026. Downloaded on 6/10/2026 10:50:53 PM.
This article is licensed under a Creative Commons Attribution 3.0 Unported Licence.

Sensors & Diagnostics Accepted Manuscript

View Article Online
DOI: 10.1039/D6SD00010J

Fig. 5. A) Probe **9** showed fluorescence response with PPi *via* off-on mechanism. B-D) Probes **10-12** were reversibly interacted with PPi and PO_4^{2-} ions. E) The associated binding representation between **13-Zn2** and ATP. F) The reversible fluorescence response between probe **14-Zn2** and PPi ions. Adapted with permission from ref.117 Copyright © 2018 Royal Society of Chemistry. Adapted with permission from ref. 122 Copyright © 2017 Royal Society of Chemistry.

Recently, ensemble probe **13-Zn2** has been reported as a secondary detecting probe for ATP ion, which was prepared from pyridine and a derivative of pyrimidine (Fig. 5E).[121] While the addition of ATP to this probe, caused to form a ternary adduct with the subsequent fluorescence quenching. Live cell bioimaging and a number of on-site detection applications, like mung bean sprout evaluations and the use of paper strips and cotton swabs as real samples were employed to detect Zn^{2+}/ATP ions. In addition, probe **14** (dinuclear Zn^{2+} complex) was constructed by the reaction between phenol and diethylendiamine with Zn^{2+} metal centre, containing nitrate, bromide, and iodide salts (Fig. 5F).[122] Addition of PPi leads to suppress its fluorescence due to the formation of stable Zn-PPi complex and subsequent restoration of **14**, which was monitored in live HCT 116 cells. The proposed structure of the aggregation between **14-Zn2** and PPi was justified using DFT calculations.

5. 1. 2. Quinoline-based fluorescence probe

A novel **15-Zn** probe was developed for the first-time in order to simultaneously detect sodium-*meta*arsenite and $H_2PO_4^-$ ions and reported for its *in vivo* applications.[123] It shows an emission band at 650 nm, which has experienced a remarkable blue shift to 566 nm, upon the addition of sodium arsenite as a result of the formation of a stable **15-Zn-AsO2** complex, none of the other anions have shown such spectral change (Fig. 6A). Though, subsequent addition of $H_2PO_4^-$ with **15-Zn-AsO2** complex led to detach the Zn^{2+} ions from this complex. Moreover, the dissociated Zn^{2+} is anticipated to form a stable complex with AsO_2^- and $H_2PO_4^-$ ions along with the consequent release of **15** as a free ligand, which was confirmed from the observed emission profile (480 nm) and ESI-MS techniques. Interestingly, the sensitivity of **15-Zn** to arsenite and dihydrogen phosphate was successfully established in living cells using zebrafish embryos (Fig. 6B).

Open Access Article. Published on 10 June 2026. Downloaded on 6/10/2026 10:50:53 PM.
This article is licensed under a Creative Commons Attribution 3.0 Unported Licence.

Sensors & Diagnostics Accepted Manuscript

View Article Online
DOI: 10.1039/D6SD00010J

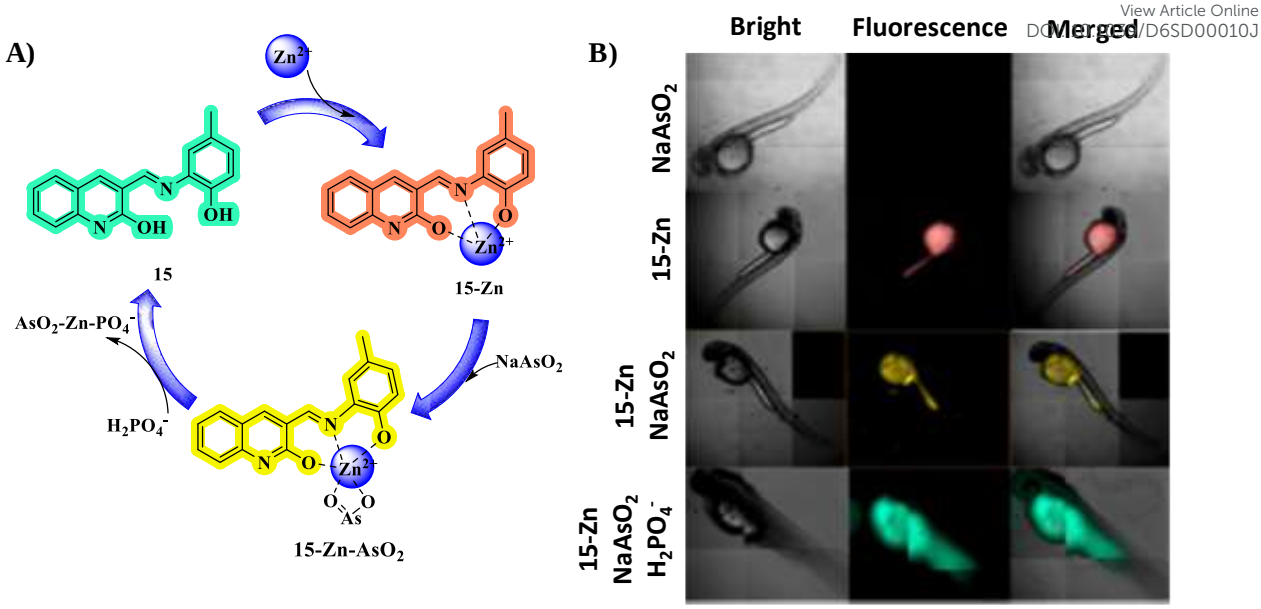

Fig. 6. A) Fluorescence response of **15-Zn** with $NaAsO_2$ towards $H_2PO_4^-$. B) Fluorescence imaging studies of **15-Zn** with $NaAsO_2$ towards $H_2PO_4^-$ on zebrafish embryos. Adapted with permission from ref. 123 Copyright 2019 Elsevier.

5. 1. 3. Pyrene-based fluorescence probes

Since, pyrene-based fluorophore has a unique chemosensing properties, a recent report has demonstrated the preparation of a monomer probe **16** from hydroxy pyridine and pyrene moiety for the identification of Zn^{2+} by generating a **16-Zn** with excimer emission of two pyrene units through face-to-face π-π stacking. The subsequent addition of $H_2PO_4^-$ with **16-Zn** led to the departure of **16** alone and generated a stable Zn-$H_2PO_4^-$ complex (Fig. 7A).[124] Likewise, Cys exhibits a similar pattern of behavior by establishing a potent interaction between Zn^{2+} and Cys and leaving out **16** as free ligand. Another strategy of Schiff base (**17**) was developed by the reaction between two equivalents of pyrene carboxaldehyde and cystamine dihydrochloride for the recognition of Zn^{2+} and PPi ions (Fig. 7B).[125] It showed an intense excimer emission at 515 nm due to the strong face-to-face π–π stacking between the two pyrene units. This excimer formation was inhibited by the addition of Zn^{2+} with **17**, and the band at 515 nm has blue shifted to 470 nm along with a slight hump at 475 nm may due to the rigid pyrene conformers, which reveals the occurred corresponding intermolecular excimer formation. The subsequent addition of PPi ion caused a distinguished change in the fluorescence of **17** from blue to green, among the various anions including phosphate-based ions. It reveals an innovative approach to detect Zn^{2+} and PPi ions by an interchange between the emissions of monomer and excimer pyrenes. In a similar manner, probe **18** has been designed from pyrene-1-carboxaldehyde and 2(2-aminoethylamino)ethanol, which showed a

Open Access Article. Published on 10 June 2026. Downloaded on 6/10/2026 10:50:53 PM.
This article is licensed under a Creative Commons Attribution 3.0 Unported Licence.

Sensors & Diagnostics Accepted Manuscript

View Article Online
DOI: 10.1039/D6SD00010J

weak monomer emission. Adding Zn^{2+} with this probe led to appeared a strong fluorescence at 456 nm due to the strong face-to-face stacking between pyrene moieties (Fig. 7C).[126] Probe **18** undergo hydrolyzes at acidic pH, while it is more stable at neutral and basic pH gradients, therefore it can be used to realize analyses at physiological pH. The fluorescence response of **18-Zn** was evaluated for a number of biologically significant phosphates, and the addition of ATP significantly (10 times) increased the fluorescence response at 460 nm was monitored with ^{31}P NMR spectral method, whereas other phosphates showed no changes in fluorescence. This observation suggests a possible role for the π–π stacking of pyrene and adenine moieties, also enables to making it as a viable option to track ATP in HeLa cells through fluorescence imaging studies.

Open Access Article. Published on 10 June 2026. Downloaded on 6/10/2026 10:50:53 PM.
This article is licensed under a Creative Commons Attribution 3.0 Unported Licence.

Sensors & Diagnostics Accepted Manuscript

View Article Online
DOI: 10.1039/D6SD00010J

Open Access Article. Published on 10 June 2026. Downloaded on 6/10/2026 10:50:53 PM.
This article is licensed under a Creative Commons Attribution 3.0 Unported Licence.

Sensors & Diagnostics Accepted Manuscript

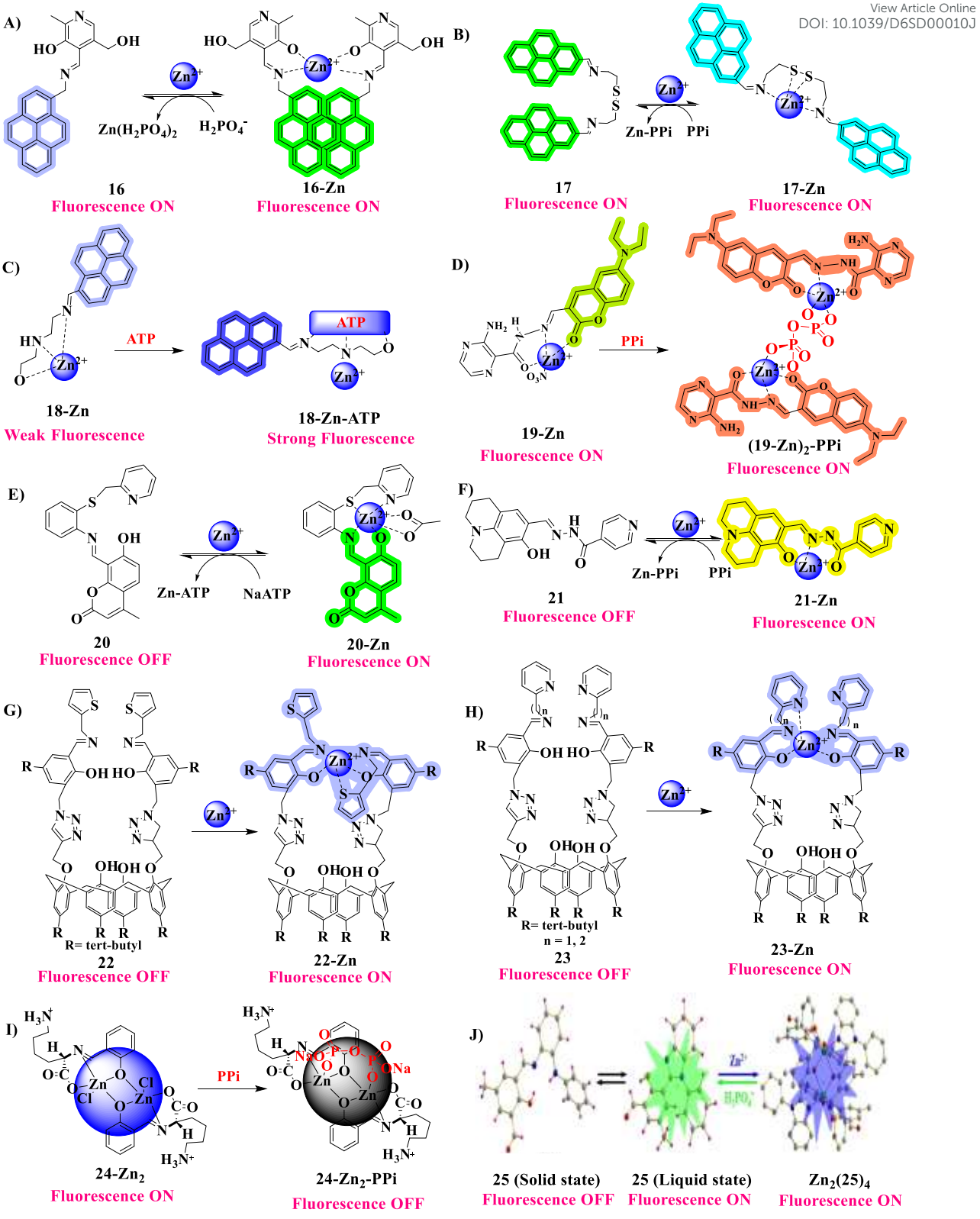

Fig. 7. Schematic representation of reversible and irreversible binding between probes **16-25** and phosphate-based biomolecules. Adapted with permission from ref. 133 Copyright © 2020 Royal Society of Chemistry.

View Article Online
DOI: 10.1039/D6SD00010J

Open Access Article. Published on 10 June 2026. Downloaded on 6/10/2026 10:50:53 PM.
This article is licensed under a Creative Commons Attribution 3.0 Unported Licence.

Sensors & Diagnostics Accepted Manuscript

5. 1. 4. Coumarin-based fluorescence probes

Coumarin acts as a fluorophore as well as a receptor against metal ions and anions. Fluorescence probe **19** as Schiff base was prepared from pyrazine and coumarin, which showed a green emission at 524 nm in DMSO and an aggregation-induced ratiometric emission (AIRE) at 555 nm in DMSO (0.5%) containing aqueous buffer (99.5%) with various solvents due to π–π stocking exist in the ligand architecture of coumarin moiety (Fig. 7D).[127] Addition of 2 equiv. of Zn^{2+} to **19** may led to quenched the existing AIRE of **19** at 555 nm, at the same time, its fluorescence emission in the far-red region at 628 nm was remarkably enhanced. Furthermore, the **19-Zn** complex was successfully used as a fluorescent ratiometric chemosensor to detect PPi. Recently, fluorescent probe **20** was constructed with pyridylthioether appended coumarin to form a Schiff (Fig. 7E).[128] It exhibited a weak yellow emission at 555 nm that originated from the combination of PET and ESIPT in the mixture of MeOH-water (3:1) solvent system at 25° C. Upon the addition of Zn^{2+} ion to **20** resulted in the observed hypsochromic shift to 512 nm along with a 240-fold enhancement in intensity according to the predicted CHEF effect. This fluorescence was then extinguished by adding ATP through the demetallation mechanism since Zn-ATP was generated

5. 1. 5. Julolidine-hydrazone-based fluorescence probe

Julolidine-hydrazone-based chemosensor (**21**) has been reported as Zn^{2+} sensor, and subsequently ensembled as **21-Zn** complex by their chelation in order to discriminate PPi from ADP and ATP (Fig. 7F).[129] The closed proximity of -OH and imine nitrogen groups as proton donor and acceptor respectively offers the ESIPT active core in probe **21** and was anticipated to demonstrate the respective enol and keto emissions. Sensing capabilities of **16** and the in-situ produced **21-Zn** and Zn-PPi complexes respectively with Zn^{2+} and PPi ions have also been evaluated in real water samples.

5. 1. 6. Calix[4]arene-based fluorescence probes

Iminothiophenyl with salicylaldehyde derivative was anchored on calix[4]arene and developed probe **22**, which showed strong fluorescence enhancement with Zn^{2+} in the HEPES buffer solution (Fig. 7G).[130] Its fluorescence was completely quenched by the addition of 0-1 equivalent of PPi to make an adduct, **22-Zn-PPi** as ternary complex. However, the excess addition of PPi with **22-Zn** led to leached out Zn^{2+} ion and generated a new Zn-PPi adduct. Additionally, further displacement of Zn^{2+} from the Zn-PPi adduct was also caused by the addition of Ca^{2+}, which retained its fluorescence emission. Interestingly, probe **23** was designed and developed on the basis of a pyridyl unit containing triazole-linked calix[4]arene conjugates, which exhibited a weak emission at ~455 nm in HEPES buffer at pH 7.4 (Fig. 7H).[131] When

View Article Online
DOI: 10.1039/D0SD00010J

Zn^{2+} interacted with this probe showed enhanced fluorescence due to the inhibition of isomerization in the imine (C=N bond) moiety and the ESIPT from salicyl -OH to the imine nitrogen and CHEF effect. Typically, all these probes were unstable at higher acidic and basic media and therefore, they exhibited poor fluorescence responses. These sensor studies were expanded to simple organic and bio-relevant molecules containing phosphate units, such as β-naphthyl phosphate, PPi, AMP, ADP, and ATP.

5. 1. 7. Phenol-based Schiff base probes

A lysine-based Schiff base probe **24** exhibited a highly fluorescent property both in the solid and solution phases in neutral aqueous media by showing a band at 453 nm. Its fluorescence was developed from the available 2-hydroxybenzylidene amino moiety in the probe's structure, in which the C=N isomerization is inhibited due to the addition of Zn^{2+} ions (Fig. 7I).[132] Later, when PPi was added, this fluorescence was suppressed; the extent of this decrease varied according to the PPi concentration. In this regard, a titration was carried out between **24-Zn$_2$** against PPi ions in a 1:4 ratio excess of Cl^- ions, which did not restore its fluorescence, illustrating the existing greater affinity between PPi and Zn^{2+} over Cl^- ions. In addition, ATP and ADP also significantly quenched the fluorescence of **24-Zn$_2$** in the following decreasing order; PPi >ATP > ADP. A novel, simple, and non-toxic two-in-one type fluorescent probe, **25** has been developed using a half-condensed organic fluorophore sequence based on 2,6-diformyl *p*-cresol derivative for the selective detection Zn^{2+} and $H_2PO_4^-$ ions as "Green-Blue-Green" emissive material for the first time (Fig. 7J).[133] It showed a strong absorption band at 335 nm, which might be due to the n-π^* charge transfer transition, *i.e.*, transitions of electrons from non-bonding orbitals on the nitrogen atoms to the π^* orbital in the phenolic ring. When incremental addition of Zn^{2+} ion to the buffer solution of **25** at 25 °C, its consistent emission at 520 nm was gradually blue shifted to 475 nm. Interestingly, this emission band (475 nm) experienced a significant red shift (520 nm) upon the addition of $H_2PO_4^-$ ion with **25-Zn** complex, by the re-generation of free probe **25** with a rigid anionic structure. A simple fluorescence probe **26** was prepared from salicylaldehyde and derivatized phthalimide (Fig. 8).[134] Upon adding Zn^{2+} to this probe showed strong fluorescence at 447 nm *via* the CHEF effect. After that, adding PPi to **26-Zn** exhibited a rapid suppression of its fluorescence through a displacement approach. Significantly, **26** has been used for the sequential detection of Zn^{2+} and PPi in zebrafish and live cells. Specifically, it is the first evidence for recognizing Zn^{2+} and PPi in living cells and zebrafish by a chemosensor.

Open Access Article. Published on 10 June 2026. Downloaded on 6/10/2026 10:50:53 PM.
This article is licensed under a Creative Commons Attribution 3.0 Unported Licence.

Sensors & Diagnostics Accepted Manuscript

View Article Online
DOI: 10.1039/D6SD00010J

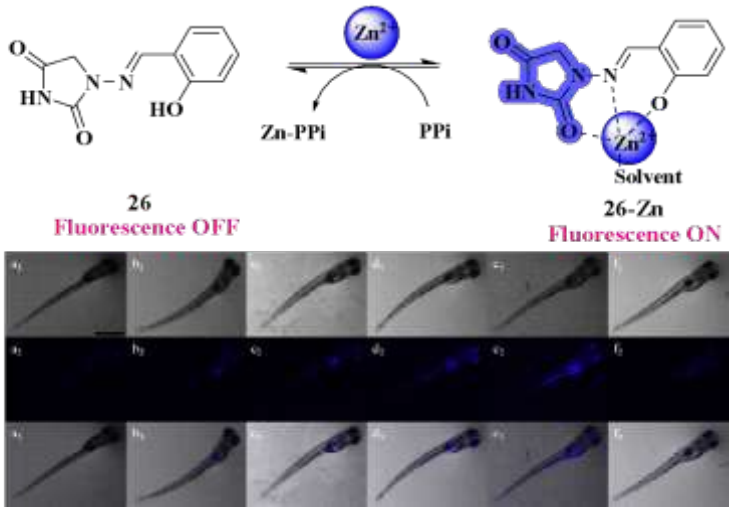

Fig. 8. The schematic representation of **26** with Zn^{2+} and PPi ions. B) The fluorescence images of zebrafish incubated with **26** and followed subject to Zn^{2+} and PPi ions. Adapted with permission from ref. 134 Copyright 2018 Elsevier.

5.2. Dipicolylamine-based (DPA) family receptor probes

5. 2. 1. Benzoxazole and benzothiazole-based fluorescence probes

DPA-based receptors may effectively bound to Zn^{2+} ions. In this series, benzoxazole-phenol-based probe **27** bearing two DPA receptor units with phenol (Fig. 9A).[135] has been developed. The available phenoxide oxygen in this probe could chelate with Zn^{2+} and generate **27-Zn$_2$** in order to disable the ESIPT process. These two Zn^{2+} ions are conveniently spaced apart, which permits the precise detection of PPi than other anions including ATP. The ternary adduct of **27-Zn$_2$-PPi** was achieved by the interaction of PPi with two Zn^{2+}, resulting in the de-coordination of a phenolic hydroxyl group from the Zn^{2+} ions, enabling the ESIPT turn-on process. Similarly, probe **28** was created from benzothiazole moiety instead of benzoxazole along with two DPA units, allowing ESIPT on-off mechanism (Fig. 9B).[136] Upon the addition of 1 equiv. of Zn^{2+} with **28** led to a remarkable fluorescence shift from green to blue region, and its fluorescence was consistent with the subsequent addition of one more 1 equiv. of Zn^{2+} ions. On the other hand, 2 equiv. of Zn^{2+} interacting with **28** to form **28-Zn$_2$**, which interacts with PPi to form **28-Zn$_2$-PPi**. Unexpectedly, this probe can be distinguishing in the detection of PPi ions from ATP in both alcohol and water solvents. Such a solvent-dependent recognition of ESIPT has confirmed its excellent sensitivity towards the adopted environments utilized and the capability to distinguish the structurally identical anions has been mechanistically investigated by NMR studies, which offers solid suggestions for extended future design of ESIPT sensor. In the sequence of these cases, the Zn^{2+} interacted with a combination of *p*-methylphenol and one DPA unit and generated a probe **29-Zn**, which disabled the ESIPT

Open Access Article. Published on 10 June 2026. Downloaded on 6/10/2026 10:50:53 PM.
This article is licensed under a Creative Commons Attribution 3.0 Unported Licence.

Sensors & Diagnostics Accepted Manuscript

View Article Online
DOI: 10.1039/D3SD00010J

process due to the phenol OH group coordinating with Zn^{2+}as our earlier discussion (Fig. 9C).[137] The stepwise deprotonation of H_2PPi with **29-Zn** was monitored by NMR spectroscopy. The addition of ADP or H_2PPi to **29-Zn** led to a significant spectral shift (from 447 to 504 nm) as a consequence of phenol moiety elimination, which turned on the ESIPT process.

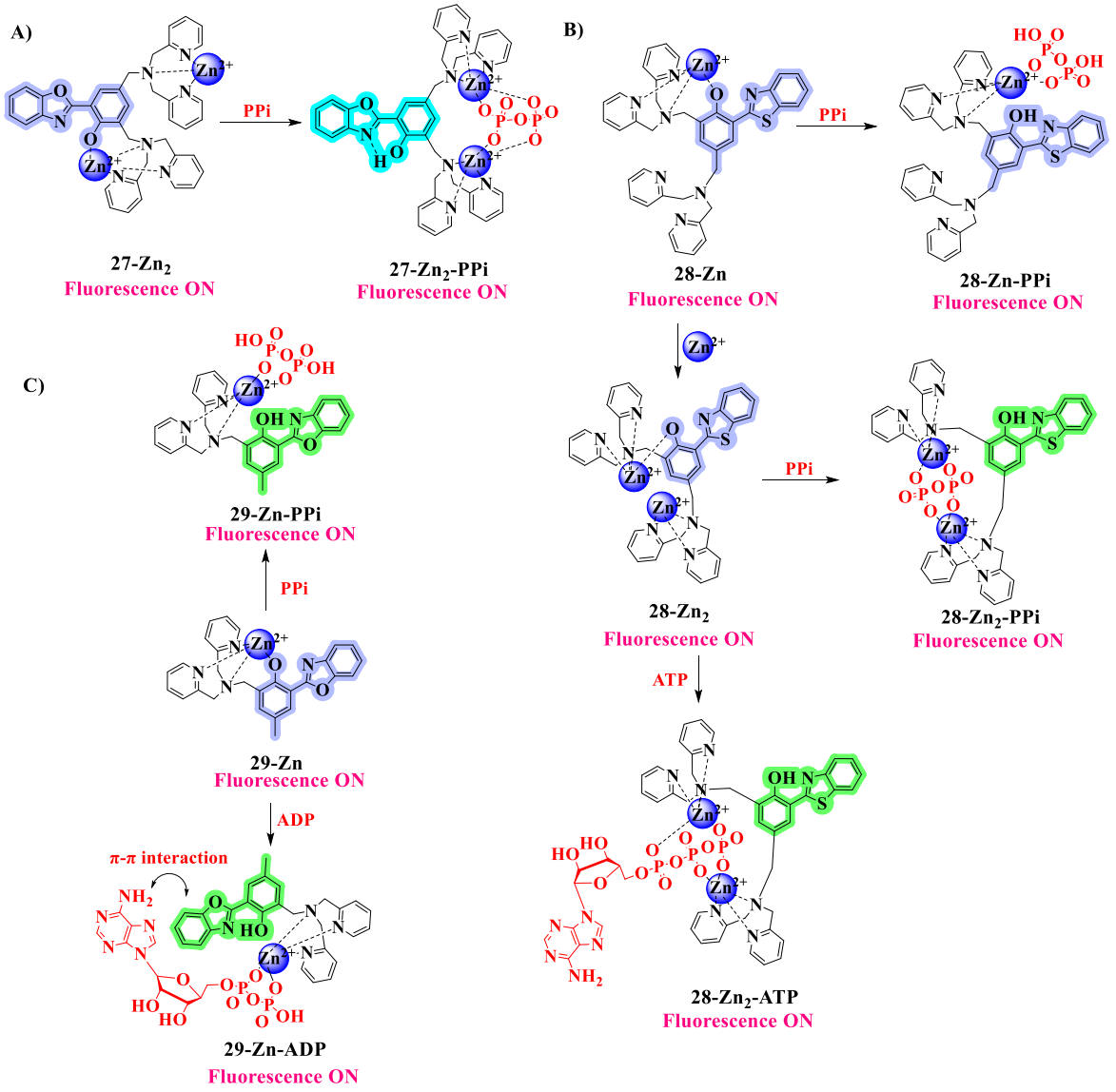

Fig. 9. The associated binding representation between Zn(II) complexes of probes (**27-29**) and PPi/ ADP/ ATP.

5. 2. 2. Naphthalene-based fluorescence probes

Probe **30** has been developed based on the naphthalene derivative, 1,1'-bi-2-naphthol (BINOL) connected with two DPA receptors (Fig. 10A).[138] In this competition, **30** illustrated a weak fluorescence in the 336-612 nm region due to the anticipated PET process from the lone pair nitrogens of DPA moiety to BINOL in HEPES buffer solution. However, the addition of Zn^{2+} ions has led to an increase in its fluorescence, meanwhile inhibiting the lone pair electron

Open Access Article. Published on 10 June 2026. Downloaded on 6/10/2026 10:50:53 PM.
This article is licensed under a Creative Commons Attribution 3.0 Unported Licence.

Sensors & Diagnostics Accepted Manuscript

View Article Online
DOI: 10.1039/D0SD00010J

transfer of DPA to BINOL (PET OFF), resulting in weak fluorescence appeared at 383 nm for **30-Zn$_2$**, thereafter turn-up of 4-fold enhancement fluorescence has achieved by the gradual addition of PPi ions. In the same way, a naphthalene tetracarboxylic dianhydride-based spacer with DPA receptor complexed with Zn^{2+} ions as probe **31-Zn$_2$** (Fig. 10B).[139] It showed high selectivity towards PPi over the other anions, and the existing Zn sites along with the π-π interaction may induced the unique 2+2 type excimer with PPi. Later, probe **32** was constructed with 1,8-naphthalimide moiety bearing two DPA arms, which showed 59-fold fluorescence enhancement by the incorporation of Zn^{2+} ions (Fig. 10C).[140] However, this fluorescence was quenched (52%) by the addition of PPi ions along with a significant blue shift (23 nm) than its related analogs, like ATP and phosphate in aqueous media. The DFT calculations have declared that one of the Zn^{2+}ions in **32-Zn$_2$** was bonded with PPi, while the other Zn^{2+} ion bound to another chelating moiety, which did not bond with PPi ions.

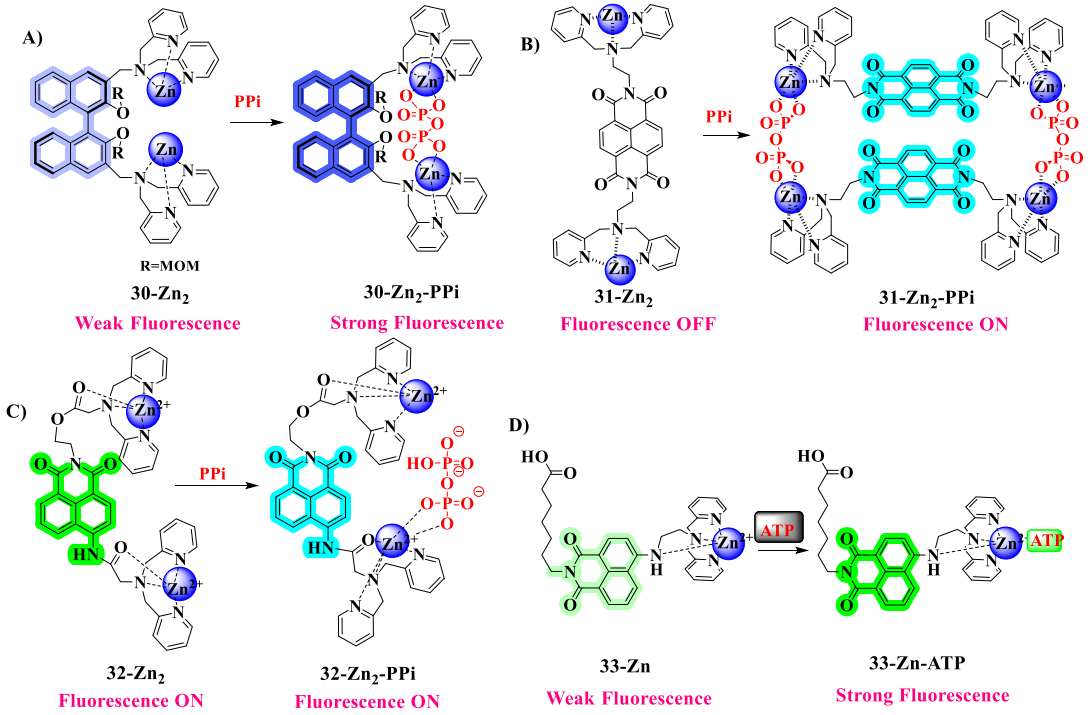

Fig. 10. The interaction between Zn(II) complexes-based fluorescence probes (**30**-**33**) and PPi /ATP.

A naphthalene derivative and DPA were connected with a spacer to generate probe **33**, it exhibited a weak fluorescence with Zn^{2+} ions due to the inhibition of PET process (Fig. 10D).[141] This PET process was activated by the interaction between **33-Zn** and ATP, yield a strong fluorescence. On the other hand, the substantial fluorescence was enhanced as a result of the interaction between ATP and **33-Zn**, which decreased the strength of the Zn-NH link. The observed loss of fluorescence intensity was found to be 40% and 25% at lower pH (5.6

Open Access Article. Published on 10 June 2026. Downloaded on 6/10/2026 10:50:53 PM.
This article is licensed under a Creative Commons Attribution 3.0 Unported Licence.

Sensors & Diagnostics Accepted Manuscript

View Article Online
DOI: 10.1039/D6SD00010J

and 6.5 respectively) compared to the neutral solution. Acedan derivatives have been used to generate some mononuclear Zn-DPA complexes that function as fluorescent probes for phosphate anion detection.[142] In particular, they were frequently portrayed as two-photon sensors for metal cations, using the acedan derivatives (**34b-d**) and the exiting aryloxy attached (**34a**) with Zn^{2+} as fluorescent probes for phosphate anion detection (Fig. 11A). Anion binding to the metal complexes can trigger the ICT in the acedan fluorophore, regardless of the abilities of donor (6-acylamido group) or acceptor (2-acyl group). As a result, the acedan system (**34b**) was made and contrasted with **34c** and **34d**, where the naphthyl nitrogen may play a vital role in metal coordination and enhance the selectivity of PPi ions over ATP. The association of Zn^{2+} ions with oxygen in the carboxamido moiety caused a modest fluorescence along with a bathochromic shift (10 nm) in the interaction between probe **34b** and Zn^{2+}. This conjugation was cleaved by the addition of PPi and led to a significant fluorescence enhancement (10-fold) by the formation of a new adduct, **34b-Zn-PPi**, while ATP caused a minor enhancement (1.86-fold) in its fluorescence. These fluorescence changes were accompanied by the ICT transfer of acedan moiety.

Open Access Article. Published on 10 June 2026. Downloaded on 6/10/2026 10:50:53 PM.
This article is licensed under a Creative Commons Attribution 3.0 Unported Licence.

Sensors & Diagnostics Accepted Manuscript

View Article Online
DOI: 10.1039/D6SD00010J

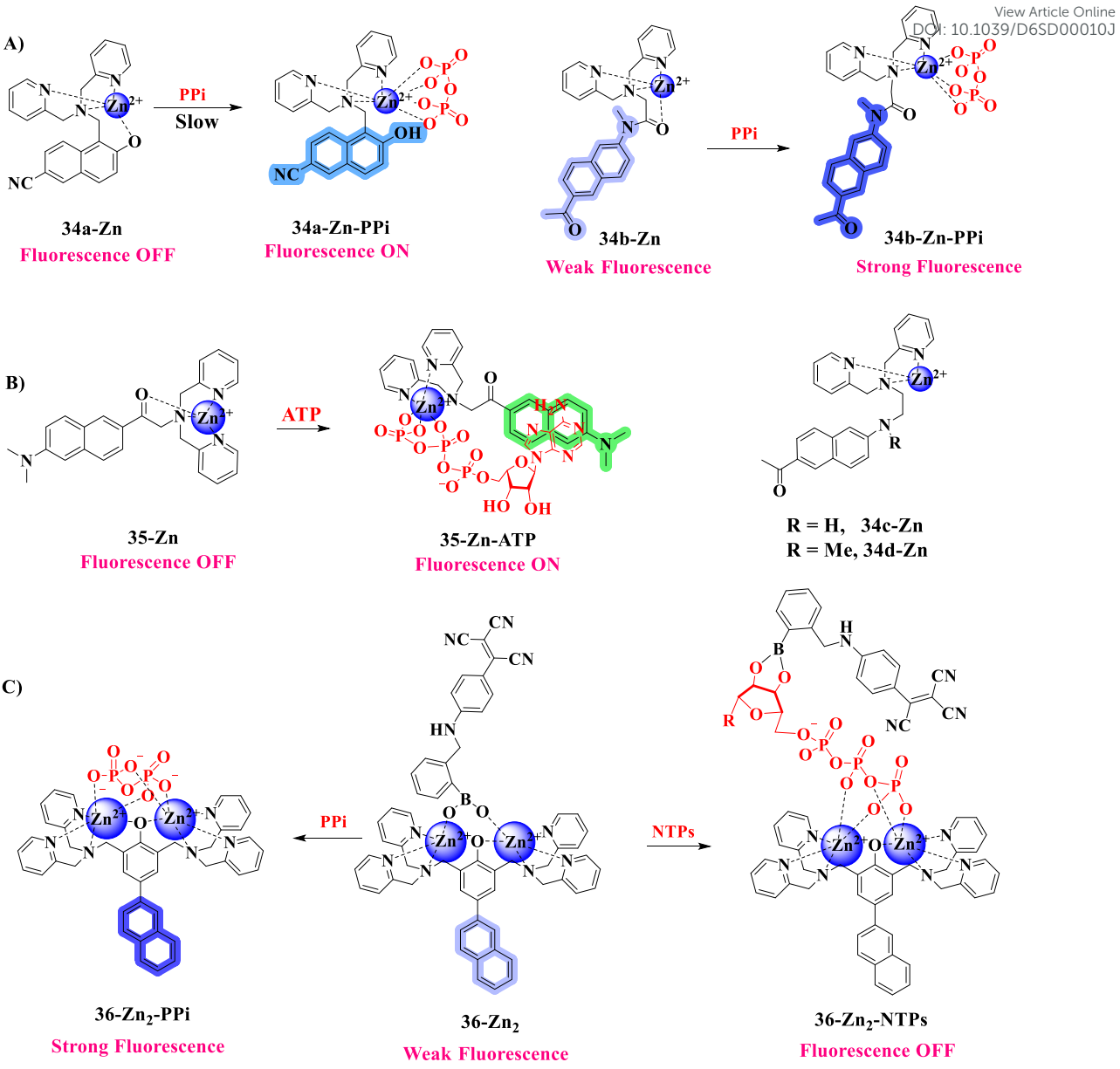

Fig. 11. Schematic illustration of the interaction between phosphate-based biomolecules and Zn(II) complex probes (**34-36**).

Similarly, **35-Zn** was designed from acedan derivative with a DPA receptor to detect the nucleosides, ATP and ADP (Fig. 11B).[143] The allowed PET process from DPA moiety to acedan, caused for a weak fluorescence response for this probe. Instead, the addition of Zn^{2+} led to a gradual suppression of its fluorescence intensity in both solid and solution states. Moreover, the conducted fluorescence titration between **35-Zn** and ATP revealed 8.5 times more fluorescence than other phosphate-containing analytes. This selectivity is explained by the π-π interaction between the acedan core and adenine base of ATP. Another method of preparing a bimetallic complex **36-Zn2** was done using naphthalene-based DPA unit receptors that were bonded to Zn^{2+} ions, subsequently it was connected to boronic acid (BA) derivatives

Open Access Article. Published on 10 June 2026. Downloaded on 6/10/2026 10:50:53 PM.
This article is licensed under a Creative Commons Attribution 3.0 Unported Licence.

Sensors & Diagnostics Accepted Manuscript

View Article Online
DOI: 10.1039/D6SD00010J

(Fig. 11C).[144] The observed weak fluorescence for the combined **36-Zn$_2$** and BA, has shown 8-fold enhancement by the addition of PPi due to the newly developed adduct, **36-Zn$_2$-PPi**. Moreover, the obtained binding affinity towards PPi is also greater than **BA** for **36-Zn$_2$**. Surprisingly, **36-Zn$_2$-BA** interaction with NTPs showed inhibited fluorescence, at the same time BA bound with NTPs to form an adduct of boronic ester, which was coordinated with **36-Zn$_2$**, which was confirmed by mass analysis. This strategy was successfully used to the accurate measurement of RNA produced during RNA transcription.

5. 2. 3. Anthracene-based fluorescence probes

Anthracene derivative of 10-azaanthracene coupled with two DPA units as probe **37** and it showed weak fluorescence with Zn^{2+} (Fig. 12A).[145] Surprisingly, its fluorescence was suppressed by the addition of PPi, while it displayed a huge fluorescent enhancement with Pi, these observations suggest that this is due to the selective CHEF effect for Pi and the CHEQ effect for PPi. The association constants of **37-Zn$_2$** with PPi and Pi were found to be 4.85×10^7 and 9.36×10^4 M^{-1} respectively. The observed enhanced fluorescence for **37-Zn$_2$** with phosphate ions could be ascribed to the additional hydrogen bonding existing between nitrogen and hydrogen atoms of acridine and Pi moieties respectively. Another approach of an excellent sensitivity property by giving PPi more selectivity than ATP and other common anions was obtained for the bridged dinuclear DPA-Zn_2 complex (Fig. 12B). This was constructed with a modified anthracene moiety with two sets of DPA containing a 2-position CH_2OH group, enabling the controlling anthracene excimer in a neutral solution.[146] In contrast, the incorporation of H instead of -CH_2OH led to suppress the fluorescence of **38-Zn$_2$** (H) with the addition of PPi. The substitution of H or CH_2OH moieties may influence certain chemical and photophysical responses in detecting analytes. Unpredictably, probe **39-Zn$_2$** was constructed from DPA units and anthracene-methyl ester with Zn^{2+} (Fig. 12C).[147] It revealed a 3-fold more intense fluorescence spectral response at 460 nm by the addition of ATP. Their binding affinity was found to be 10 and 30 times greater than ADP and AMP respectively. Their structural binding mode was evaluated by ^{31}P NMR technique, in that the observed NMR signals of β- and γ-phosphate of ATP have shown a clear and notable shift to the downfield (2.5 and 2.1 ppm, respectively) upon the addition of 1 equiv. of **39-Zn$_2$**, instead, a very poor chemical shift was observed for α-phosphate.

Open Access Article. Published on 10 June 2026. Downloaded on 6/10/2026 10:50:53 PM.
This article is licensed under a Creative Commons Attribution 3.0 Unported Licence.

Sensors & Diagnostics Accepted Manuscript

View Article Online
DOI: 10.1039/D6SD00010J

Open Access Article. Published on 10 June 2026. Downloaded on 6/10/2026 10:50:53 PM.
This article is licensed under a Creative Commons Attribution 3.0 Unported Licence.

Sensors & Diagnostics Accepted Manuscript

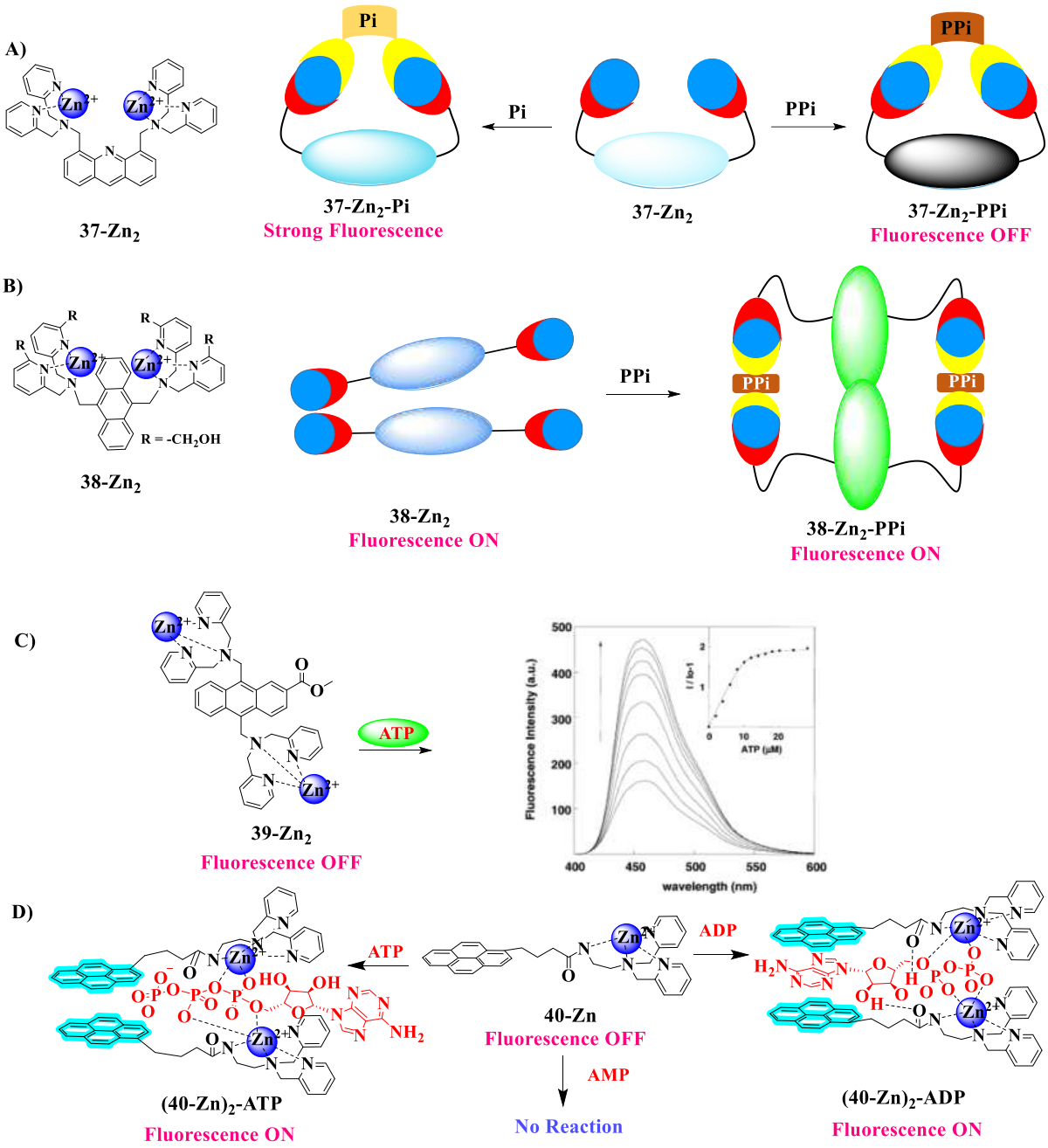

Fig. 12. The distinct associative behavior expressed between Zn (II) complex probes (**37-40**) with phosphate-based molecules. Adapted with permission from ref. 147 Copyright 2002 Elsevier.

5. 2. 4. Pyrene-based fluorescence probe

Probe **40-Zn** has been prepared from pyrene coupled DPA unit and employed for the detection of phosphate-based analytes, such as PPi, AMP, ADP, and ATP through their fluorescence responses (Fig. 12D).[148] Addition of 0.5 equiv. of PPi to **40-Zn**, illustrated a drastic fluorescence enhancement at 482 nm, indicating the formation of the **40-Zn-Ppi.**

View Article Online
DOI: 10.1039/D6SD00010J

Similarly, addition of 0.4 equivalent ATP or ADP to this probe showed an increased excimer emission, and the consecutive excess of ATP or ADP showed monomer emissions. These results indicated that the adenine aromatic ring might be inside the pyrene dimer to provide a fully intramolecular sandwich structure for the **40-Zn-ADP** complex. Conversely, AMP did not exhibit any changes in fluorescence signal with **40-Zn**, indicating no discernible interaction occurred in between AMP and **40-Zn**.

5. 2. 5. Coumarin-based fluorescence probes

Nitro-substituted coumarin benzene ring was directly connected to the DPA receptor to make **41**, which was connected with Cu^{2+}, Zn^{2+}, and Cd^{2+} ions and acted as respective probes towards various anions, exclusively they have excellent affinity toward phosphate anions (Fig. 13A).[149] Amongst, the PPi has been shown to be more strongly coordinated with **41-Zn** than **Cu-41** and **Cd-41**. Therefore, it could be employed for the quantitative detection of PPi under physiological conditions along with developing a real-time "turn-on" (for **41-Zn** and **41-Cu**) and "turn-off" (**41-Cd**) fluorescence assay to assess enzyme activity of alkaline phosphatase (ALP). In this series, the coumarin benzene ring was connected to a DPA receptor through a spacer to create **42**, upon interacting with Zn^{2+} showing a weak fluorescence (**42-Zn**). It experienced an enhanced fluorescence response after interacting with ATP, and also showed a greater selectivity towards nucleoside polyphosphates. The interaction was analyzed by NMR spectroscopy, illustrating the binding nature between the ATP phosphate moiety and the Zn^{2+} centre (Fig. 13B).[150] Interestingly, the benzocoumarin dye with DPA has shown an elevated fluorescence response at 595 nm, indicating a quick and reversible interaction between nuclear ATP and probe **43-Zn**. This was caused by a significant alteration in the coordination mode, which resulted in an off-on change in fluorescence (Fig. 13C).[151] Probe **43-Zn** was inert with other compounds such as nucleotides, RNAs, or DNAs, and has a better affinity to ATP than ADP. This probe has been employed to examine the ATP levels in cell nuclei of healthy and cancerous tissues in various mouse organs. They used as a special imaging technique called two-photon microscopy, and used to found the level of nuclear ATP in tumor cells is 3.9-7.8 times more than healthy cells, which can be linked to their rapid growth. Moreover, some separate tests have confirmed that the observed high level of nuclear ATP formation during cell division (mitosis) in tumors. Tumor and normal tissue differentiation were investigated using the fluorescent probe **43-Zn**, which was related to nuclear ATP-associated biological activity.

Open Access Article. Published on 10 June 2026. Downloaded on 6/10/2026 10:50:53 PM.
This article is licensed under a Creative Commons Attribution 3.0 Unported Licence.

Sensors & Diagnostics Accepted Manuscript

View Article Online
DOI: 10.1039/D6SD00010J

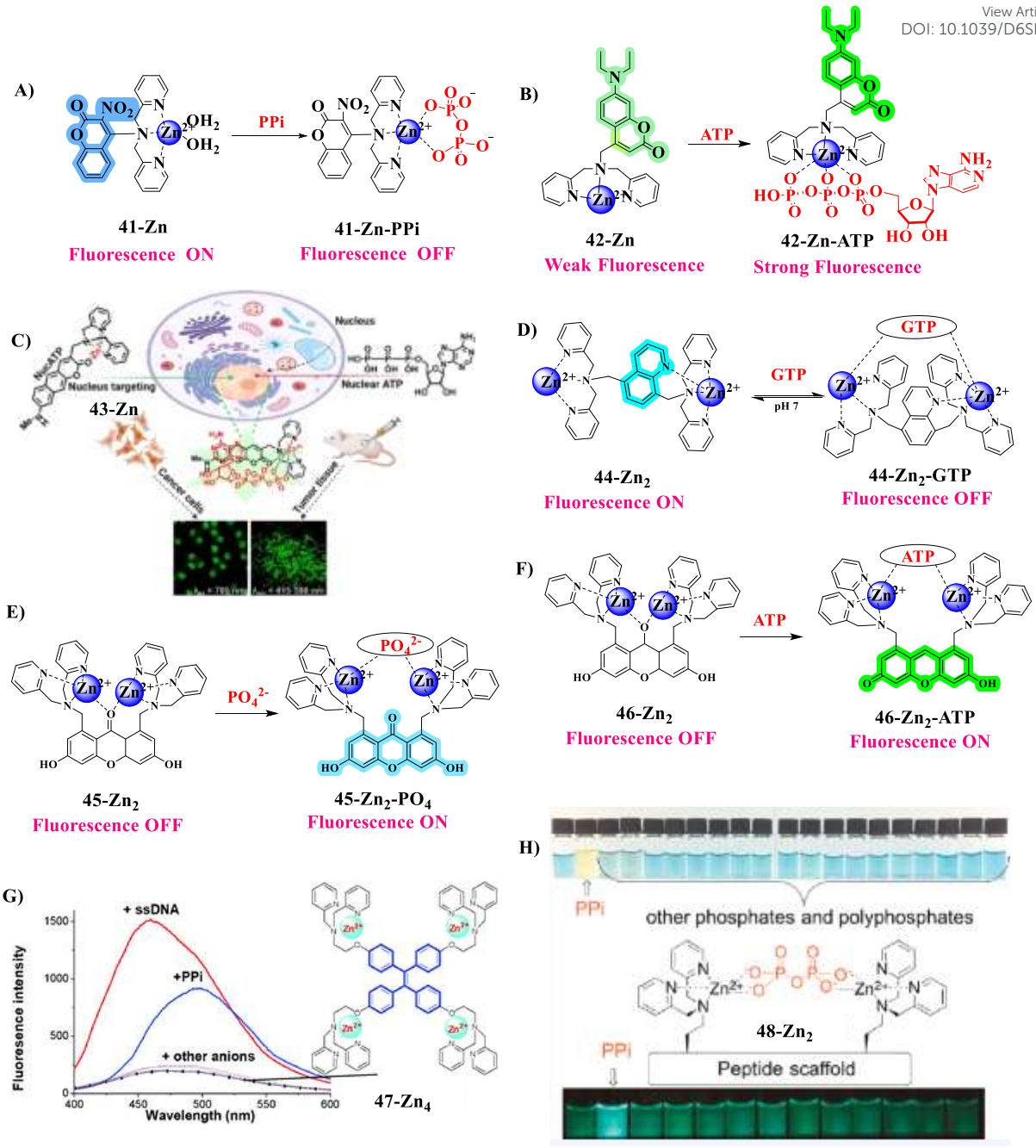

Fig. 13. A, B) Reaction between probes (**41-Zn** and **42-Zn**) with PPi and ATP respectively. C) Probe **43-Zn** was reached nuclear ATP and showing the images of cancer cells and tissues in the fluorescence scope. D, E, F) Interaction of probes with GTP, PO_4^{2-} and ATP. G) Structure of probe **47-Zn$_4$** and its fluorescence response with PPi and ssDNA. H) Structure of **48-Zn$_2$** and its interaction with PPi in visible and fluorescence lamp. Adapted with permission from ref. 151 Copyright © 2023 John Wiley and Sons. Adapted with permission from ref. 155 Copyright © 2014 Royal Society of Chemistry. Adapted with permission from ref. 156 Copyright 2017 American Chemical Society.

Open Access Article. Published on 10 June 2026. Downloaded on 6/10/2026 10:50:53 PM.
This article is licensed under a Creative Commons Attribution 3.0 Unported Licence.

Sensors & Diagnostics Accepted Manuscript

View Article Online
DOI: 10.1039/D6SD00010J

Open Access Article. Published on 10 June 2026. Downloaded on 6/10/2026 10:50:53 PM.
This article is licensed under a Creative Commons Attribution 3.0 Unported Licence.

5. 2. 6. Quinoline-based fluorescence probe

There are relatively few literature studies that are exclusively available for the recognition of ATP and GTP by metal-based receptors. In this regard, a binuclear Zn^{2+} complex was prepared by utilizing a DPA receptor linked to quinoline to make **44-Zn$_2$** (Fig. 13D).[152] This probe showed fluorescence quenching with GTP compared to common anions such as PPi, ATP, GDP, CTP, and UTP. This quenching process can be explained by a static anion-complexation PET mechanism in both the excited and the ground states. Additionally, NMR spectroscopic experiments and DFT calculations showed that the GTP is bound with **44-Zn$_2$** through three points involving the simultaneous coordination of the N7 atom of the guanosine motif and two phosphate groups towards two Zn atoms. This probe can detect GTP in the micromolar concentration range even in the presence of coexisting species in the plasma and urine.

5. 2. 7. Xanthene-based fluorescence probe

Probe **45-Zn$_2$** was has been developed from the combination of xanthene and DPA with Zn^{2+} and it is utilized for the detection of the phosphate anions (Fig. 13E).[153] The DPA receptors and xanthene moiety of carbonyl oxygen atom was coordinated with bimetallic Zn centres (**45-Zn$_2$**). However, one of the Zn^{2+} atom undergo de-coordination from the carbonyl group of xanthene due to its interaction with phosphate ion, yield a turn-off fluorescence signaling. On the other hand, the other Zn^{2+} centre has strongly coordinated with carbonyl atoms, which was confirmed by an X-ray crystallographic study. Another compact probe of binuclear zinc complex (**46-Zn$_2$**) was prepared from xanthene fluorophore and DPA receptors, which, showed an astonishingly 30-fold increase in fluorescence upon binding with a nucleoside polyphosphate like ATP in neutral aqueous conditions (Fig. 13F).[154] Remarkably, **46** reacted with Zn^{2+} ions in methanol to form **46-Zn$_2$** with a water molecule. When this water molecule came into contact with two Zn^{2+} centers, it led a nucleophilic attack on the xanthene ring at neutral pH, which caused it to lose its fluorescence. Due to the deconjugation involved nucleophilic attack of a metal-bound water molecule, the deconjugated xanthene fluorophore structure was formed, resulting in turn-on fluorescence. The first approach stated on the interaction between nucleoside polyphosphates and **46-Zn$_2$** demonstrated the recovery of the conjugated structure of the xanthene ring.

5. 2. 8. Tetraphenylethene-based fluorescence probe

The **47-Zn$_4$** complex was developed from tetraphenylethene (TPE) anchoring with four DPA receptors, which showed an effective fluorescence enhancement with PPi ions compared to other anions (Fig. 13G).[155] Subsequently, this probe showed significant fluorescence

Sensors & Diagnostics Accepted Manuscript

View Article Online
DOI: 10.1039/D6SD00010J

enhancement upon the addition of ssDNA, consequently restricting the intramolecular rotation of TPE upon Zn^{2+}–DPA units binding to DNA through the coordination. Titration of **47-Zn$_4$** against PPi has shown that it may bind PPi to produce 1 : 1 and 1 : 2 complexes with emission bands respectively at 480 and 490 nm. Similarly, this emission was considerably different from the emission of **47-Zn$_4$**-DNA complexes, which demonstrated that TPE-Zn may bind diverse phosphate derivatives with different binding modes.

5. 2. 9. Peptide-scaffold fluorescence probe

Two **48-Zn$_2$** have been positioned in the presence of DPA anion receptors employing novel peptide scaffolds, which has been successful in generating receptors with an exceptional ability to differentiate PPi from other comparable molecules with phosphate groups, such as nucleoside triphosphates (Fig. 13H).[156] These structural constructions could enable the fusion of small receptor libraries, where the two binding site configurations were slightly changed in order to evaluate the factors affecting the selectivity and affinity of PPi binding. It led to alter several structural elements, such as the length of the peptides, the size of the cyclic peptide rings, the makeup of the amino acids, the orientation of the binding sites about each other, and the relative stereochemistry of the peptides. Backbone-modified cyclic peptides from the *Lissoclinum class* of natural products were used to provide the receptors as additional levels of preorganization. On the other hand, short and flexible bis-**48-Zn$_2$**-functionalized linear peptides, were found to be effective scaffolds for selective PPi identification in the far more complex biological cell samples in the later findings.

5. 2. 10. Boron-based fluorescence probe

A non-fluorescence probe **49** was constructed from the BODIPY system with the DPA receptor, showing an enhanced fluorescence (at 549 nm) by treating with Zn^{2+} to generate **49-Zn** (Fig. 14A).[157] It was quenched by adding PPi to **49-Zn** and yield the detection limit of 17.5 μM. The binding strengths of **49-Zn** and **49-Zn**-PPi complexes were investigated by NMR titration and DFT calculations. Also, this system could be employed as an efficient method to detect the Zn^{2+} and PPi ions in live cells.

5. 2. 11. Dicyanomethylene-benzopyran-based fluorescence probe

Open Access Article. Published on 10 June 2026. Downloaded on 6/10/2026 10:50:53 PM.
This article is licensed under a Creative Commons Attribution 3.0 Unported Licence.

Sensors & Diagnostics Accepted Manuscript

View Article Online
DOI: 10.1039/D6SD00010J

Open Access Article. Published on 10 June 2026. Downloaded on 6/10/2026 10:50:53 PM.
This article is licensed under a Creative Commons Attribution 3.0 Unported Licence.

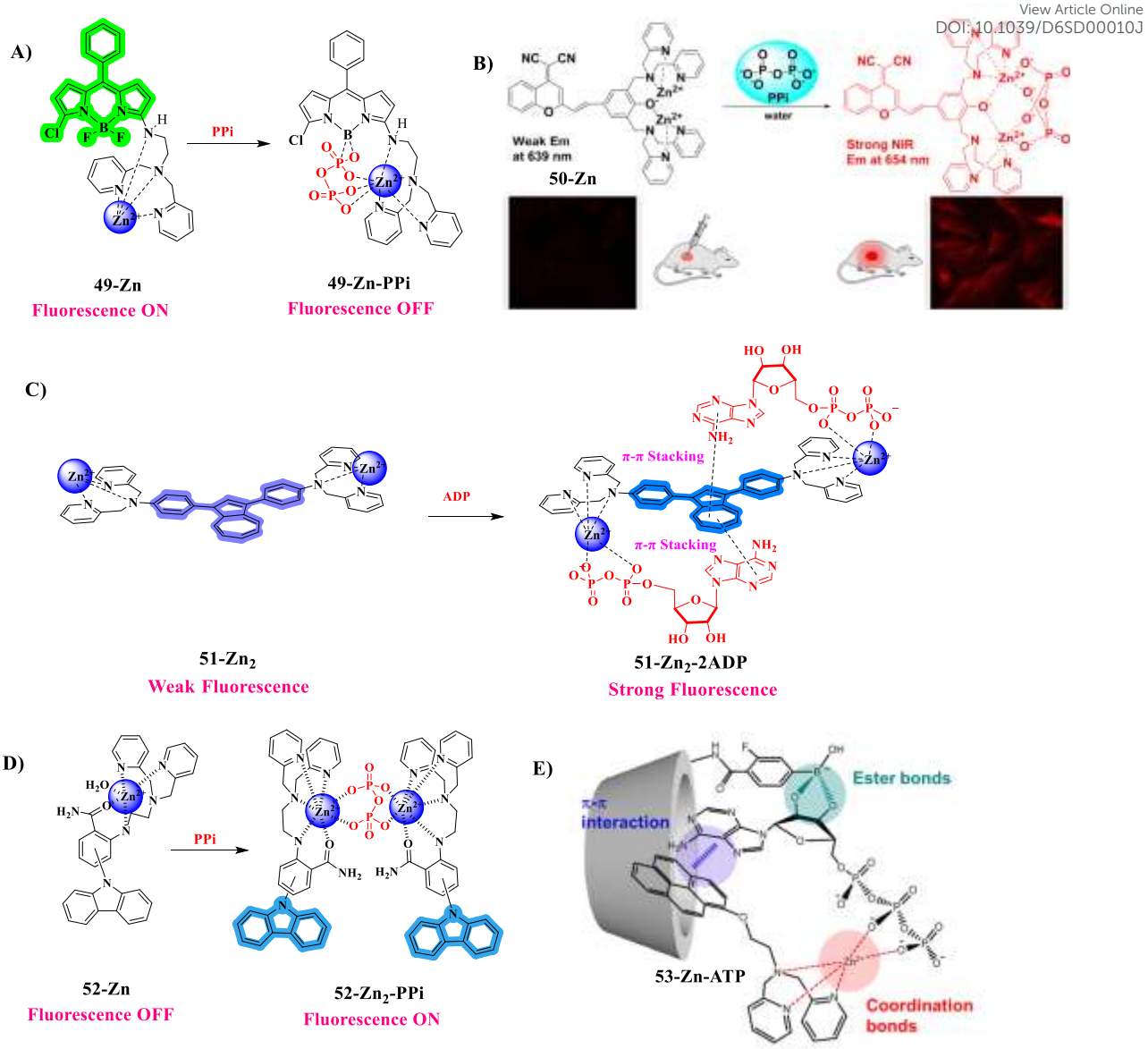

Fig. 14. A) Schematic representations of the binding mode between **49-Zn** and PPi, B) Weak fluorescence probe **50-Zn**$_2$ interacted with PPi and their tissue images. C, D) Interaction between **51-Zn**$_2$ and ADP; **52-Zn**$_2$ and PPi, and E) Structure of **53-Zn-ATP** and their interaction with pyrene and boronic units. Adapted with permission from ref. 158 Copyright © 2018 John Wiley and Sons. Adapted with permission from ref. 161 Copyright © 2023 Royal Society of Chemistry.

A distinctive near-infrared fluorescent probe **50-Zn** was obtained from dicyanomethylene-benzopyran and DPA receptor (Fig. 14B).[158] This probe showed unique variations in the NIR region of fluorescence signal for PPi, as well as a significant stokes shift with the nanoscale level detection. It provided two types of turn-off and turn-on fluorescence mechanisms. The addition of a small amount of PPi to this probe, its fluorescence has been quenched due to the increased electron density in the nitrogen atom of two DPA receptors,

Sensors & Diagnostics Accepted Manuscript

View Article Online
DOI: 10.1039/D6SD00010J

which consequently triggered the PET process. However, the excess addition of PPi to this probe, a stable **50-Zn-PPi** was formed. This resulted in a weaker bond between the phenolate oxygen atom and the two Zn^{2+} ions, leaving the negatively charged phenolate oxygen atom. It thus contributed greater electron density to the phenyl ring, which induced the ICT process subsequently enhancing the fluorescence. Further, this probe was a proof-of-concept that PPi detection *in vitro* and *in vivo* has tremendous potential for biological applications and was supplied by its capacity to demonstrate that PPi may be suitably exploited for imaging in living cells and animals.

5. 2. 12. Azulene-based fluorescence probe

The azulene fluorophore was bound with two Zn-DPA receptor motifs at positions 1 and 3 (p-phenylene and m-phenylene), which were connected with a spacer that generate **51-Zn$_2$** (Fig. 14C).[159] It exhibited a significant fluorescence response with the additions of ADP and ATP, while other anions showed only a poor response except PPi. The nucleobase–fluorophore–nucleobase π-π stacked arrangement has been hypothesized as the obtained 2:1 ratio of binding stoichiometry between ADP and **51b-Zn$_2$**. This predicted assembly can explain the comparatively inadequate response to both PPi (lack of π-πstacking) and ATP (binding of triphosphate to Zn-DPA may cause the wrong coordination of purine ring for π-π stacking). These observations were confirmed by changing the p-linker to m-phenylene (to provide an isomeric probe **51b-Zn$_2$**), which eliminates the ability to distinguish between ADP and ATP.

5. 2. 13. Carbazole-based fluorescence probe

Probe **52** was designed from a 2-aminobenzamide skeleton appended to the DPA receptor and carbazole fluorophore moieties (Fig. 14D).[160] Its strong fluorescence may be quenched by the addition of Zn^{2+} ion, and yield **52-Zn**. However, the fluorescence was restored by adding PPi, and produced a sandwich structure of **52a** (carbazole at 4-position) and **52b** (carbazole at 5-position) with 48- and 43-fold fluorescence enhancements respectively. Whereas, the addition of ADP and ATP showed a slight fluorescence response (6-12 times). The binding affinities of **52a** and **52b** with Zn^{2+} were validated by theoretical and experimental methods in the absence and presence of PPi. These observed results reveal that the occurred synergistic coordination between Zn^{2+} and **52**, moreover, existing H-bonding of NH groups may play a vital role in the significant detection of PPi.

5. 2. 14. Cage-type-pyrene-based fluorescence probe

The host-guest interaction type of systems is also actively participated in this competition. In such a way, γ-cyclodextrin (γ-CyD) was encapsulated with boronic acid to form FBγCyD (**53**) (Fig. 14E).[161] Its interaction with a pyrene-attached Zn-DPA may yield **53-Zn**.

Open Access Article. Published on 10 June 2026. Downloaded on 6/10/2026 10:50:53 PM.
This article is licensed under a Creative Commons Attribution 3.0 Unported Licence.

Sensors & Diagnostics Accepted Manuscript

View Article Online
DOI: 10.1039/D6SD00010J

This supramolecular complexation was occurred between positive Zn-DPA moiety and negative species of **53** *via* electrostatic attraction in the solution. This probe has shown a remarkably enhanced fluorescence by the incorporation of ATP, while poor response with various phosphate anions including PPi. Notably, ATP bound with **53-Zn** in three ways as follows; the phosphate oxygen, ribose moiety and the adenine group were coordinated to the Zn metal centre, boron moiety, and pyrene moiety by π-π stacking respectively, in which provide a strong binding in the nanomolar detection limitations.

5. 3. Terpyridine family receptor probes

Terpyridines-based organic compounds are most important ligand system for the preparation of metal complexes, among them, Zn(II) complexes have shown distinct reactivities and peculiar behavioral changes in fluorescence studies. In this sequence, pyrene anchoring with terpyridine coordinated Zn^{2+} has been utilized to generate **54-Zn**, which showed a large bathochromic shift (>100 nm) in fluorescence spectra due to the ICT effect (Fig. 15A).[162] This probe showed green fluorescence at 542 nm, while adding PPi, it underwent blue fluorescence at 442 nm, indicating the dissociation of **54-Zn**. Instead, a non-fluorescence ability has been reported for the **55-Zn**, which was constructed with Zn^{2+}-terpyridine receptor connected coumarin instead of pyrene moiety (Fig. 15B).[163] Addition of PPi to **55-Zn** led to observe a significant 'turn on' fluorescence band at 505 nm. Moreover, the 2:1 ratio of interaction between **55-Zn** and PPi with multi-hydrogen bonds, which was confirmed by Job-plot and the obtained binding constant was 1.27×10^4 M^{-1}. Fluorescence imaging evaluations of PPi with **55-Zn** in Hi-5 cells and *C. elegans* has been efficiently accomplished. In this connection, instead of coumarin, dimethoxy phenolate was coupled with a terpyridine unit and developed the new receptor, **56-Zn** for PPi detection in aqueous media at a physiological pH gradient (Fig. 15C).[164] This probe showed 50-fold enhanced fluorescence at 502 nm when adding 10 μL of aqueous PPi solution, resulting in the formation of PPi and **56-Zn** adduct in 1:3 binding ratio was confirmed by Job's plot analysis. In this series, **57-Zn** was prepared from coumarin moiety attached to terpyridine with a spacer (Fig. 15D).[165] The role of binding between PPi/ATP/ATP and this probe plays a choice in the solvent ratios in acetonitrile-water solution. In such a way that an aq. HEPES buffer-CH_3CN (1:4, v/v) medium, **57-Zn** can bind to PPi ions even in the presence of an excess of other general anions, instead it showed a more distinct affinity with AMP/ADP compared to ATP and PPi in aq. HEPES buffer-CH_3CN (2:3, v/v) medium. These binding properties between **57-Zn** and different phosphate ions were validated by DFT calculations. Furthermore, a weak fluorescence has been observed for N,N-

Open Access Article. Published on 10 June 2026. Downloaded on 6/10/2026 10:50:53 PM.
This article is licensed under a Creative Commons Attribution 3.0 Unported Licence.

Sensors & Diagnostics Accepted Manuscript

View Article Online
DOI: 10.1039/D0SD00010J

dimethylaniline appended terpyridine with Zn^{2+} instead of coumarin to make **58-Zn** receptor (Fig. 15E).[166]

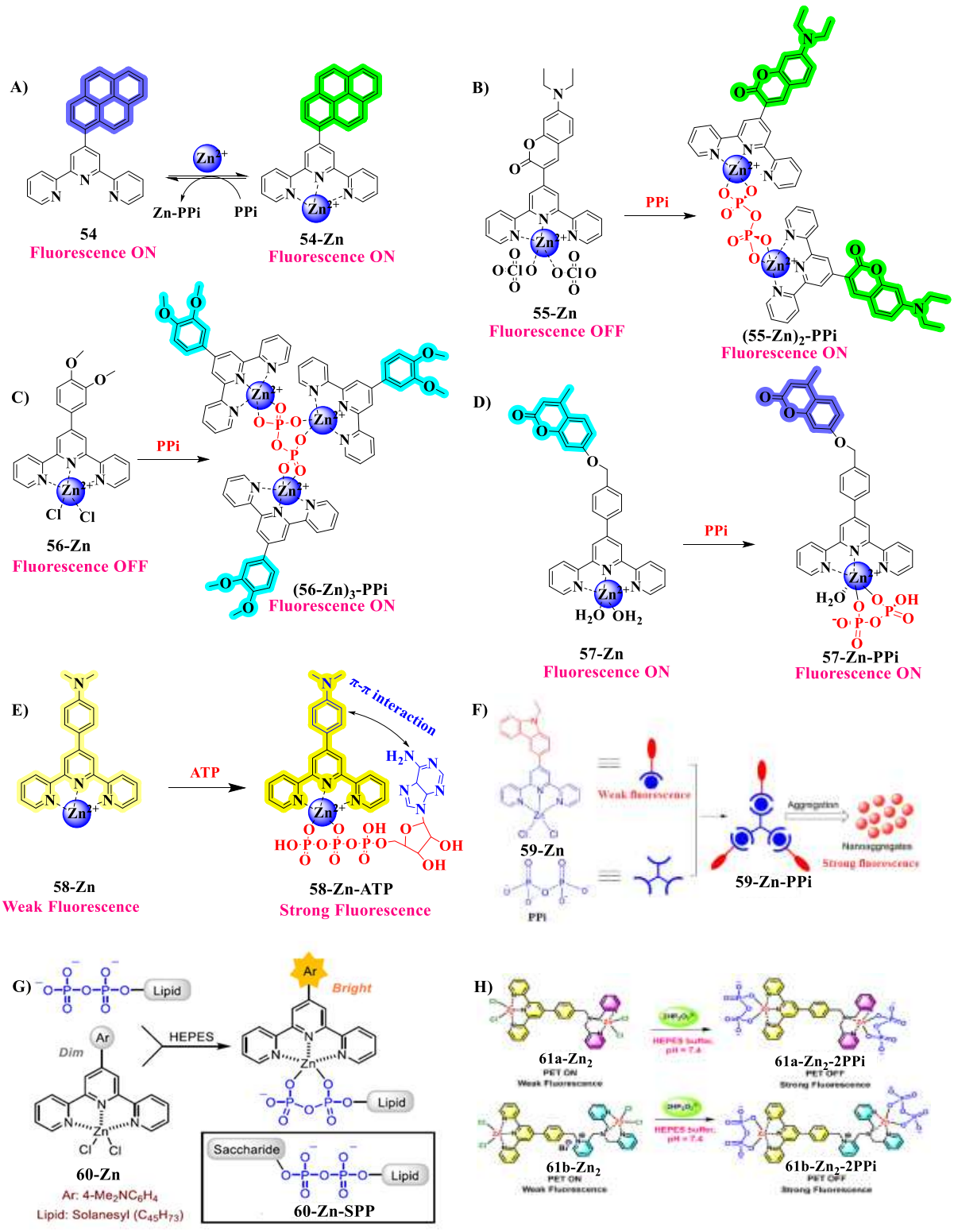

Fig. 15. Schematic representation of Zn(II) complex probes (**54-61**) with phosphate-based molecules. Adapted with permission from ref. 167 Copyright © 2016 Springer Nature. Adapted with permission from ref. 168 Copyright 2020 American Chemical Society.

Open Access Article. Published on 10 June 2026. Downloaded on 6/10/2026 10:50:53 PM.
This article is licensed under a Creative Commons Attribution 3.0 Unported Licence.

Sensors & Diagnostics Accepted Manuscript

View Article Online
DOI: 10.1039/D6SD00010J

In the presence of ATP, **58-Zn** displayed a 5-fold increase in fluorescence, which was validated by DFT calculations to be the result of a π-π interaction between the adenine moiety's ATP and **58-Zn** of aniline. Since this receptor could be able to detect ATP with very low detection limit (0.15 μM), it can also be employed to detect the same in real water samples. On the other hand, the terpyridine Zn(II) complex (**59-Zn**), was feasibly prepared from carbozole and terpyridine moiety with Zn^{2+}. It can function as a selective and effective fluorescent receptor for PPi detection (Fig. 15F)[167] When PPi was added, its weak fluorescence at 570 nm in aqueous environments has shown a green fluorescence at 515 nm as a result of anion-induced aggregation emission. Similarly, amine-functionalized terpyridine based **59-Zn** was displayed a bright fluorescence at 520 nm in the presence of PPi. The carbazole–modified and amino-modified **59-Zn** showed a detection limit of 5.37 and 9.72 nM respectively. In addition, this high affinity reported receptors towards PPi, can also be evaluated through the cell imaging studies. Another approach has been reported with a fluorescence receptor **60-Zn** prepared from 4-(dimethylamino) benzaldehyde (Ar) anchoring terpyridine was utilized for the detection of long-chain lipid pyrophosphate monoesters (SPP) (Fig. 15G).[168] Upon excitation at 375 nm, the intense band at 551 nm was suppressed with the addition of incremental concentrations of SPP. The obtained Job plot for these observed fluorescence changes have been revealed that the formation of **60-Zn**-SPP complex through a 1:1 binding stoichiometry between the **60-Zn** and SPP. Additionally, probe **61a** was established by connecting DPA and terpyridine, while probe **61b** (Fig. 15H) was formed by coupling three DPA to another pair of terpyridine.[169] These probes complexed with Zn^{2+} to produce **61-Zn**$_2$, and the job plot confirmed their 1:2 binding mode. When adding PPi, both of these probes displayed a high fluorescence by generating the respective adducts in the 1:2 binding ratio. The experiments demonstrated that both probes were biocompatible, or safe for use with living cells. Since additional research verified their efficacy in monitoring PPi levels in breast cancer cells, this opens the door for their application in disease diagnosis. In contrast to traditional molecular sensing techniques, the pincer type of terpyridine-based Zn(II) complexes was prepared from terpyridine with anchoring 2-furyl or N-dimethyl benzyl-based derivative to generate (**62a-Zn** and **62b-Zn**) upon their interaction with Zn^{2+} (Fig. 16).[170] Subsequently, these probes were investigated for gelation ability tests in organic and pure aqueous media, resulting in no gel formation in heating and cooling processes. The **62a-Zn** showed gelation formation by interacting with ATP and did not with other phosphate ions, instead only a white precipitate was observed. The intramolecular π-π stacking between the planar nucleobases of ATP and the metal-hybrid aromatic ring of the pincer complex had a significant impact on the coordinated adduct

Open Access Article. Published on 10 June 2026. Downloaded on 6/10/2026 10:50:53 PM.
This article is licensed under a Creative Commons Attribution 3.0 Unported Licence.

Sensors & Diagnostics Accepted Manuscript

View Article Online
DOI: 10.1039/D6SD00010J

geometry and potential molecular self-assembly process, even though the **62b-Zn** interaction with AMP, ADP, or ATP (2 wt%) was not entirely dissolved after heating under the same gelation process, partial gel formation was observed with the soluble portion of the sample containing ATP. Moreover, **62-Zn** has been successfully used in the possible application of ATP detection in HeLa cells because of its low cytotoxicity and ATP detectable concentration level in water, which further supports the hypothesis that ATP discrimination is conceivable.

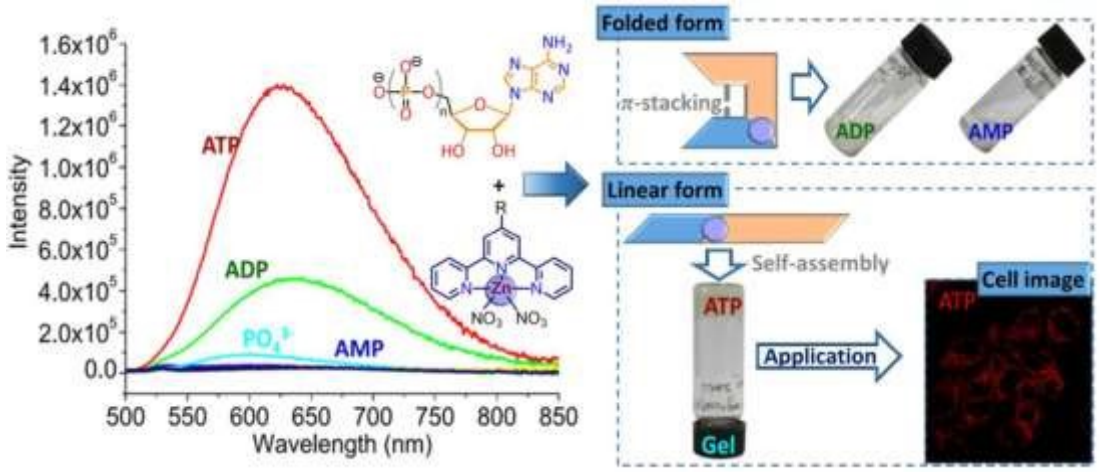

Fig. 16. Fluorescence responses of probe **62** with ATP and ADP in spectral and cell imaging studies. Adapted with permission from ref. 170 Copyright 2016 American Chemical Society.

5. 4. Duality of receptor and fluorophore-based family probes for the detection of phosphate-based biomolecules

In this competition, non-Schiff base, DPA and terpyridine based receptor families also contribute to the detection of phosphates biomolecules through duality character of fluorophore and receptor as follow below.

5. 4. 1. Anthracene-based fluorescence probes

An unexpected mono-nuclear probe **63-Zn** was designed by using two anthracene moieties connected pyridine receptor with Zn^{2+}, which showed an extraordinary selectivity for ADP (Fig. 17A), by showing its elevated fluorescence responses at 416 and 441 nm, whereas adding AMP and PPi did not show significant fluorescence enhancement, instead its fluorescence was quenched by the addition of ATP.[171] The π-π stacking interactions obtained between adenine ADP and one in the anthracene group could be generate an intense fluorescence by forming a pentacoordinate complex between the oxygen atom of one phosphate in ADP and the Zn^{2+} metal center. Likewise, the two pyridine receptors connected to anthracene in the center of the cyclic system were used to form a bimetal complex probe **64-Zn$_2$** (Fig. 17B).[172] This probe showed a stronger fluorescence enhancement with ADP, moderate fluorescence with ATP, and

Open Access Article. Published on 10 June 2026. Downloaded on 6/10/2026 10:50:53 PM.
This article is licensed under a Creative Commons Attribution 3.0 Unported Licence.

Sensors & Diagnostics Accepted Manuscript

View Article Online
DOI: 10.1039/D0SD00010J

minor response with AMP/PPi. These results reveal that the facile discrimination between ATP, ADP, AMP, and PPi anions. Interestingly, this probe showed a strong binding affinity with ATP because of π–π stacking interaction between the adenine group of ATP and the anthracene moiety. Probe **65** was subsequently established by modifying the pyridine receptor to a macrocyclic system and connecting it to two side arms with anthracene (Fig. 17C).[173] This probe first displayed a green fluorescence with Zn^{2+} ions due to the excimer emission provided by the π–π stacking of two anthracene. When ATP was added, the probe displayed a blue fluorescence because, two anthracene moieties were removed from the contact and ATP formed a sandwich between anthracene moieties.

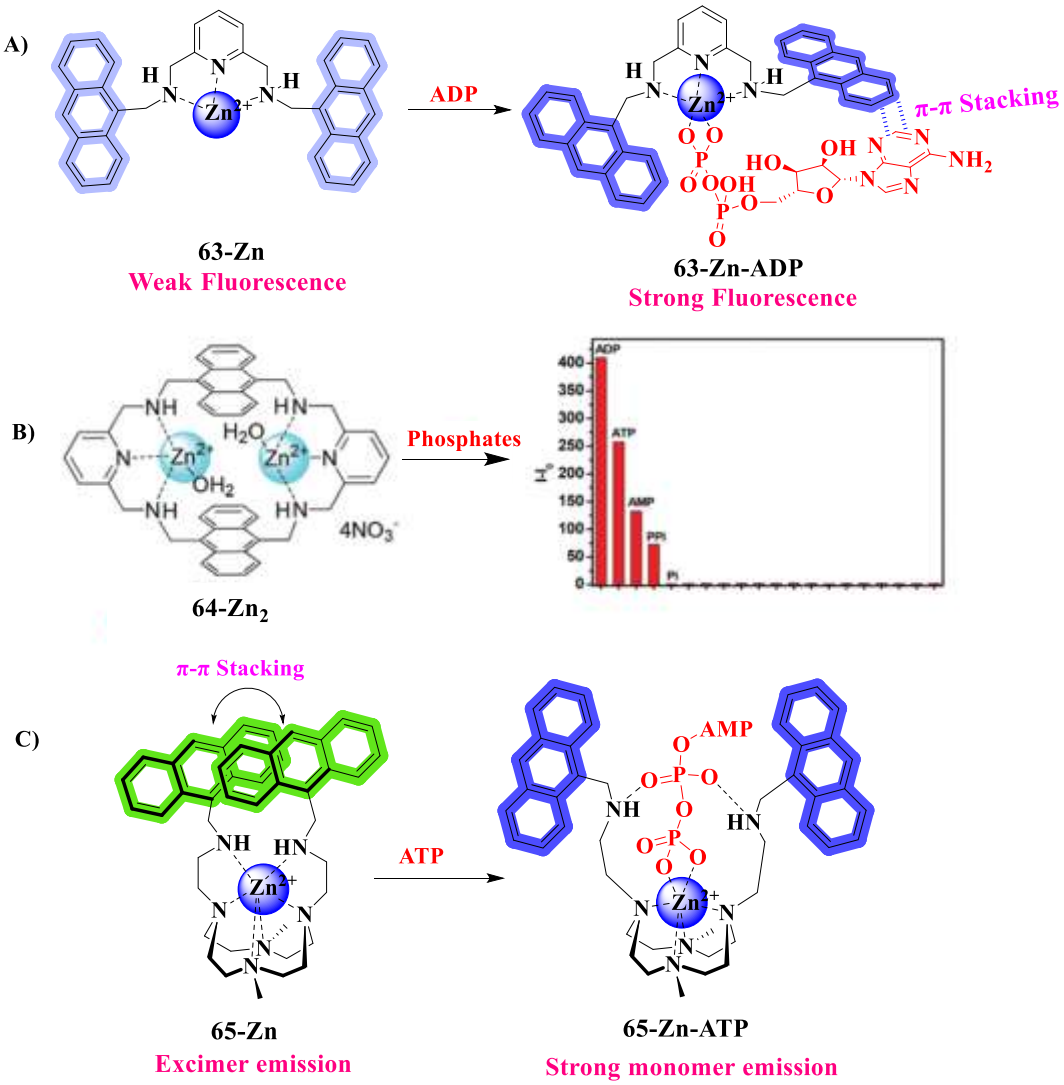

Fig. 17. The interaction between probes (**63-65 -Zn**) and ATP/ADP/AMP. Adapted with permission from ref. 172 Copyright © 2014 Royal Society of Chemistry.

5. 4. 2. Quinoline-based fluorescence probes

Quinoline derivatives act as fluorophores and chelating receptors, they have strong coordination ability with metal centres. In such way, dinuclear Zn(II) complexes were prepared

Open Access Article. Published on 10 June 2026. Downloaded on 6/10/2026 10:50:53 PM.
This article is licensed under a Creative Commons Attribution 3.0 Unported Licence.

Sensors & Diagnostics Accepted Manuscript

View Article Online
DOI: 10.1039/D6SD00010J

from 2-hydroxy-1,3-diaminopropane and quinoline derivatives (such as 2-quinoline, 8-quinoline, and isoquinoline) (Fig. 18A).[174] The 2-quinoline-based probe (**66-Zn$_2$**) showed a strong fluorescence enhancement with PPi (1 equivalent) due to the intramolecular excimer of two quinoline rings, which was suppressed by the excess addition of PPi ions. To extend this ligand architecture, 8-quinoline was modified with the methoxy group and reacted with 2-hydroxy-1,3-diaminopropane to create **67-Zn$_2$** (Fig. 18B).[175] It showed a 2-fold enhancement in intensity at 406 nm upon the addition of 0.5 equiv. of PO_4^{3-} ($\phi = 0.159$) by forming a bridged [((**67**-Zn$_2$)$_2$-μ_4-PO$_4$)]] ternary complex. The excess addition of PO_4^{3-} leads to a gradual decrement in its fluorescence intensity due to the anticipating demetallation. X-ray crystallography studies confirmed the formation of **67-Zn$_2$** and [((67-Zn$_2$)2-μ_4-PO$_4$)] and suggested a simple fluorescent molecule system through a novel approach for anion-sensing functionalities. A binuclear **68-Zn$_2$** receptor has been developed using diethylenetriamine-derived hexaazamacrocycle and two quinoline units as shown in Fig. 18C.[176] Interestingly, its weak fluorescence brought in to a strong enhancement by the addition of 1 equivalent of $HPPi^{3-}$ ion due to excited-state intramolecular charge transfer (ESICT) in the quinoline ring. Adding an excess of $HPPi^{3-}$ to this probe led to quench its fluorescence and simultaneously eliminated the Zn^{2+} ions from **68-Zn$_2$**. Although Zn^{2+} and Cd^{2+} ions bind differently, the fluorescent sensor based on a quinoline molecule can discriminate between them. Additionally, the complex generated between probe **69** and Zn^{2+} (**69-Zn**) can be employed as another sort of sensor to detect PPi and ATP (Fig. 18D).[177] Its blue fluorescence band (416 nm) was disappeared and the subsequent appearance of green fluorescence along with a remarkable red shift to 498 nm by adding Zn^{2+}. The fluorescence profile of **69-Zn** (at 498 nm) was gradually decreased (76 and 82%, respectively) when PPi and ATP were incorporated incrementally along with the remarkable blue shift to 416 nm. This probe **69-Zn** may theoretically distinguish between these two anions in this manner. The amide group's oxygen and the two nitrogen atoms (one in the amide group and one in the aromatic form) may greatly boost the capacity of quinoline unit to donate electrons. This might then obstruct the electron transfer from amide group (PET process), which would cause a remarkable shift in light absorption towards longer wavelengths (bathochromic shift) and light emission from chelation with Zn^{2+}. This was successfully observed in mung bean sprouts with little damage to the plants. Another method for relay detection of Zn^{2+} and $H_2PO_4^-$ in an aqueous solvent system has been reported using pincer-type probe **70**.[178] This dual fluorescence receptor **70** displayed a distinct fluorescence enhancement at 496 nm upon the interaction with Zn^{2+} ions (Fig. 18E). The fact that, probe **70** did not display fluorescence, might be due to the transfer of

Open Access Article. Published on 10 June 2026. Downloaded on 6/10/2026 10:50:53 PM.
This article is licensed under a Creative Commons Attribution 3.0 Unported Licence.

Sensors & Diagnostics Accepted Manuscript

View Article Online
DOI: 10.1039/D6SD00010J

an electron from the nitrogen atom to the quinoline ring moiety, coupled with PET and ESIPT process that was carried out by the involvement of keto-enol tautomerism of amide proton. Though, all three nitrogen atoms may associate with Zn^{2+} ions in the complexation of **70-Zn**, which can hinder the PET and ESIPT processes along with enhanced the CHEF effect. In order to find out its dynamic binding ability, fluorescence titration was carried out with successive addition of $H_2PO_4^-$ ions. As the concentration of $H_2PO_4^-$ increased, the emission band at 496 nm progressively began to decline, which might be due to the formation of the ternary complex, **70-Zn-$H_2PO_4^-$**.

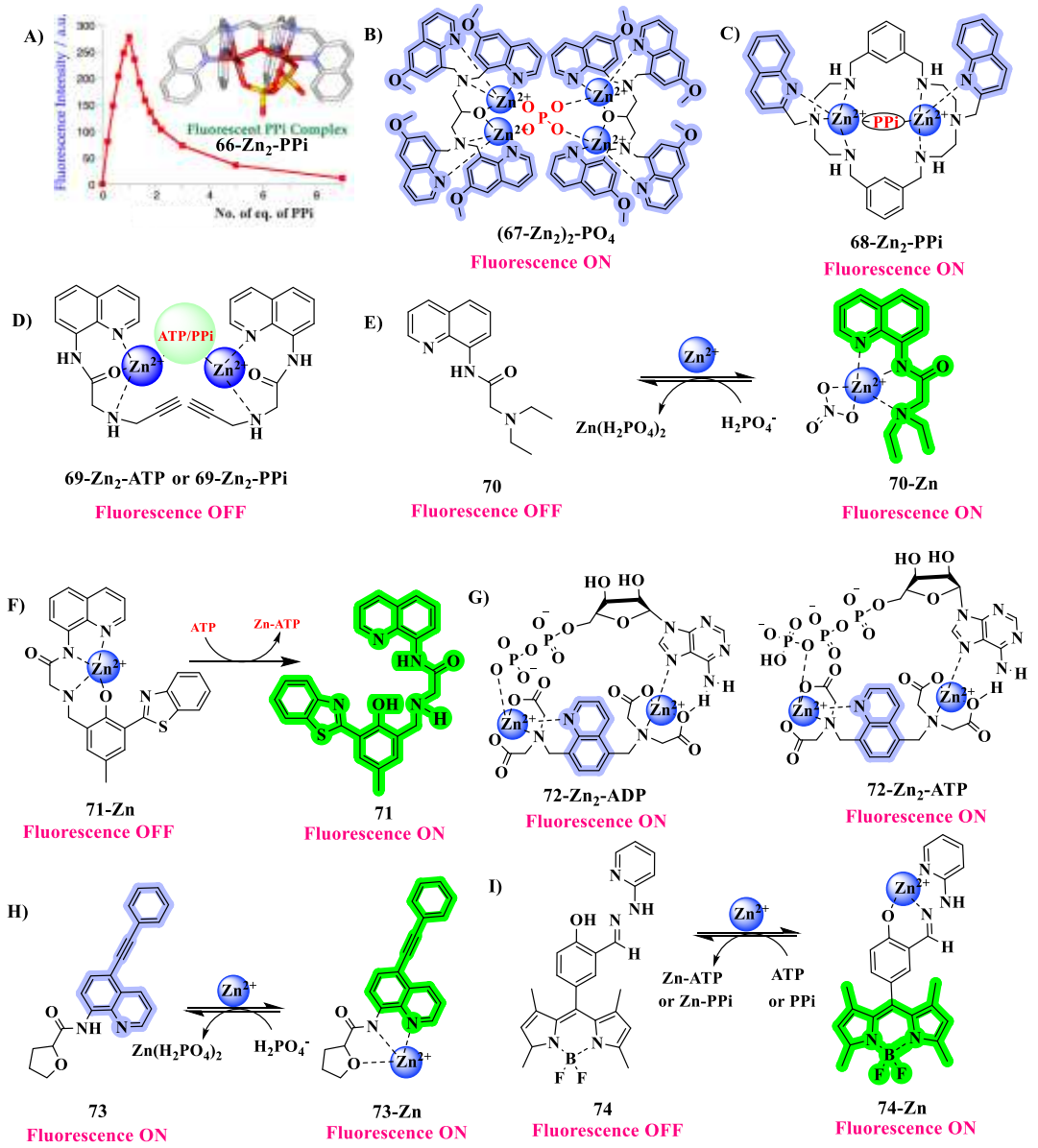

Fig. 18. The schematic representations of binding between probes (**66-74**) and phosphate-based biomolecules. Adapted with permission from ref. 174 Copyright 2013 American Chemical Society.

Open Access Article. Published on 10 June 2026. Downloaded on 6/10/2026 10:50:53 PM.
This article is licensed under a Creative Commons Attribution 3.0 Unported Licence.

Sensors & Diagnostics Accepted Manuscript

View Article Online
DOI: 10.1039/D6SD00010J

In this series, the carboxyamidoquinoline (**71**) showed strange fluorescence responses involving Zn^{2+} ions that were recovered by adding ATP, ADP, PPi, and Pi anions to the demetallation (Fig. 18F).[179] Furthermore, the detection of low levels of phosphates in biological fluids such as urine and saliva can be quantitatively measured by these studies. Another simple probe **72-Zn2** was constructed in the combination of quinoline and two sets of acid receptors, which showed a turn-on fluorescence and high selectivity with ATP and ADP biomolecules (Fig. 18G).[180] Based on the observed spectral data (^{1}H NMR, electronic, fluorescence) and DFT calculations, it most probably occurred through the supporting coordination bonds and hydrogen bond in the obtained maximal binding affinity between **72-Zn2** and ADP. The combined coordination of the N7 atom of the adenosine unit and a phosphate moiety with two Zn^{2+} ions in a 2:1 M ratio revealed the successful ADP detection. A simple ratiometric sensing probe **73** has been reported for the selective detection of Zn^{2+} and $H_2PO_4^-$ ions, based on the ICT mechanism (Fig. 18H).[181] It exhibited a strong emission band at 430 nm, indicating the incorporation of the phenylene-ethylene moiety in its ligand architecture. This band was dramatically suppressed by the addition of a slight excess of Zn^{2+} ions and the simultaneous emergence of new band at 525 nm, together with a remarkable red-shift (95 nm) due to the formation of **73-Zn**, However, which was gradually decreased upon the increamental addition of $H_2PO_4^-$, led to the appearance of the band at 430 nm indicating the regenerated probe **73**, due to the subsequent formation of new complex, $Zn(H_2PO_4)_2$ by the interaction between $H_2PO_4^-$ with Zn^{2+}ions. These observations suggest that the **73-Zn** complex is a promising candidate for use in cell imaging studies, as it may be able to diffuse through cells and be further developed as a biomaterial for probing bioactive analytes in the cellular environment through changes in fluorescence emission. A new hydrolysis-resistant BODIPY-based probe (**74-Zn**) was reported as a selective "turn-on" fluorescence sensor for PPi and ATP in aqueous media (Fig. 18I).[182] Probe **74** has moderate fluorescence, which undergoes dramatic quenching with the addition of Zn^{2+}, while only a minor spectral change was observed by the additions of Co^{2+}, Cu^{2+}, and Cd^{2+} ions. Additions of different concentrations of Zn^{2+} with **74** led to a gradual decrement in its original fluorescence and reached saturation with 1 equiv. of Zn^{2+} ions, suggested that the obtained 1:1 binding stoichiometric **74-Zn** complex. It showed a strong fluorescence with PPi and ATP, and a moderate fluorescence response was observed with ADP, but AMP did not show any fluorescence alterations. Zn-2PPi or Zn-2ATP occurs in a binary form, along with the formation of recovery compound **74**. Probe **75** was developed by a different cavity approach using quinoline moieties and exhibited a strong fluorescence at 510 nm by adding Zn^{2+}, leading to the CHEF mechanism in aqueous medium (Fig. 19).[183] Further,

Open Access Article. Published on 10 June 2026. Downloaded on 6/10/2026 10:50:53 PM.
This article is licensed under a Creative Commons Attribution 3.0 Unported Licence.

Sensors & Diagnostics Accepted Manuscript

View Article Online
DOI: 10.1039/D0SD00010J

the addition of various phosphate anions of ATP and ADP with **75-Zn** exhibited 2.5 and 1.4-fold fluorescence enhancements respectively, while additions of PPi, HPO_4^{2-} (~50%), and AMP (~20%) ions led to suppress its fluorescence intensity. Addition of ATP led to generate the corresponding emissions from the quinoline monomer and intramolecular excimer of **75-Zn** at 445 and 510 nm respectively. The idea behind this study was that the stabilization of ATP and ADP by secondary interactions between the aromatic adenosine and quinoline groups, may led to form the excimer by elevating the emission intensity. Furthermore, it has been shown that **75-Zn** may function as a biological fluid simulation agent to track the real-time hydrolysis of ATP catalyzed by apyrase.

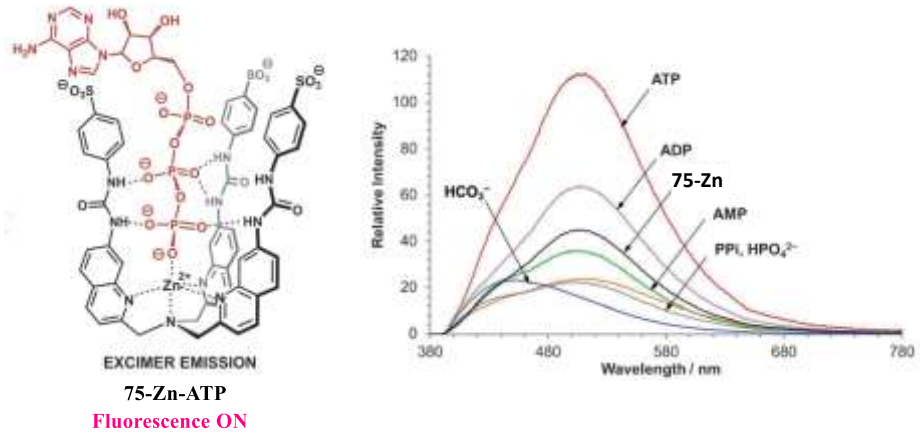

Fig. 19. Fluorescence spectra of **75-Zn** with various phosphates and bicarbonate. B) The interaction of **75-Zn** with ATP excimer formation. Adapted with permission from ref. 183 Copyright © 2014 John Wiley and Sons.

Noteworthy, tri-arm 8-hydroxyquinoline-based fluorescent receptor **76** showed a selective and ratiometric fluorescent response with Zn^{2+} and PPi ions (Fig. 20A).[184] **76-Zn$_3$** was generated by treating Zn^{2+} ions with **76** in an aqueous-organic solution, which displayed a substantially enhanced fluorescence at 491 nm. **76-Zn$_3$** have shown a strong fluorescence by its interaction with PPi and Pi ions. Moreover, **76-Zn$_3$** might be used to track Zn^{2+} ions in living cells due to its cell permeability nature. This sensor, **76-Zn$_3$**, has shown excellent fluorescence response and selectivity against PPi, suggesting that its potential utilization in analytical and biochemical applications.

5. 4. 3. Naphthalene-based fluorescence probes

A novel and water-soluble ratiometric fluorescent receptor **77-Zn** has been developed for the efficient recognition of PPi than the other phosphate-containing anions in aqueous media and blood serum at physiological pH gradients (Fig. 20B).[185] **77** was constructed with a naphthalene fluorophore that showed a weak fluorescence response to Zn^{2+} ions at 415 nm,

Open Access Article. Published on 10 June 2026. Downloaded on 6/10/2026 10:50:53 PM.
This article is licensed under a Creative Commons Attribution 3.0 Unported Licence.

Sensors & Diagnostics Accepted Manuscript

View Article Online
DOI: 10.1039/D6SD00010J

even its low concentrations (as low as 0.4 mM). On the other hand, PPi can behave as a template for its complexation-induced self-assembly with **77-Zn**. Furthermore, since no discernible changes were noticed in the UV region, the observed strong fluorescence at 415 nm might be attributed to the face-to-face position favoring the formation of an intramolecular excimer by π-π interaction, while the charge-transfer mechanism may not be anticipated at higher concentrations of PPi. Eventually, these unique results allowed us to use **77-Zn** to observe the hydrolysis of PPi through ratiometric fluorescence measurements in real-time analysis, which will be optimistic for its potential to prevent environmental disruption. Similarly, cyclam-based colorimetric probe **78-Zn** was prepared from the cyclam with (E)-4-((4-(dimethylamino)phenyl)diazenyl)benzene-1-sulfonyl group (Fig. 20C).[186] Probes **78** and **78-Zn** showed their respective absorption bands at 422 and 453 nm respectively, with the visible color change from pale yellow to pale orange. This observed bathochromic shift from 422 nm to 453 nm for **78-Zn** was illustrated for a more feasible π-π* intercomponent charge transfer (CT) transition. Further, its binding properties with various anionic analytes have been evaluated using different spectral techniques. Among them, ATP has shown a better affinity compared to the other similar anions like cytidine triphosphate (CTP), and ADP and showed a peak at 503 nm along with the noticeable bathochromic shift (40 nm). The reversible binding of **78-Zn** with ATP was demonstrated by adding an aqueous sodium citrate to **78-Zn-ATP.** Which exhibited a restored absorption band at 463 nm responsible for probe **78-Zn**. Similarly, the systematic spectral properties of **78-Zn** or [**α-CD-78-Zn**] were verified with increasing additions of ATP in the HEPES buffer medium. The absorption around 457 nm was decreased with subsequent growth of absorption at 503 nm for **78-Zn** and it was observed along with obvious isosbestic points at 420 and 466 nm, and [**α-CD-78-Zn**] has shown a band at 499 nm with an isosbestic point at 468 nm. The color change observed when **78-Zn** and [**α-CD-78-Zn**] bind to ATP suggests that they could be useful for staining live eukaryotic (Yeast) and prokaryotic (bacterial) cells. This is because these microbes likely produce ATP on their cell surfaces during metabolism, allowing us to monitor their growth dynamics based on this color change.[187]

5. 4. 4. Thiazole-based fluorescence probe

Thiazole-based fluorescent probe **79** was developed for the highly precious detection of Zn^{2+} and phosphate ions (Fig. 20D).[188] According to the anticipated ESIPT, it produces minor fluorescence responses at 382 and 535 nm, respectively, *via* the enamine and ketamine peaks of the ESIPT molecular route. However, by blocking the ESIPT, Zn^{2+} incorporation and subsequent chelation could be able to generate a stable complex with **79**. This revealed the

Open Access Article. Published on 10 June 2026. Downloaded on 6/10/2026 10:50:53 PM.
This article is licensed under a Creative Commons Attribution 3.0 Unported Licence.

Sensors & Diagnostics Accepted Manuscript

View Article Online
DOI: 10.1039/D6SD00010J

emergence of a new emission band at 460 nm with a higher quantum yield (Φ = 0.0653) compared to the low quantum yield (Φ = 0.0059) of free 79 that was obtained due to CHEF. Remarkable fluorescence quenching was observed by the addition of $HP_2O_7^{3-}$ and H_2PO_4 ions to the stable **79-Zn** complex due to their maximum affinity with Zn^{2+} ion. Interestingly, the addition of $HP_2O_7^{3-}$ and $H_2PO_4^-$ may led to diminish the band at 460 nm, followed by the restoration of bands belonging to ketamine and enamine respectively at 382 and 535 nm, due to the demetallation of Zn^{2+} from **79-Zn** and activate the ESIPT.

5. 4. 5. Imidazole and thiozole-based fluorescence probes

The ensemble probe **80** was prepared from 2,3-diamino-phenazine and 2-pyridylaldehyde, it showed a fluorescence band at 540 nm, which was switched to 600 nm by the formation of **80-Zn** due to its interaction with Zn^{2+} ions (Fig. 20E).[189] This fluorescence change has been occur due to the twisted intramolecular charge transfer (TICT) from pyridine to phenazine moiety. When, **80-Zn** interacts with $H_2PO_4^-$ ions, a stable **80-$H_2PO_4^-$** complex is formed, which restores the fluorescence band at 540 nm for **80** free. Another pyridine-based set of hydroxide-bridged Zn^{2+} complexes (**81**) provide cavity-based synthetic scaffold probes for the detection of biomolecules (Fig. 20F)[190]. The five analogs that have Zn^{2+} atoms coupled with phosphate groups as arene sites for the detection of adenine fragments, and hydrogen bonds to govern the cavity structure for the selective recognition of ATP. The cavity angles for probes **81b-e** coordinated with Zn^{2+} were found to be 117º, 90º, 83º, and 125º respectively. The cavity angle in **81b-Zn_2** was reduced to **81c** and **81d** with Zn^{2+} ions, which showed 90º and 83º with the H-bond acceptor from the heterocyclic ring and the H-donor from the protonated heterocyclic ring, and resulted in the cavity being locked. In contrast, the probe **81e-Zn_2** was further supported to the H-bond donor and the acceptor does not exist and shows a large cavity angle of 125º. The cavity-based **81-Zn_2** receptor has exhibited a fluorescence band at 510 nm in HEPES buffer solution containing DMSO-water (9:1) mixture. ATP treated with **81a-Zn_2** and **81b-Zn_2** caused to exhibit a 6-fold fluorescence enhancement, whereas other phosphates (ADP, AMP, PPi) did not show any fluorescence changes. However, the addition of phosphates (like ATP) did not significantly alter the fluorescence of **81d** and **81e** with Zn-based probes; the detection was in good agreement with the acquired binding experiments, which included binding constants and cell imaging investigations.

Open Access Article. Published on 10 June 2026. Downloaded on 6/10/2026 10:50:53 PM.
This article is licensed under a Creative Commons Attribution 3.0 Unported Licence.

Sensors & Diagnostics Accepted Manuscript

View Article Online
DOI: 10.1039/D6SD00010J

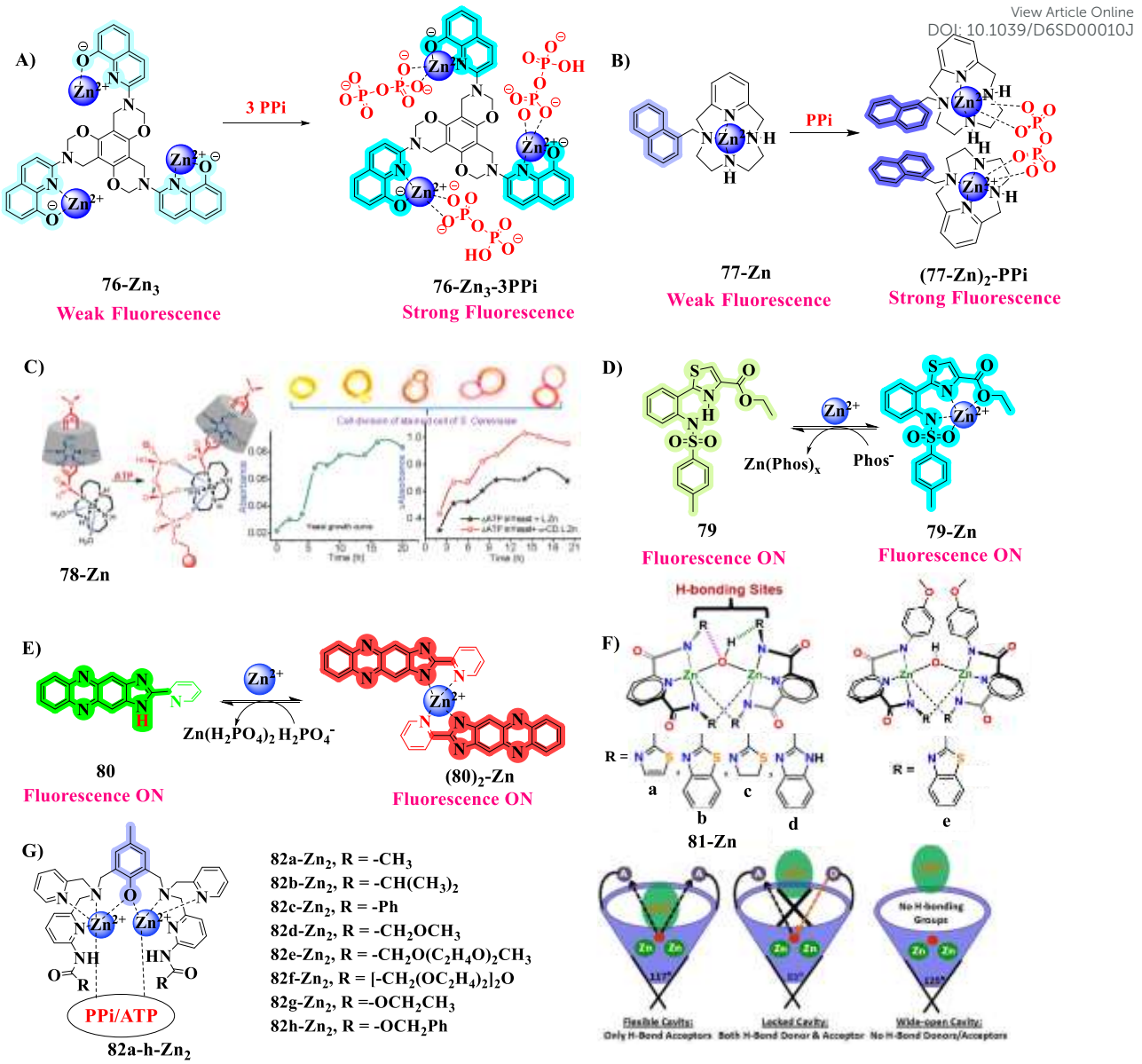

Fig. 20. A, B) The relationship between **76-Zn$_3$** with PPi ion and **77-Zn** with PPi. C) Interaction between **78-Zn** and ATP, their corresponding absorbance changes with cell division-stained cell studies. D, E) The reversible binding nature between probes (**79**, **80**) with Zn^{2+} and Pi ions, F) The designed concept and recognition of ATP by **81-Zn$_2$** in H-bonding donor and acceptor mechanism and G) Probe **82-Zn$_2$** modified with various structural changes and studied PPi and ATP binding properties. Adapted with permission from ref. 186 Copyright 2011 American Chemical Society. Adapted with permission from ref. 190 Copyright © 2019 Royal Society of Chemistry.

The bis(Zn-DPA) complex has implanted in the 6-position of dipicolylamine (DPA) based on amide moiety containing probe **82(a-i)** has been developed for the selective detection of PPi ions (Fig. 20G).[191] Its binding with guest molecules containing PPi ion may be impacted

Open Access Article. Published on 10 June 2026. Downloaded on 6/10/2026 10:50:53 PM.
This article is licensed under a Creative Commons Attribution 3.0 Unported Licence.

Sensors & Diagnostics Accepted Manuscript

View Article Online
DOI: 10.1039/D6SD00010J

both thermodynamically and kinetically by the different substituents on the 6-position of DPA in **82a-Zn$_2$** complex. When receptor, **82c-g-Zn$_2$** were added to the adducts **82aZn$_2$-PPi** or **82a-ATP**, their respective fluorescence intensities were decreased. This indicates that the receptors **82c-g-Zn$_2$** could be able to reduce the amount of bound PPi or ATP from their respective complexes, which would allow for a possible exchange of guest PPi towards **82c-g-Zn$_2$** because of their higher affinity than **82a-Zn$_2$**. Especially, the association constants of **82c-Zn$_2$** and **82g-Zn$_2$**-PPi were preferentially enhanced, indicating that the introduction of steric hindrance into a receptor molecule may influence the selectivity towards PPi, other receptors have also demonstrated comparable association constants. Furthermore, **82h-Zn$_2$** and **82i-Zn$_2$** extended their structural motifs by the addition of α-alkoxyacetyl substituents, which showed a stronger affinity with PPi than other probes. Amongst, **82h-Zn$_2$** demonstrated a selective recognition of PPi over ATP, due to their structural construction with anionic guests, which is efficient due to their preferred orientation of the lone pair of electrons on the SP^3-hybridized oxygen atoms. These findings implied that steric effects would be primarily responsible for selectivity, with the acidity of hydrogen bond donors perhaps having very little effect.

5. 5. Pyridine and phenol-based receptors for the detection of phosphate-based biomolecules by colorimetrically

Another chromophore, 7-nitrobenz-2-oxa-1,3-diazole (NBD) bridged dinuclear Zn^{2+} complex, **83-Zn$_2$** has been identified as sensor due to its long wavelength absorption (~500 nm), which facilitated the colorimetric detection of PPi even in the presence of a large quantity of ATP and inorganic phosphate ions, which also yield a suitable way to access pyrophosphatase in real samples, while it could not be able to recognize inorganic phosphates (Fig. 21A).[192] A remarkable color change from pink to purple was observed only with its interaction towards PPi, may be due to the strong complexation and the consequent formation of **83-Zn$_2$-PPi** complex.

Open Access Article. Published on 10 June 2026. Downloaded on 6/10/2026 10:50:53 PM.
This article is licensed under a Creative Commons Attribution 3.0 Unported Licence.

Sensors & Diagnostics Accepted Manuscript

View Article Online
DOI: 10.1039/D6SD00010J

Open Access Article. Published on 10 June 2026. Downloaded on 6/10/2026 10:50:53 PM.
This article is licensed under a Creative Commons Attribution 3.0 Unported Licence.

Sensors & Diagnostics Accepted Manuscript

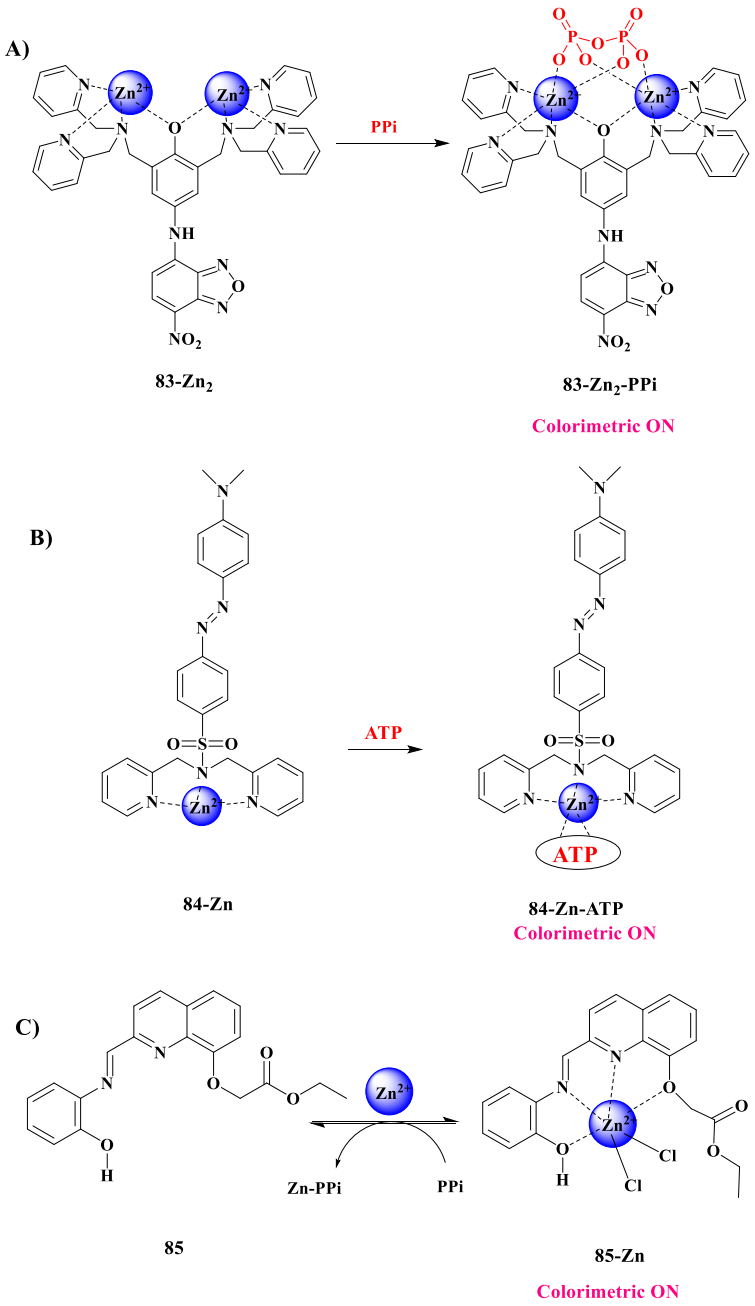

Fig. 21. Colorimetric changes occurred by the interaction between probes (**83-85**) and phosphates anions.

A simple chromogenic probe **84-Zn** has been designed and established in order to study its interactions with important bio-phosphates such as ATP in aqueous media (Fig. 21B).[193] Its emission was significantly suppressed as soon as ATP was added to **84-Zn**, and the reaction solution instantly became pink from pale yellow because of the excitation that formed at 463 nm. While, other phosphates did not cause any spectral changes, even at higher concentrations, except ADP, which displayed a much smaller redshift (8 nm). The observed downfield shift on ^{31}P signal for the phosphorous atoms exists in the ATP due to its strong interaction with **84-Zn**. This shift was more prominent for the γ and *β*-phosphorous atoms, while the α-

View Article Online
DOI: 10.1039/D5SD00010J

phosphorous atom underwent a small chemical shift (δ). So, the observed ^{31}P NMR spectral data has also employed to confirm the obtained binding affinity order as; ATP > ADP >> AMP. Most probably, the anticipated stronger electrostatic interaction between **84-Zn** and ATP may essential for the obtained effective binding of **84-Zn-O** (phosphate). As a consequence, the observed **84-Zn** binding order of ATP > ADP >> AMP may be explained by differing the numbers of anionic charges on phosphate species. The existing pyrimidone functionality in CTP caused for its weaker electron donor, which is reflected in the obtained lower binding constant compared to the ATP. Though, as a triphosphate, it efficiently bound to **84-Zn**, as compared to ADP and AMP. The obtained maximum selectivity against ATP and the appeared visual colour change on binding with **84-Zn**, it could be employed as reagent for the staining of living yeast cells and allowed to detect under normal light microscopy. A naked-eye detection of PPi using simple probe **85-Zn** was prepared from Schiff base formation between aminophenol and quinoline derivative with Zn^{2+} (Fig. 21C).[194] Its absorbance band at 504 nm, which was suppressed by the addition of PPi due to the coordination of PPi with Zn^{2+} and **85** was restored.

6. Detection of amino acids using Zn(II) complexes

6. 1. Salen-type receptor probes

The salen type of probe **86** was designed from anthracene-9-carboxaldehyde and 4-amino-5-phenyl-4H-1,2,4-triazole-3-thiol.[195] Its weak emission displayed at 456 nm with a quantum yield value of 0.008, exhibiting aggregation-induced enhanced emission (AIEE) between water and ethanol from 3 to 97%, resulting in a fluorescence band being moved from 456 to 470 nm due to the PET on-off process (Fig. 22A). This probe has shown a green fluorescence with Zn^{2+} ion and led to form **86-Zn** complex in the 2:1 ratio. Furthermore, **86-Zn** interaction was cleaved by Tyr, resulting in a turn-off fluorescence response and forming a **Zn-Tyr** complex. According to the obtained Job plot, HR-MS, ^{1}H-NMR, and DFT investigations, the 2:1 and 1:1 stoichiometry convincingly supported the binding mechanism between **86**, Zn^{2+}, and Tyr respectively. Additionally, by employing the current AIEE-based sensory system and its sensors in the presence of Zn^{2+} and Tyr in cellular and zebrafish imaging experiments, its potential for use in both *in vitro* and *in vivo* (using zebrafish and B16-F10 cells) scenarios in a variety of biological samples has been established (Fig. 22B).

Open Access Article. Published on 10 June 2026. Downloaded on 6/10/2026 10:50:53 PM.
This article is licensed under a Creative Commons Attribution 3.0 Unported Licence.

Sensors & Diagnostics Accepted Manuscript

View Article Online
DOI: 10.1039/D6SD00010J

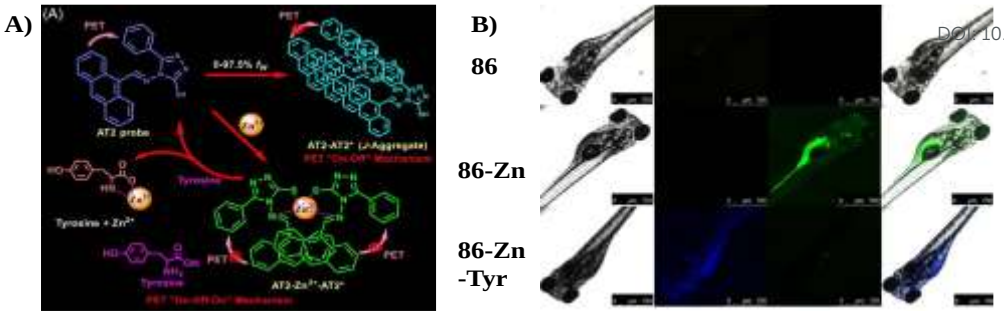

Fig. 22. A) Schematic representation of **86-86*** excimer-tuned *J*-aggregate formation and its reversibility with Tyr. B) Zebrafish images of **86**, **86-Zn**, and **86-Zn** with Tyr. Adapted with permission from ref. 195 Copyright © 2022 MDPI.

A significant fluorescent enhancement at λ = 655 nm has been observed by the interaction between D-methionine (D-Met, 100 equiv.) and the ensemble probe **87(R)-Zn**, upon the excitation at 420 nm (Fig. 23A).[196] Similarly, L-Met also displayed a fluorescence at 655 nm, but its emission is significantly lower than D-Met. The solution containing a 1:9 ratio of mixture of **87**(R) and **87a**(S) was gradually changed from green to red during the increased (D-Met) from 0 to 100 %, according to the use of a mixture of **87**(R) and **87a**(S) with varying ratios in combination with $Zn(OAc)_2$ to interact with Met samples at varying percentages of D-Met under UV lamp at 365 nm. Similarly, the interaction of a 1:1 mixture of **87**(R) and (S)-1,1'-bi-2-naphthol dialdehyde **87a**(S) containing Zn^{2+} ions with various percentages (0 to 100) of His has shown noticeable colour changes from green to yellow, orange, and red respectively, which led to determine the enantiomeric content of amino acid by this the fluorescence sensor. Furthermore, asparagine, arginine, and lysine interacted with a mixture of 1:4 combinations of **87**(R) and **87a** (S) and $Zn(OAc)_2$ at different enantiomeric compositions and induced some significant color changes. In such a way, pair of probes can be used for the first time to detect two enantiomers of a chiral amino acid simultaneously at two distinct wavelengths (Δ = 150 nm). Provided, if the enantiomers of such substrates are exist, the unique color shift of this sensor system could be used to visually quantify the enantiomeric composition. Additionally, a new and universal method for developing fluorescent probes for the quantitative visual identification of chiral compounds was established by this technology. In the continuation of (S)-1,1'-bi-2-naphthol dialdehyde, (S)-BINOL was converted into the MOM-protected dialdehyde as probe **88**(S) and it is utilized for the detection of Ser (Fig. 23B) in the presence of Zn^{2+} ions using HEPES buffer at physiological pH gradient.[197] The observed very weak fluorescence response for the interaction between **88**(S) and 2 equiv. of Zn^{2+} ions have been displayed a notable fluorescence by the addition of 20 equiv. of L-Ser. On the other hand, if D-

Open Access Article. Published on 10 June 2026. Downloaded on 6/10/2026 10:50:53 PM.
This article is licensed under a Creative Commons Attribution 3.0 Unported Licence.

Sensors & Diagnostics Accepted Manuscript

View Article Online
DOI: 10.1039/D0SD00010J

Ser was treated with **88**(S)-Zn^{2+}, it exhibited a strong fluorescence response at 550 nm. In such a way, D-Ser has experienced a great enhancement in its fluorescence with **88**(*R*), but L-Ser caused only a much minor fluorescence response. Such mirror image association has confirmed the observed enantioselective recognition in their fluorescence responses. Further, this probe showed an enantioselective fluorescent enhancement in the presence of L-Met (at 523 nm), L-Phe (at 520 nm), L-Leu (at 510 nm), and L-Thr (at 516 nm). These observations clearly demonstrated that this sensor system could be able to discriminate the structurally different chiral amino acids in an enantioselective manner.

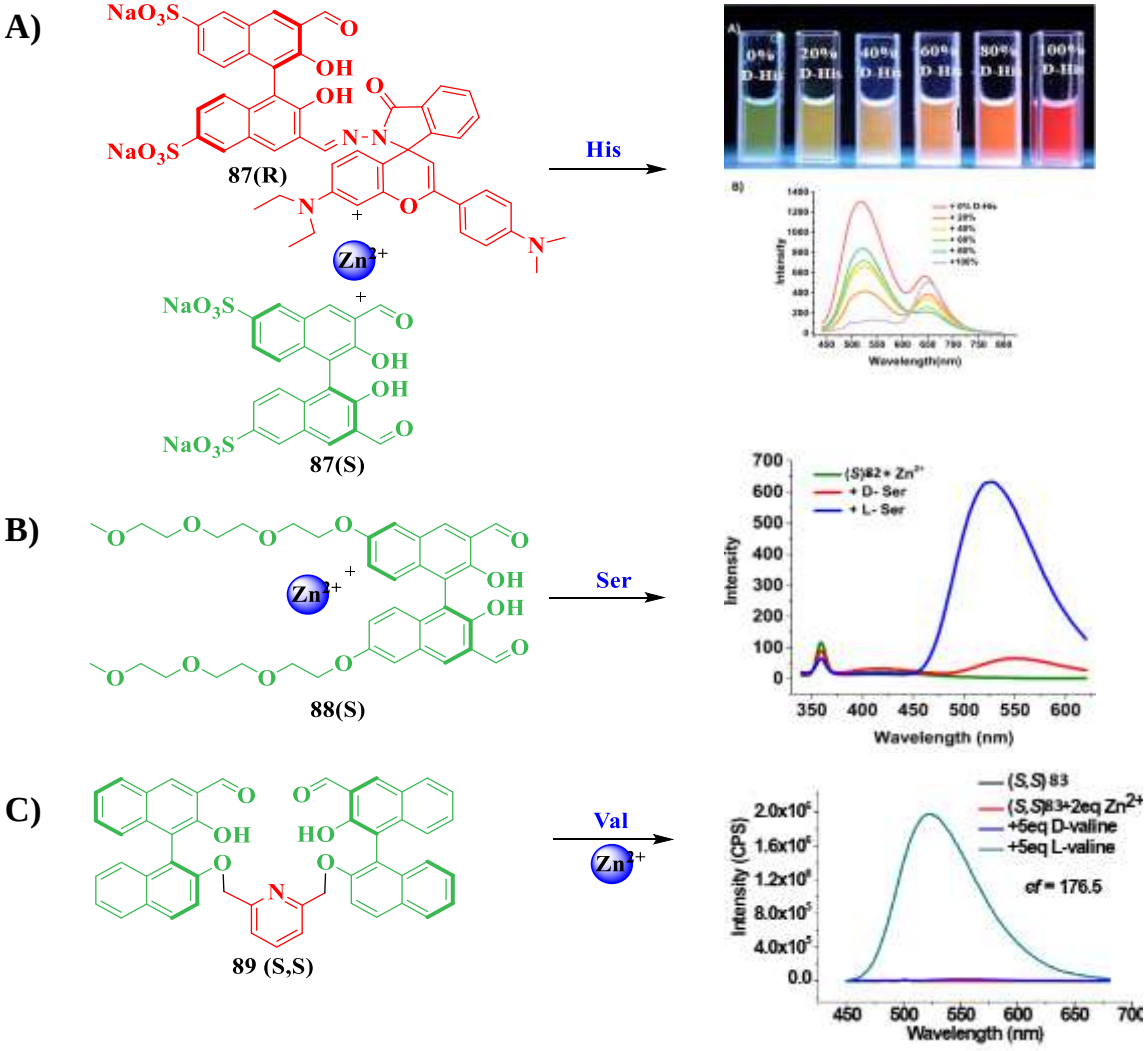

Fig. 23. The interaction of probes and excess of Zn^{2+} with isomers of His (A), Ser (B), and Val (C) to exhibit the corresponding fluorescence spectrum independently. Adapted with permission from ref. 196 Copyright 2021 American Chemical Society. Adapted with permission from ref. 197 Copyright © 2018 John Wiley and Sons. Adapted with permission from ref. 198 Copyright 2019 American Chemical Society.

Open Access Article. Published on 10 June 2026. Downloaded on 6/10/2026 10:50:53 PM.
This article is licensed under a Creative Commons Attribution 3.0 Unported Licence.

Sensors & Diagnostics Accepted Manuscript

View Article Online
DOI: 10.1039/D6SD00010J

In addition, probe **89**(S,S) consists of two chiral BINOL aldehydes linked with a pyridine unit. It could be able to discriminatively exhibited an excellent enantioselective fluorescence response towards 13 common chiral amino acids after its conjugation with Zn^{2+} ions (Fig. 23C).[198] The new bisBINOL based probe **89**(S,S) can interact with Zn^{2+} ions and showed a little fluorescence response. Upon addition of L-Val (10 equiv.) one of the two enantiomers of Val exhibited a remarkable fluorescence enhancement at 522 nm and stable after 3 h, whereas only a poor fluorescence change was attained with D-Val instead of L-Val under the same experimental conditions and which was saturated after 5h. These results displayed that the interaction between the probe **89**(SS) and L-enantiomers of these tested amino acids might dramatically increase the fluorescence response around 500 nm, while the D-enantiomers were unable to do so. In this regard, it showed a very high enantiomeric fluorescent enhancement ratio only when it [**89(SS)**] interacted with a few specific amino acids that showed on-off enantioselectivity, like Val, Ala, Met, Phe, and Leu. If it comes to the fluorescence detection of free amino acids, the observed high enantioselectivity and the range of substrates are unique. Additionally, this fluorescent probe can be used to determine the enantiomeric composition of structurally diverse chiral amino acids. NMR and mass spectroscopic techniques were also used to examine the interaction probe and tested amino acids.

6. 2. Terpyridine-based receptor probes

L-His can be detected by some novel fluorescent sensors (**90a,b**), they have been designed and developed based on crown ether terpyridine (Tpy) complexed with Zn^{2+} ion even in the presence of Cys and other amino acids (Fig. 24A).[199] Additionally, they could be able to differentiate His from other imidazole derivatives. There was no fluorescence responses observed when terpyridine (Tpy) interacted with Zn^{2+} in response to different amino acids. Thus, 1,1'-bi-naphthol-Tpy molecules has been introduced to this ligand architecture to enhance the interaction between Zn-Tpy and amino acids. Among these probes, **90a-Zn_2** did not exhibit any notable alterations with different amino acids. Which motivated the authors develop another probe which can led fluorescence response with amino acids, in this regard, **90a** receptor has been modified with crown ether, consequently they have developed **90b** and it has been constantly treated with various amino acids, Though, none of the other amino acids have demonstrated the formation of such a product under comparable experimental conditions. The formation of **90b-Zn_2-His** adduct as a white precipitate by the interaction between **90b-Zn_2** and **His**, suggested that the probe **90b-Zn_2** could be performed as a highly selective

Open Access Article. Published on 10 June 2026. Downloaded on 6/10/2026 10:50:53 PM.
This article is licensed under a Creative Commons Attribution 3.0 Unported Licence.

Sensors & Diagnostics Accepted Manuscript

View Article Online
DOI: 10.1039/D3SD00010J

fluorescence sensor for L-His. Furthermore, it has been found that imidazole and its 2-methyl or N-methyl derivatives, as well as O- and N-protected histidine, were unable to induce any fluorescence signal in the **90b-Zn$_2$** complex. Consequently, the interaction between the whole histidine molecule and the complex has only been detected by the fluorescent sensor and the imidazole ring of the substrate.

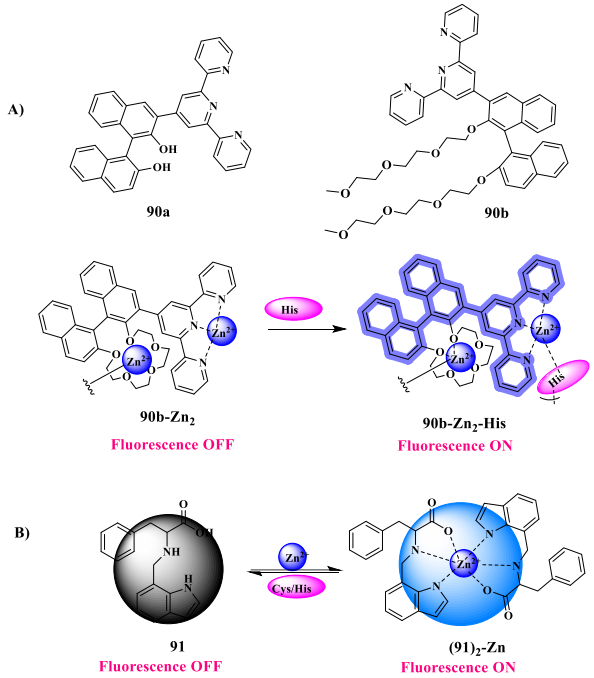

Fig. 24. The interaction between probes and His/Cys amino acids.

Besides this approach, phenylalanine derivative connected with an indole moiety-based fluorescent probe **91** have shown a selective and sensitive detection ability towards Zn^{2+} and Cys/His among the other amino acids in tandem (Fig. 24B).[200] This probe **91** has shown an enhanced fluorescence with the addition of Zn^{2+} and their binding stoichiometry was found to be 2:1. The observed fluorescence intensity of **91-Zn** was significantly altered by adjusting the pH gradients. It displayed an insufficient fluorescence response at pH 6, due to the simple protonation of **91**. Furthermore, it underwent hydroxylation (-OH) at a pH value of greater than 11, which hindered the formation of the complex with Zn^{2+} ions as **91-Zn** complex; instead, Zn^{2+}-hydroxide complex has been generated, which reduced the fluorescence response. Interestingly, receptor **91-Zn** displayed a good "On-Off" fluorescence flexibility in the pH range between 3 - 9. When Cys/His was added to the **91-Zn** complex, the fluorescence band was gradually decreased, until the amount of Cys/His was equal to that of **91-Zn**, which may cause for the demetallation of Zn^{2+} ions and subsequently coordinated with Cys and His respectively. Furthermore, **91** and **91-Zn** did not exhibit any cytotoxicity in HeLa cells, while

Open Access Article. Published on 10 June 2026. Downloaded on 6/10/2026 10:50:53 PM.
This article is licensed under a Creative Commons Attribution 3.0 Unported Licence.

Sensors & Diagnostics Accepted Manuscript

View Article Online
DOI: 10.1039/D5SD00010J

exhibiting good biocompatibility and cell membrane permeability. Fluorescence imaging analysis have been carried out for the significant detection of Zn^{2+} and Cys/His in HeLa cells by **91**. This implies that the phenylalanine-based chemosensor has a lot of intriguing advantages for the consecutive detection of Zn^{2+} and Cys/His in biosystems. All these observed results contribute to the development of an effective multi-target fluorescence receptor with conceivable applications in the biological and medical domains by offering hints.

6.3. Detection of sulphide, nitrate and nitric oxide ions using Zn(II) complexes

6.3. 1. Phenol-based fluorescence and receptor probes

Salen-type of Zn^{2+} complexes as a fluorescent probe, **92** have been developed for the recognition of H_2S and its hydrosulfide (HS^-) on their binding at Zn centre by flowing H_2S gas (Fig. 25A).[201] These substituted complexes of **92a–d** have shown their respective absorption spectra after flowing HS^-, leading to attain significant shifts in their visible and UV regions corresponding to metal-ligand charge transfer transitions (MLCT). The ICT effect of the electron-donating amines / electron-accepting cyanine pairs caused to the fluorescence quenching of complex **92c** with HS^-, while the other complexes demonstrated significant enhancement in their respective fluorescence responses with HS^-. When H_2S gas was directly exposed to the powder sample of complex **92d**, caused a color change from dark purple to bright orange. The ^1H NMR spectrum of the free complex in DMSO-d_6 solution, obtained after bubbling H_2S gas in the NMR tube, displayed the signals of both free complex **92d-Zn** and simple **92d** as free ligand, brief the mechanistic pathway occurred when complex **92d** was exposed in an H_2S atmosphere. This finding implies that the displacement of zinc center from the **92d-Zn** by the flowing H_2S gas might have happened in a different way from the result of the interaction between **92d-Zn** and HS^-. These results obtained from bioimaging investigations, revealed the possibility of utilizing all of these complex probes to detect H_2S in live cells (HepG2). In order to selectively recognize Zn^{2+} ions, a simple water-soluble hydrazone-based receptor as **93-Zn** complex was developed with a set of O_2N donor architecture, which exhibited a distinguished fluorescence enhancements with the cation. It also has the potential to function as an S^{2-} ion reversible on-off sensor (Fig. 25B).[202] It displayed a weak fluorescence at 450 nm, while the coordination of Zn^{2+} ions caused to obtain an intense emissive band at 440 nm. This intensive emission might be quenched with the selective addition of S^{2-} anion, while other anions did not show any impact. The fluorescence intensity of **93-Zn**-S^{2-} was roughly restored to the original emission of **93**, which strongly confirmed the displacement Zn^{2+} from the **93-Zn** complex by the addition of S^{2-}. The recognition of this cation

Open Access Article. Published on 10 June 2026. Downloaded on 6/10/2026 10:50:53 PM.
This article is licensed under a Creative Commons Attribution 3.0 Unported Licence.

Sensors & Diagnostics Accepted Manuscript

View Article Online
DOI: 10.1039/D6SD00010J

and anion by this probe **93** was thoroughly studied by using UV-vis, ^{1}H NMR, ESI-MS, time-resolved fluorescence, and DFT calculations. Moreover, this probe **93** has exhibited extremely low toxicity to normal cells. Therefore, its sensitive and selective off-on-off sensing system towards Zn^{2+} and S^{2-} ions was also assessed in cell imaging studies using living mitochondrial cells under physiological circumstances. Likewise, a multiple targeted of (E)-5-((4-(diethylamino)-2-hydroxybenzyldene)amino)-1H-imidazole-4-carboxamide as probe **94** has been designed and developed for the fluorometric and colorimetric detections of Zn^{2+} / S^{2-} ions and $Fe^{3+/2+}$ ions respectively in aqueous media (Fig. 25C).[203] This receptor **94** has displayed a very weak fluorescence response at 484 nm when it excited at 420 nm. Upon the incorporation of Zn^{2+} ions exhibited an instant and significant alterations in its fluorescence intensity among the 21 equivalents of various cations. The gradual increasing additions of S^{2-} ions caused to decrease in its fluorescence intensity and reached the saturation level after 34 equivalent additions of S^{2-} towards **94**. During the additions, the absorbance bands at 300 and 500 nm experienced a significant augmentation, whereas the band at 450 nm was dropped, which led to observe an isosbestic point at 472 nm. Diverse cations were added to evaluate the fluorescence fluctuation of **94** for Zn^{2+}. Among them, $Fe^{3+/2+}$, Co^{2+}, Cu^{2+}, and Cr^{2+} were able to quench the fluorescence response; this may observe due to their inherent fluorescence quenching properties. Interestingly, Cd^{2+} did not exhibit any interference, therefore it can understand that **94** could be successfully distinguish Cd^{2+} from Zn^{2+} ions as discussed earlier in this section. Furthermore, between pH gradients of 7 and 11, Zn^{2+} was utilized to sustain the fluorescence intensity of **94**. This non-toxic probe **94** has also been used to detect Zn^{2+} ions in living cell imaging studies using HeLa cells in real sample analysis. Interestingly, no appreciable fluorescence was observed in the cells without Zn^{2+}, instead an enhanced fluorescence was noticed only in the presence of Zn^{2+}. Additionally, after being treated with S^{2-} ions, the cell lines containing the **94–Zn** complex did not show any fluorescence. These obtained results revealed that Zn^{2+} and S^{2-} in living cells may be successively identified by **94**.

Open Access Article. Published on 10 June 2026. Downloaded on 6/10/2026 10:50:53 PM.
This article is licensed under a Creative Commons Attribution 3.0 Unported Licence.

Sensors & Diagnostics Accepted Manuscript

View Article Online
DOI: 10.1039/D6SD00010J

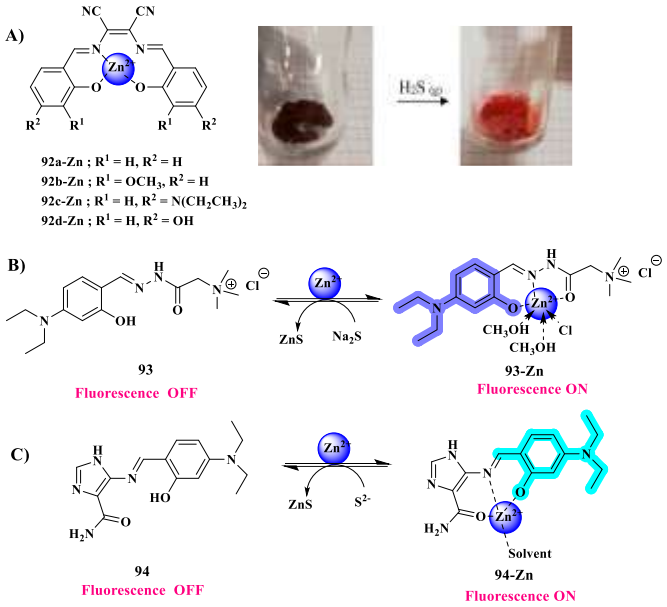

Fig. 25. A) The structures of **92a-d** with Zn^{2+} and **92d-Zn** exposed H_2S gas to form colour changes from brown to orange, and B) Probe **93** and **94** reacts with Zn^{2+} and after that reversible with the addition of S^{2-} ion. Adapted with permission from ref. 201 Copyright 2020 American Chemical Society.

6.3.2. Quinoline-based fluorescence and receptor

Quinoline-based fluorescent probe **95** was developed for the successful detection of Zn^{2+} and PPi/ S^{2-} ions (Fig. 26A).[204] Addition of Zn^{2+} ions led to a distinct 52-fold fluorescence enhancement among the other common metal ions. Such a significant fluorescence responses and distinguished color change from colorless to green upon the addition of Zn^{2+} can be attributed to the inhibition of the PET effect, which occurs when the electron-donating picolinohydrazide moiety transfers, its electrons to the electron-receptor 8-aminoquinoline moiety. Fluorescence emissions were elevated in the pH range of 7-9, while they diminished in basic (pH>10) and acidic (pH<6) conditions. S^{2-} and PPi have triggered to quench the fluorescence responses of **95-Zn**, but the other anions showed only slight alterations, as a result of competing coordination of PPi or S^{2-} with the Zn^{2+} from the **95-Zn** complex, which caused the displacement of Zn^{2+} ions from **95-Zn**, and thus **95** could activate the PET process. Probe **95** has demonstrated a higher cellular vitality (95%) at concentrations between 0 and 10 µM and around 82% at concentrations of 25 µM when administered to HepG2 cells. These results suggested that this **95** could exhibit a strong biocompatibility but no discernible cytotoxicity. Moreover, it also suggested that this quinoline-based fluorescence probe has a wide range of prospective applications for the *in vivo* detection of intracellular Zn^{2+} and PPi ions. A quinoline and morpholine-based probe **96-Zn** has been successfully synthesized with the ability to detect

Open Access Article. Published on 10 June 2026. Downloaded on 6/10/2026 10:50:53 PM.
This article is licensed under a Creative Commons Attribution 3.0 Unported Licence.

Sensors & Diagnostics Accepted Manuscript

View Article Online
DOI: 10.1039/D6SD00010J

mercury (Hg^{2+}) and HS^- (Fig. 26B).[205] Addition of Zn^{2+} to an aqueous solution of the non-fluorescent probe **96** yield an enhanced fluorescence response at 510 nm. Its fluorescence response did not undergo any significant change by treating it with Hg^{2+}. However, a quantitative fluorescence quenching to the baseline was observed for **96-Zn** by the titration of Hg^{2+} ions. The detection limit of Hg^{2+} was determined as 0.79 μM based on the obtained binding constant value. Similarly, addition of HS^- was used to monitor the fluorescence quenching of **96-Zn**, and the resulting fluorescence was rapidly recovered by adding Zn^{2+}. Once Zn^{2+} ions connected to **96**, the single pair of electrons on the amide nitrogen has no longer prevented the fluorescence of **96-Zn**. The enhanced binding strength of Hg^{2+} allows it to displace Zn^{2+} ions when it comes into contact with the **96-Zn** complex. The Hg^{2+} was coordinated to **96** as **Hg-96**, although this was not visible in the UV-vis spectra. The binding constant for Hg^{2+} ions was found to be 1.3×10^5 M, which was extremely similar to the binding constant for Zn^{2+} ions. Elimination of Zn^{2+} ions from the **96-Zn** has been occurred by its exposure with HS^- and the amide electrons were subsequently able to diminish the fluorescence of **96-Zn**. The treatment of HeLa cells to the **96**, and subsequently with Zn^{2+} exhibited an intense fluorescence due to the existing Zn^{2+}. The fluorescent cells that were subjected to about 1-10 concentrations of Hg^{2+} had declined the fluorescence, thus this probe **96** could efficiently detect Zn^{2+} ions in living cells. Instead of morpholine employed in probe **96**, and 3-morpholinopropan-1-amine has been employed to develop **97** including the quinoline moiety as water-soluble and extremely high real sample fluorescent probe in order to investigate its sequential binding to Zn^{2+} and S^{2-}ions through various spectroscopic techniques (Fig. 26C).[206] The observed weak emission for **97** in the range of 400-650 nm has been altered as an emerald-green emission at 500 nm by the incorporation of Zn^{2+} among the various other common metal ions in a 1:1 stoichiometric ratio and generated **97-Zn** complex. The ability of **97** to differentiate between the chemically similar analogies of Zn^{2+} and Cd^{2+}, which have comparable chemical properties. This emission of **97-Zn** was gradually dropped at 500 nm after the gradual and incremental addition of S^{2-}. The viability of spotting Zn^{2+} and S^{2-} in zebrafish was investigated by fluorescence imaging techniques. Following the incubation of **97** alone with zebrafish, its entire body showed only a very slight green fluorescence, while, its heart and eyes have exhibited an enhanced green fluorescence upon the incorporation of Zn^{2+} and S^{2-}, indicating that the fluorescence intensity of zebrafish heart has increased only in the presence of Zn^{2+}. Various spectroscopic methods, theoretical computations, and bioimaging applications were used to validate the sensing ability of **97** in the detections of both Zn^{2+} and S^{2-}. Similarly, quinoline-based fluorescent probe **98** was prepared and constructed for the

Open Access Article. Published on 10 June 2026. Downloaded on 6/10/2026 10:50:53 PM.
This article is licensed under a Creative Commons Attribution 3.0 Unported Licence.

Sensors & Diagnostics Accepted Manuscript

View Article Online
DOI: 10.1039/D6SD00010J

consecutive sensing of Zn^{2+} and S^{2-} (Fig. 26D).[207] The observed weak fluorescent emission of **98** (ex = 340 nm, Φ = 0.0045), was enhanced by the incorporation of Zn^{2+} with a large quantum yield (Φ = 0.0878). As similar to the receptor **97**, it can also efficiently distinguish the Zn^{2+} ion from its physical analogous of Cd^{2+}, confirming that this probe could act as an excellent discriminatory fluorescent sensor for the Zn^{2+} ion. The absorption bands observed at 250 and 350 nm responsible for **98** alone underwent gradual suppression upon the addition of Zn^{2+}, meanwhile, two new bands have been emerged at 290 and 410 nm. This complexation between Zn^{2+} and **98** was also confirmed by using ESI-MS, NMR techniques and DFT calculations. The Zn^{2+} ion can be separated from the **98-Zn** complex by adding S^{-}. This could be observed in the UV-vis spectroscopic technique, which can also be measured using ESI-MS and NMR spectroscopic techniques, none of the any other interference anions show spectral response with **98**, except S^{-} ions. These results demonstrated the superiority of **98-Zn** as a potential sulphide ion sensor. The detection limits of Zn^{2+} ion and S^{2-} were found to be 0.06 µM and 2.33 µM respectively in real water samples, these values are much higher than the suggested levels of 76.0 µM and 14.7 µM, respectively by WHO. Moreover, Zn^{2+} measurement in real water samples and imaging investigations using live zebrafish larvae both showed excellent results with **98**. To a certain extent, probe **99** of a quinoline-based derivative, has been developed as an effective fluorescence sensor for Zn^{2+} ions, which may then be able to detect the PPi and S^{2-} ions.[208] A remarkable 32-folds of fluorescence augmentation has been observed by the interaction between Zn^{2+} and this non-fluorescent receptor **99** at 506 nm with excellent selectivity in methanol-tris buffer (1/1, v/v, 10 mM, pH 7.2) due to the suppression of the PET process (Fig. 26E). ^{1}H NMR, HR-MS analysis, and DFT studies were also supported for the provided mechanistic interacting pathway of the probe **99** with Zn^{2+}. Additionally, the fluorescence imaging results obtained in HeLa cells demonstrated an appropriate level of conviction for the applications of this simplest sensor **99**, which may be established as an excellent choice for the detection of Zn^{2+} ions in biological systems.

Open Access Article. Published on 10 June 2026. Downloaded on 6/10/2026 10:50:53 PM.
This article is licensed under a Creative Commons Attribution 3.0 Unported Licence.

Sensors & Diagnostics Accepted Manuscript

View Article Online
DOI: 10.1039/D6SD00010J

Open Access Article. Published on 10 June 2026. Downloaded on 6/10/2026 10:50:53 PM.
This article is licensed under a Creative Commons Attribution 3.0 Unported Licence.

Sensors & Diagnostics Accepted Manuscript

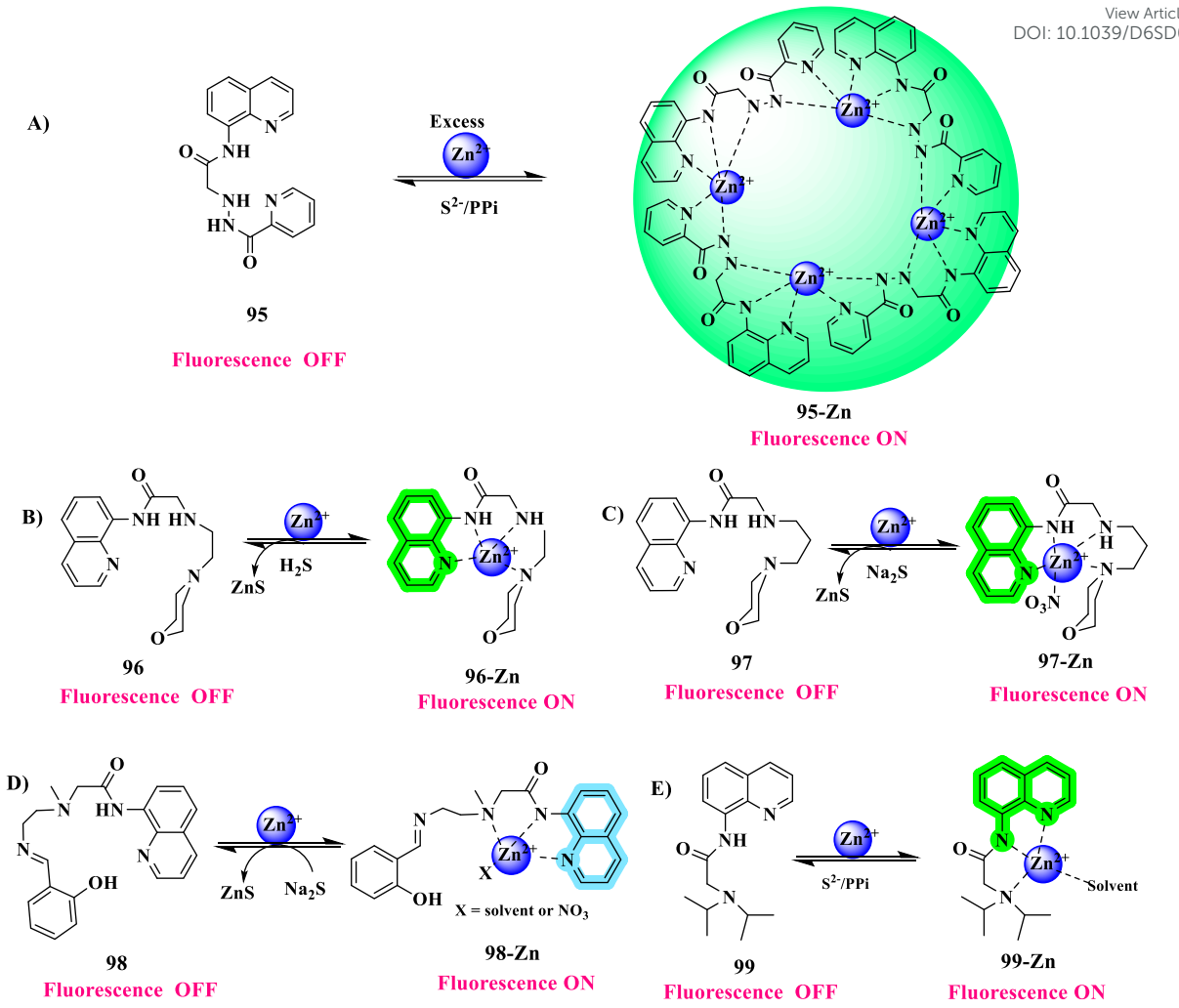

Fig. 26. The reversible interactions between the probes and S^{2-}

Another simple imidazo-pyridine-based Zn^{2+} complexes with N, O bidentate ligands as probe **100-Zn** has been constructed for the detection of HS^-/H_2S (Fig. 27A).[209] The NMR spectral technique has been adopted to examine the binding ability of HS^- at the Zn^{2+} of **100-Zn** and their prospective application as HS^- fluorescence sensors through their coordination. The interaction between HS^- and **100c-Zn** has resulted with a shift in the ^1H NMR pattern and a change in the multiplicity of the majority of the signals. The key outcome is the appearance of a high field resonance at -2.31 ppm in the NMR spectra. Similar results were also observed for the interaction between complexes **100a-Zn**, **100b-Zn** and HS^- too, in these cases the ^1H NMR spectra have shown a broad band at -3.5 ppm responsible for free HS^- due to the presence of excess NaSH. Complexes, **100a-Zn**, **100b-Zn**, and **100d-Zn** have shown their respective absorption bands in the range of 350-370 nm, while **100c-Zn** showed two medium-intense absorptions at 345 and 432 nm, may confirmed the formation of new species, and also coincide with the observed NMR spectral results. When HS^- was added, all of these complexes exhibited a similar blue shift in their lower energy bands, among them, complex **100d-Zn** displayed a

View Article Online
DOI: 10.1039/D6SD00010J

greatest variation. While, complex **100c-Zn** displayed a remarkable absorption enhancement of its intensity at 432 nm with a weak blue shift. In particular, complexes **100c-Zn** and **100d-Zn** showed a maximum fluorescence switching than their other counterparts, **100a-Zn** and **100b-Zn**. Among them, the latter has shown a slight hypsochromic emission shift. Furthermore, the acquired brightfield images of HepG2 cells demonstrated that the exposure of these complexes did not affect the morphology of the cells, indicating their minimal impact on the viability of cells. The ratiometric fluorescent probe **101** based on alizarin red S has been described as the receptor for H_2S in an aqueous buffer solution (Fig. 27B).[210] Addition of Zn^{2+} ions led to suppressed the existing band at 465 responsible for **101** along with a subsequent formation of new band at 520 nm and an isosbestic point at 465 nm suggested the formation of **101-Zn** as new species. This spectral band was disappeared by the incorporation of H_2S and restored the absorption of **101**, confirmed the occurred coordination between S^{2-} and Zn^{2+} ion, consequently left out the **101** as free ligand, which also reflected in the emission spectra. The addition of increasing concentration of Zn^{2+}ion resulted in a six-fold enhancement of its (**101**) fluorescence intensity in the orange region at 625 nm. This was primarily caused by an ICT mechanism in conjunction with CHEF. Such strong fluorescence at 625 nm of **101-Zn** underwent a sudden drop by the addition of different concentrations of H_2S, which indicated the generation of new species ZnS by displacing the Zn^{2+} ion from **101-Zn**. These results supported the viability of employing **101-Zn** as an appropriate sensor for H_2S detection in aqueous buffer solutions. However, its selectivity towards H_2S was also examined in the presence of analytes such as glutathione (GSH), cysteine (Cys), and $H_2PO_4^-$, they showed only weak emission responses due to the non-bonding interaction with Zn^{2+}center. It is determined that this **101-Zn** is appropriate for live cell imaging investigations based on their spectroscopic characteristics. Consequently, the potential of cultivated C6 cell lines for the detection of H_2S in biological cells were also investigated. Images of C6 cells were acquired after 30 minutes of incubation with compound **101**, and no fluorescent signal was noticed. Rather, the addition of Zn^{2+} ions caused a high fluorescence in the cells, which was eradicated by the addition of H_2S. It illustrated the use of probe **101-Zn** for H_2S detection in cultured cells. In light of its reversible on-off-on mode fluorescence change with H_2S and Zn^{2+}, this H_2S sensor was reusable. Additionally, fluorescent response with H_2S was used for live cell imaging. The use of sensing ensemble **101-Zn**-based fluorescence assays as an effective tool to track the release of H_2S from biological and pharmacological substances is anticipated in the future.

Open Access Article. Published on 10 June 2026. Downloaded on 6/10/2026 10:50:53 PM.
This article is licensed under a Creative Commons Attribution 3.0 Unported Licence.

Sensors & Diagnostics Accepted Manuscript

View Article Online
DOI: 10.1039/D6SD00010J

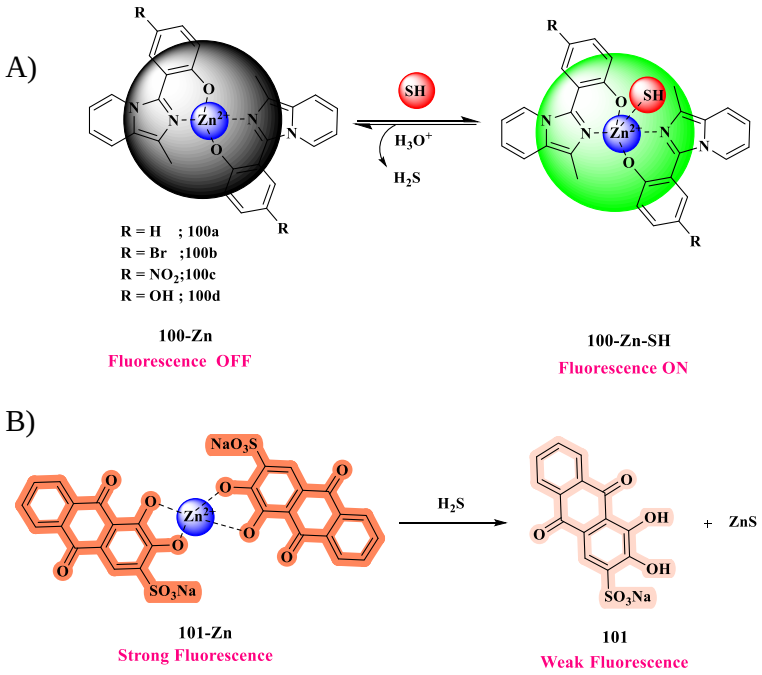

Fig. 27. The proposed interaction between probes-Zn (**100**, **101**) and H_2S ions.

7. Detection of nitric oxide using Zn (II) complexes

Fascinatingly, a novel probe **102** has been developed as an ultrasensitive receptor for the selective recognition of Zn^{2+} and NO^{2-} ions based on the control of C=N isomerization (Fig. 28A).[211] It showed three absorption bands at 325, 338, and 380 nm in acetonitrile-H_2O (9:1) HEPES buffer solution at pH 7.4, 25 °C. The increasing addition of Zn^{2+}, Cu^{2+}, and Ni^{2+} exhibited notable spectral changes among the other tested common metal ions. Among them, addition of Zn^{2+} ion led to suppressed the existing absorption bands along with the formation of a new band at 309 nm. A weak fluorescence band was observed for probe **102** (quantum yield of 0.002) while, addition of Zn^{2+} led to enhanced the fluorescence at 495 nm among other various metal ions and consequently showed an excellent off-on process, due to the inhibited C=N isomerization. The interference of **102-Zn**+Cl^- was studied with different anions, among them NO_2^- has illustrated a very significant fluorescence response at 495 nm, by displacing the existing Cl^- ion from the **102-Zn**+Cl^- complex and generated a new ternary complex, **102-Zn**+NO_2^-, which might have strongly inhibited the C=N isomerization process. The fluorophore and receptor moieties of free probe **102** have respectively shown a planar structure with a dihedral angle of about 45.99°, suggesting its flexible molecular structure due to the C=N isomerization. After its interaction with $ZnCl_2$, a relatively rigid **102-Zn^{2+}-Cl^-** ternary complex was generated, which could reduce the dihedral angle between the fluorophore and receptor as 6.87°, along with a reasonable enhanced fluorescence response due to the occurred partial inhibition of C=N isomerization. Moreover, a rigid and coplanar **102-Zn^{2+}-NO_2^-** ternary

Open Access Article. Published on 10 June 2026. Downloaded on 6/10/2026 10:50:53 PM.
This article is licensed under a Creative Commons Attribution 3.0 Unported Licence.

Sensors & Diagnostics Accepted Manuscript

View Article Online
DOI: 10.1039/D6SD00010J

complex was obtained due to the displacement of Cl^- by NO_2^-, with the dihedral angle of 1.27° indicating the acquired extreme suppression of C=N isomerization in the whole molecule. All these observed experimental results were also reflected in the theoretical calculations.

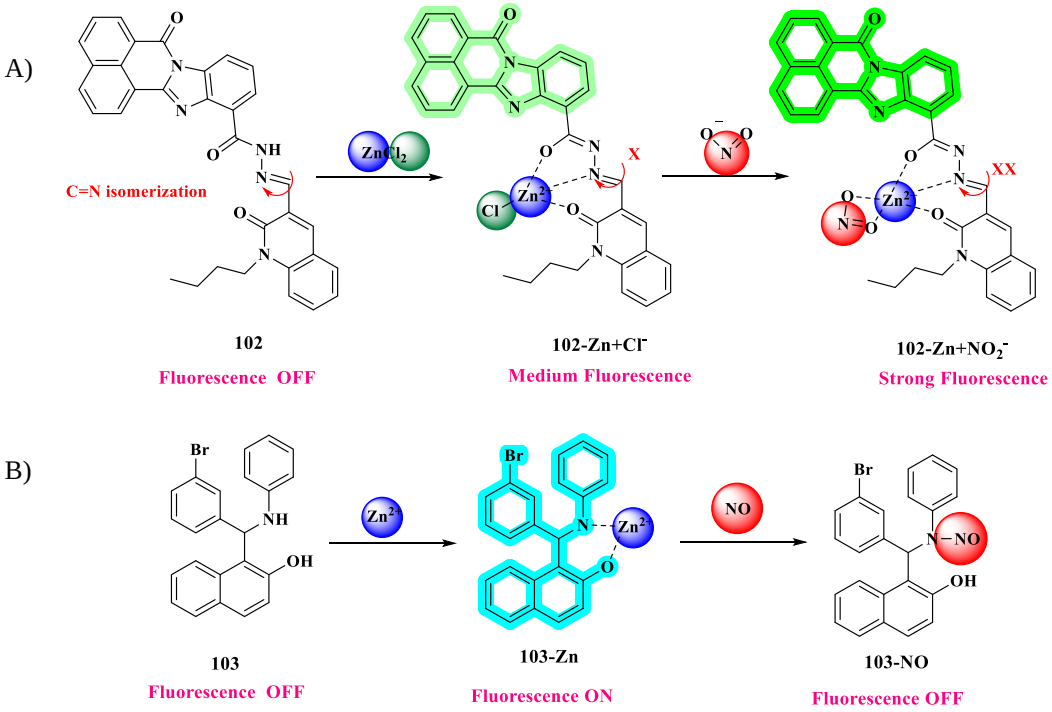

Fig. 28. The interaction of probes (**102**, **103**) with Zn^{2+} and NO^{2-} or NO ions.

Another important anion, nitric oxide (NO) has been recognized by a novel receptor **103** was constructed with aminomethylnaphthol moiety through an off-on-off behavior (Fig. 28B).[212] The addition of Zn^{2+} might trigger the previously discussed CHEF and ICT processes, and caused to observe an absorption band at 295 nm along with a minor redshift of spectral bands in the range of 220 to 230 nm. Similarly, **103** displayed an increased fluorescence response at 365 nm with the addition of Zn^{2+}. It illustrated a maximum fluorescence in the pH gradients between 4 - 9, while it showed a weak fluorescence with Zn^{2+} at alkaline pH gradients, due to the formation of Zn-hydroxide. No visible quenching was observed with the addition of various anions with **103-Zn**, and NO was the only anion that caused noticeable emission responses. These findings highlighted its particular selectivity among the vast variety of possible competing reactive oxygen and nitrogen species in the **103-Zn** solution. Further, the interaction between Zn^{2+} and probe **103** was examined using ^1H NMR spectroscopic analysis. After one to two hours of mixing, the proton signal for α-naphthol moiety (11.34 ppm) and -NH proton for amide (4.13 ppm) were disappeared. This observation suggested that the coordination of **103** with Zn^{2+} ion might be occurred via -OH and –NH groups, which confirmed its attained strong coordination with Zn^{2+} in buffer solution. The signal for the α-

Open Access Article. Published on 10 June 2026. Downloaded on 6/10/2026 10:50:53 PM.
This article is licensed under a Creative Commons Attribution 3.0 Unported Licence.

Sensors & Diagnostics Accepted Manuscript

View Article Online
DOI: 10.1039/D6SD00010J

naphthol moiety proton underwent a chemical shift from 11.34 to 10.1 ppm after **103** was treated with NO for an hour, along with the peak for the chiral C proton also shifted from 6.14 to 5.31 ppm. Further, the single peak for the amide -NH proton disappeared. These chemical changes indicated that the added NO has displaced the Zn^{2+} ion by its direct coordination through the N atom with the Zn^{2+}centre and consequently eliminated the -OH group. Subsequently, after the **103-Zn** complex was exposed to NO for two hours, the α-naphthol proton shifted from 10.1 to 8.62 ppm, and the signal peak associated with the chiral proton also shifted from 5.31 to 8.09 ppm. These spectral changes suggested that the newly developed intramolecular hydrogen bonding between the chiral proton and NO group. Moreover, the observed excellent anti-interference ability of **103** led it to be established as a bio-receptor towards the bioactive substances within the cellular system.

8. Future opportunities for optical imaging investigations

Optical molecular imaging approaches have emerged as indispensable techniques offering novel perspectives on the root cause of diseases, development of drugs, and understand the effects of therapeutic interventions by studying with small animal models. Thus, optical imaging has shown a significant influence on both fundamental and applied medical research fields. Recently, optical imaging has become a high-sensitivity technique that allows multiple imaging of several biomolecules or structures by employing various fluorophores. Since, fluorescence imaging technique does not require further processing or image reconstruction, so it provides real-time imaging compared with other existing techniques. One of the main obstacles to the use of light in medicine is its deep tissue penetration, which can range from a micron to a centimeter, depending on the wavelength.[213] Fluorescence imaging has become increasingly popular owing to its potential usefulness in preclinical technology. Only with the advent of fluorescence imaging probe technology have stronger contrast chemicals become detectable at their incredibly low (pico- to femtomolar) concentrations.[214] The brief research reports published by different research groups over the past few decades to generate new probes and proposed their interaction with biomolecules have been discussed in this overview. Especially, the chelator groups of the Schiff base, pyridyl, and DPA ligand systems may bound with Zn^{2+} ions, consequently forming their complexes, which could be utilized as receptors that have been reported in this review. Such interactions enabled various existing fluorescence processes, such as charge transfer, ICT, PET, ESIPT, and C=N isomerization.

A major challenge in detecting small biomolecules using Zn(II)-based probes is maintaining complex stability, as target biomolecules can compete for Zn(II) coordination and disrupt the probe structure. However, chelators such as terpyridine and dipicolylamine offer

Open Access Article. Published on 10 June 2026. Downloaded on 6/10/2026 10:50:53 PM.
This article is licensed under a Creative Commons Attribution 3.0 Unported Licence.

Sensors & Diagnostics Accepted Manuscript

View Article Online
DOI: 10.1039/D6SD00010J

improved stability and low detection limits. In many cases, sensing involves the formation of a more stable ternary Zn (II) complex, leading to enhanced their fluorescence response. Additionally, fluorophores play a crucial role in determining optical properties; units such as quinoline, imidazole, benzothiazole, coumarin, and BODIPY provide distinct and tunable emission consequently improving sensitivity and selectivity. It has been demonstrated that the interaction between biomolecules and probes is might be concentration-dependent system, which highlights that the significance of low-level detection. In this connection, phosphates have been detected using probes **1**, **3**, **7**, **9**, **14, 30, 50, 53, 61** and **73**, adenine-based phosphates were found with **13**, **42** and **53**; sulphide was identified with **93**, and **101** at the nanomolar level was discussed in this review. Probes **2** and **102** showed remarkable ability to detect PPi and NO_2 respectively at the picomolar level, whereas the remaining probes could detect their respective biomolecules at the micromolar level (Table 1).

Fluorescence imaging through *in vitro* and *in vivo* analysis is another tactic connected to new developments in clinical research; in this context, the recognition of biomolecules requires meticulous consideration.[215-220] In *in vitro* studies of the reported probes with HeLa, Raw, HePG-2, C2C12, A549, HCT116, MCF-7, PC3, B16, and C6 cell lines are briefly discussed. HeLa cell lines were used for the majority of the *in vitro* fluorescence imaging studies. In addition to human semen, *C. elegans*, Jurkat, yeast, and bean sprouts have been investigated for the detection of biomolecules using probes **25**, **46**, **55**, **69**, and **84** respectively. The efficient implementation of probes **15**, **26**, **86**, **97**, and **98** to detect Pi, PPi, ATP, amino acids, and S^{2-}, respectively, through the *in vivo* fluorescence imaging investigations using zebrafish as animal models is the most interesting subject in this review article. Selective detection of biomolecules using Zn(II)-based probes through both in vitro and in vivo analysis may depends on several key factors: (i) appropriate fluorophore selection, (ii) solubility, (iii) cellular permeability, (iv) sensitivity and selectivity, (v) suitable excitation and emission wavelengths, (vi) effective binding receptors, (vii) low detection limits, (viii) long fluorescence lifetimes, (ix) low toxicity, (x) incorporation of targeting groups (e.g., mitochondria or lysosome), and (xi) favorable pharmacokinetic and pharmacodynamic properties, including efficient excretion. Future research should focus on developing new sensory devices with non-invasive, highly specific, sensitive biomarkers with high diagnostic values in order to examine the molecular-level interaction phenomena linked to the metabolic changes. Additionally, it should make it easier to evaluate and appraise the prospective biosensors with markers before introducing them into clinical use. Furthermore, it should be shown that good and efficient laboratory and clinical results can be incorporated. Therefore, further design and generation of

Open Access Article. Published on 10 June 2026. Downloaded on 6/10/2026 10:50:53 PM.
This article is licensed under a Creative Commons Attribution 3.0 Unported Licence.

Sensors & Diagnostics Accepted Manuscript

View Article Online
DOI: 10.1039/D6SD00010J

novel sensors may be supported in order to detect biomolecules in real samples and HeLa cells in a selective and efficient manner. In this connection, it is anticipated that researchers may shortly come across concepts for designing and structurally constructing novel fluorescent probes to detect biomolecules in the human body, which is a pressing concern. These probes may yield significant information that will help us understand the regulation of active molecules in various diseases.

Open Access Article. Published on 10 June 2026. Downloaded on 6/10/2026 10:50:53 PM.
This article is licensed under a Creative Commons Attribution 3.0 Unported Licence.

Sensors & Diagnostics Accepted Manuscript

Open Access Article. Published on 10 June 2026. Downloaded on 6/10/2026 10:56:53 AM.
This article is licensed under a Creative Commons Attribution 3.0 Unported

Table 1. Zn (II) complexes that respond to biomolecules

Probe	Detection of analyte	Binding mode		Solvent and pH	$\lambda_{ex,}$ nm	$\lambda_{em,}$ nm		Binding constant		Limit of detection (LOD)		Cell line / live cell imaging	Ref
		Probe : Zn	Probe - Zn: analyte			Probe	Probe-Zn	Probe-Zn	Probe-Zn + analyte	Probe-Zn	Probe-Zn + analyte		
1	$P_2O_7^{4-}$	1:1		HEPES buffer,7.4	417	543	475	4.53×10^4 M^{-1}		7 nM	60 nM	HeLa	[109]
2	$P_2O_7^{4-}$	1:1		EtOH-H_2O (1:1)	430		510	1.25×10^5 M^{-1}	$1.4\times10^5 M^{-1}$	71 ppb	480 pM	HeLa	[110]
3	$P_2O_7^{4-}$	1:2		DMSO-H_2O (1:9) HEPES buffer, 7.4.	440		515	9.3×10^7 M^{-1}		0.28 nM	0.87 nM	A549	[111]
4	ATP	1:1		EtOH	370		560	2.20×10^4 M^{-1}		0.17 μM			]112]
5	$P_2O_7^{4-}$	1:1		DMSO-H_2O (1:9), HEPES buffer, 7.4	410		525	2.36×10^6 M^{-1}		0.52 nM		HeLa	[113]
6	HPO_4^{2-}	2:1		DMF-H_2O (2:1)	440		520			27.8 nM	3.12×10^{-7} M		[114]
7	$P_2O_7^{4-}$	1:1		EtOH		576	507				2.7 nM		[115]
8	$P_2O_7^{4-}$	1:1		DMSO-H_2O (1:9) HEPES buffer, 7.4	450		525	4.53×10^4 M^{-1}		0.52 μM	0.58 μM	HeLa	[116]
9	$P_2O_7^{4-}$	1:1	1:1	DMSO-H_2O (1: 9)	400		521	1.69×10^4 M^{-1}		4.48×10^{-7} M	574 nM	HeLa	[117]
10	$P_2O_7^{4-}$	1:1		EtOH-H_2O (9:1) tris buffer, 7.4	340		484	1.19×10^5 M^{-1}		1.29×10^{-8} M			[118]
11	$H_2PO_4^-$	1:2		H_2O	440		502 534	2.06×10^5		3.79 nM		RAW 264.7	[119]
12	$H_2PO_4^-$	1:1		CH_3CN	380	447	450						[120]
13	ATP	1:2	1:1	DMF-Tris HCl buffer (9:1), 7.4	335	406	590		$3.45\times10^5 M^{-1}$		38.2 nM	C2C12	[121]

Sensors & Diagnostics Accepted Manuscript

Open Access Article. Published on 10 June 2026. Downloaded on 6/10/2026 10:50:53
This article is licensed under a Creative Commons Attribution 3.0 Unported

14	$P_2O_7^{4-}$	1:1		HEPES buffer, 7.4	360		467	$31.64\times10^4 M^{-1}$	$13.69\times10^5 M^{-1}$	6.72×10^{-9} M	5.12 nM	HCT 116	[122]
15	$H_2PO_4^-$	1:1		Aqueous DMSO solution	390	480	650		9.6×10^{-3} M		5.7 μM	Zebrafish embryos	[123]
16	$H_2PO_4^-$ /Cys	2:1		DMSO-H_2O (1950μL: 50μL)	325	378 397 417	485			2.34×10^{-6} M	2.18×10^{-7} M	HeLa	[124]
17	$P_2O_7^{4-}$	1:1		CH_3CN-HEPES buffer, (3:7), 7.4	340	515	412, 475	4.4×10^4 molL^{-1}					[125]
18	ATP	1:1		PBS buffer, 7.4	340	456		$0.948\times10^4 M^{-1}$		4.82×10^{-7} M		HeLa	[126]
19	$P_2O_7^{4-}$	1:1	2:1	H_2O-DMSO (99.5 : 0.5)	470	555	628	$5.59\times10^3 M^{-1}$		3.52 μM	2.45 μM	HeLa	[127]
20	ATP	1:1		MeOH-Water (3:1)	315	512	555	$6.49\times10^4 M^{-1}L$		0.078 μM	6.6 μM	RAW 264.7	[128]
21	$P_2O_7^{4-}$	1:1		HEPES-DMSO (6:4), 7.4	420		610	2.78×10^5 M		47×10^{-9} M	1.7 μM		[129]
22	$P_2O_7^{4-}$ / ATP	1:1		HEPES buffer,7.4	390		454					HeLa	[130]
23	ATP	1:1		Aqueous CH_3OH HEPES (1:2) buffer, 7.4	390	455		$9.3\times10^4 M^{-1}$, $7.2\times10^4 M^{-1}$				HeLa	[131]
24	$P_2O_7^{4-}$	1:1		HEPES buffer,7.4	352		453		$4.06\times10^5 M^{-1}$				[132]
25	$H_2PO_4^-$	2:1		H_2O-DMSO (3:1) HEPES, 7.4	355	520	475	$3.644\times10^4 M^{-1}$		0.1- 3.5 μM	1.23 μM	Human semen sample	[133]
26	$P_2O_7^{4-}$	1:1		Bis-tris buffer, 7	357		447	$3.5\times10^3 M^{-1}$	$5.65\times10^2 M^{-1}$	0.32 μM	21.9 μM	HeLa, Zebrafish	[134]
27	$P_2O_7^{4-}$	1:2	1:1	HEPES buffer,7.4		420	518		$9.2\times10^7 M^{-1}$				[135]
28	$P_2O_7^{4-}$ / ATP	1:2	1:1	EtOH	357								[136]
29	$P_2O_7^{4-}$ / ADP	1:1	1:1	EtOH	352	530	445						[137]

Sensors & Diagnostics Accepted Manuscript

Open Access Article. Published on 10 June 2026. Downloaded on 6/10/2026 10:56:53
This article is licensed under a Creative Commons Attribution 3.0 Unported

30	$P_2O_7^{4-}$	1:2	1:1	HEPES buffer 7.4	316	336-612	383	$5.06 \times 10^{10}\ M^{-1}$	$6.7 \times 10^5\ M^{-1}$		95 nM	HeLa	[138]
31	$P_2O_7^{4-}$/ ATP	1:2	1:1	HEPES buffer	383				$4.1 \times 10^5\ M^{-1}$				[139]
32	$P_2O_7^{4-}$ / ATP	1:2	1:1	CH_3CN-HEPES (5:95)	360		505				1.5 μM	C2C12	[140]
33	ATP	1:1		HEPES buffer, 7.4	450		535						[141]
34	$P_2O_7^{4-}$	1:1	1:1	1% CH_3CN HEPES, 7.4	295			$2 \times 10^4\ M^{-1}$		0.1 μM			[142]
35	ATP	1:1	1:1	1%CH_3CN HEPES buffer, 7.4	370	538			$6.2 \times 10^6\ M^{-1}$			A549, MCF-7, PANC-1, PC3, PNT-2, AsPC-1 SNU-216	[143]
36	ATP	1:2	1:1	CAPS buffer	317		~ 460						[144]
37	$P_2O_7^{4-}$ / PO_4^{3-}	1:2		HEPES buffer	359		462	$4.85 \times 10^7\ M^{-1}$					[145]
38	$P_2O_7^{4-}$	1:2	1:1	HEPES buffer	380		480		$5.39\text{-}7.68\times10^5\ M^{-1}$				[146]
39	ATP	1:1		HEPES buffer, 7.2	380		460		$2.2 \times 10^6 M^{-1}$				[147]
40	ATP / ADP	1:1	2:1	HEPES buffer, 7.4					$3.6 \times10^{10}\ M^{-2}$ $7.1 \times 10^9\ M^{-2}$				[148]
41	$P_2O_7^{4-}$	1:1	1:1	HEPES buffer, 7.4	320		428		$3.18\times10^5\ M^{-1}$				[149]
42	ATP	1:1	1:1	HEPES buffer	400		500				8.4 nM	RAW 264.7	[150]
43	ATP	1:1	1:1	HEPES buffer, 7.4	400		595					PC3	[151]
44	GTP	1:2		MOPS buffer	325		410				0.9 μM		[152]
45	ATP/ ADP AMP/	1:2	1:1	HEPES buffer, 7.2	397		447		$4.2 \times 10^5 M^{-1}$				[153]

Sensors & Diagnostics Accepted Manuscript

Open Access Article. Published on 10 June 2026. Downloaded on 6/10/2026 10:50:53
This article is licensed under a Creative Commons Attribution 3.0 Unported

	Pi												
46	ATP	1:2	1:1	HEPES buffer	488		523		$1.3 \times 10^6\ M^{-1}$			Jurkat	[154]
47	$P_2O_7^{4-}$	1:4	1:1	H_2O-DMSO (99:1)	330		465						[155]
48	$P_2O_7^{4-}$	1:2	1:1	HEPES buffer	390		485						[156]
49	$P_2O_7^{4-}$	1:1	1:1	H_2O-MeOH HEPES (49:1), 7.4	465		549	$5.9 \times 10^4\ M^{-1}$	$6.9 \times 10^4\ M^{-1}$	0.59 µM	17.5 µM	RAW 264.7	[157]
50	$P_2O_7^{4-}$	1:2	1:1	HEPES buffer solution, 7.4	504		639				42 nM	A549 and mice	[158]
51	ADP	1:2	1:2	HEPES-MeCN (1:1) buffer, 7.3	380		435					HeLa	[159]
52	$P_2O_7^{4-}$/ ADP	1:1	2:1	HEPES buffer, 7.4	350	426		$3.45 \times 10^5\ M^{-1}$	$2.56\times10^{10}\ M^{-2}$				[160]
53	ATP	1:1	1:1	DMSO-Water (1:99)	350				$7.71 \times 10^6\ M^{-1}$		18.9 nM		[161]
54	$P_2O_7^{4-}$	1:1		CH_3CN-HEPES (9 : 1)	346	442	542		7.0×10^{-5} M				[162]
55	$P_2O_7^{4-}$	1:1	2:1	CH_3CN-HEPES (5:5), 7.2	430		512		$1.27 \times 10^4\ M^{-1}$		2.18×10^{-6} M	Hi-5, *C.elegans*	[163]
56	$P_2O_7^{4-}$	1:1	3:1	HEPES buffer, 7.4	400				$2.94\times 10^6\ M^{-1}$				[164]
57	$P_2O_7^{4-}$	1:1	1:1	HEPES-CH_3CN (1:4)	315		379 460		5.0×10^{-4} M				[165]
58	ATP	1:1	1:1	EtOH:H_2O (9:1)	440		610				0.15 µM		[166]
59	$P_2O_7^{4-}$	1:1	3:1	H_2O-DMSO (7:3)	400						5.37 nM	HeLa and HepG2	[167]
60	Modified $P_2O_7^{4-}$	1:1	1:1	EtOH-$CHCl_3$ (1:1)	375		551				5.8 µM		[168]
61	$P_2O_7^{4-}$	1:2	1:2	HEPES buffer, 7.4	283		367 365		$7.72\times10^5\ M^{-2}$, $6.74\times10^4\ M^{-2}$		0.47 nM 0.17 nM	MCF-7	[169]

Sensors & Diagnostics Accepted Manuscript

Open Access Article. Published on 10 June 2026. Downloaded on 6/10/2026 10:56:53 AM.
This article is licensed under a Creative Commons Attribution 3.0 Unported

62	ATP / ADP	1:1		Water, 7	448						1.85 μM	HeLa	[170]
63	ADP	1:1	1:1	HEPES-DMF buffer (75:25)	380		416		1.1×10^6 M^{-1}				[171]
64	ATP / ADP / $P_2O_7^{4-}$/ AMP	1:2	1:1	HEPES buffer, 7.2	380	420			2.0×10^6 M^{-1} 3.9×10^5 M^{-1} 9.1×10^4 M^{-1} 3.1×10^4 M^{-1}				[172]
65	ATP	1:1	1:1	H_2O-MeOH (9:1) HEPES buffer, 7.4	370		515	1.7×10^7 M^{-1}					[173]
66	$P_2O_7^{4-}$	1:2	1:1	DMF-H_2O (1:1)	317	455							[174]
67	PO_4^{3-}	1:2	2:1	DMF-H_2O (1:1) HEPES, 7.5	341	406				15 nM			[175]
68	$P_2O_7^{4-}$	1:2		MOPS buffer	302						300 nM		[176]
69	ATP / PPi	1:1		CH_3CN-H_2O (2:98) HEPES buffer, 7.4	321	416	498	1.4×10^4 M^{-1}	4.5×10^3 M^{-2} 5.8×10^3 M^{-2}			Bean sprouts	[177]
70	$H_2PO_4^-$	1:1	2:1	CH_3CN-H_2O (8:2)	310	496		3.28×10^4 M^{-1}	1.87×10^{-7} M	8.8×10^{-9} M	5.5×10^{-8} M		[178]
71	ATP	1:1		DMSO-HEPES (3: 97) buffer, pH=7.	365	550							[179]
72	ATP / ADP	1:2	1:1	MOPS buffer	324								[180]
73	$H_2PO_4^-$, Cys	1:1		DMSO-H_2O (8:2)	390	430	525	1.94×10^4 M^{-1}		41 nM	49 nM	HepG-2	[181]
74	ATP / PPi	1:1		CH_3OH-HEPES (2:1) buffer, 7.2	500		512	1.1×10^7 M^{-1}			2.4 μM 1.0 μM		[182]
75	ATP / ADP	1:1	1:1	HEPES buffer, 7.4	344	445	510						[183]

Sensors & Diagnostics Accepted Manuscript

Open Access Article. Published on 10 June 2026. Downloaded on 6/10/2026 10:50:53
This article is licensed under a Creative Commons Attribution 3.0 Unported

76	$P_2O_7^{4-}$	1:3	1:3	DMSO-H_2O (4:1) in HEPES buffer, 7.4	267	405	491			9.87 μM		RAW	[184]
77	$P_2O_7^{4-}$	1:1	2:1	HEPES buffer, 7.4	280		223	4.4×10^6 M^{-1}	2.1×10^8 M^{-2}	0.4 μM	0.2 μM		[185]
78	ATP	1:1	1:1	CH_3CN-CH_2Cl_2) (1:1)				3.45×10^4 M^{-1}					[186]
79	$HP_2O_7^{3-}$ / $H_2PO_4^-$	1:1		EtOH	337	382 535	460	$0.98 \times 10^4 M^{-1}$	1.40×10^5 M^{-1} 5.66×10^5 M^{-1}	20 μM	1 μM 1 μM		[188]
80	$H_2PO_4^-$	2:1		DMSO-H_2O (8:2) HEPES buffer, 7.24	400	540	600	5.76×10^6 M^{-2}					[189]
81	ATP	1:1		DMSO-Water (9:1) HEPES buffer, 7.2	330			7.5×10^5 M^{-1}	6.2×10^5 M^{-1}		5.9×10^{-8} M	B16	[190]
82	$P_2O_7^{4-}$/ ATP	1:2	1:2	1% DMSO HEPES buffer, 7.42		450							[191]
83	$P_2O_7^{4-}$/ ATP	1:2	1:1	HEPES buffer, 7.4 Naked eye					2.9×10^8 M^{-1}				[192]
84	ATP	1:1	1:1	CH_3CN								Yeast	[193]
85	$P_2O_7^{4-}$	1:1		EtOH-H_2O (10%) Naked eye									[194]
86	Tyr	2:1		EtOH-Water	418		520				1.39×10^{-7} M^{-1}	B16-F10, Zebrafish	[195]
87	D-His D-Met	1:1	1:1	CH_2Cl_2-MeOH (7:1)	420								[196]
88	L-Ser, L-Met, L-Phe, L-Thr		1:1:1	1% THF HEPES buffer	320								[197]
89	L-Val, L-Met,	1:1		CH_3CN-H_2O (99:1)	435								[198]

Sensors & Diagnostics Accepted Manuscript

Open Access Article. Published on 10 June 2026. Downloaded on 6/10/2026 10:56:53 AM.
This article is licensed under a Creative Commons Attribution 3.0 Unported

	L-Leu, L-Ala												
90	L-His	1:2	1:1	1% THF HEPES buffer, 7.35	343								[199]
91	L-Cys / L-His	2:1		Tris buffer	298		363				2.43×10^{-5} M 2.81×10^{-5} M		[200]
92	HS^-	1:1		DMSO	560, 414, 442, 570		~ 600-800					HepG2	[201]
93	S^{2-}	1:1		HEPES buffer, 7.4	360		440			66 nM	32.6 nM	HeLa	[202]
94	S^{2-}	1:1		Bis-tris buffer, 7.0	420		484	$1.7\times10^4\ M^{-1}$	$2.0\times10^3\ M^{-1}$	1.59 μM	8.03 μM	HeLa	[203]
95	PPi / S^{2-}	1:1		MeOH-Tris buffer, (7:3)	353			$6.7\times10^5\ M^{-1}$			3.7×10^{-7} M 4.9×10^{-7} M	HepG2	[204]
96	HS^-	1:1		Bis-tris buffer	357		447			0.63 μM		HeLa	[205]
97	Na_2S	1:1		Bis-tris buffer	345		500	$1.67\times10^4\ M^{-1}$	$3.4\times10^3\ M^{-1}$	0.29μM	2.39 μM	Zebrafish	[206]
98	Na_2S	1:1		Bis-tris buffer	340			$5.28\times10^5\ M^{-1}$	$1.79\times10^4\ M^{-1}$	0.06 μM		HeLa, Zebrafish	[207]
99	PPi/S^{2-}	1:1		MeOH-Tris buffer	355			$4.9\times10^5\ M^{-1}$			0.63 μM 0.66 μM	HeLa	[208]
100	H_2S	2:1		Milli-Q water solution								HepG2	[209]
101	H_2S	2:1		MeOH-PBS (3:1) buffer	530		625	$13826\ M^{-1}$			92 nM	C6 cell	[210]
102	NO_2	1:1		CH_3CN-H_2O (9: 1) HEPES	370			$5.38\times10^7\ M^{-1}$	$4.15\times10^9\ M^{-1}$	2.6×10^{-9} M	1.2 pM		[211]
103	NO	1:1		EtOH-Water (1:1), 7.4	295		365			2.97×10^{-8} M			[212]

Sensors & Diagnostics Accepted Manuscript

View Article Online
DOI: 10.1039/D6SD00010J

9. Conclusions and Future recommendations

Fluorescent Zn(II) complexes have emerged as highly promising tools for the sensitive and selective detection of various biomolecules, owing to their unique photophysical properties and tunable binding affinities. This review comprehensively examined the recognition of diverse biomolecules, including phosphates (Pi, PPi), nucleotides (AMP, ADP, ATP), amino acids, and key signaling molecules such as sulfide (S^{2-}), nitric oxide (NO), and nitrite (NO_2^-). We discussed structural and binding modulations influence fluorescence responses such as on/off switching, binding constants, and detection limits in different Zn(II) complexes. These insights enable the development of highly sensitive and selective Zn(II)-based biosensors for bioimaging applications in complex cellular environments. Achieving exceptional selectivity toward specific biomolecules, even in the presence of competing species within biological samples, remains a critical challenge. Strategies to address this include employing dynamic combinatorial chemistry to tailor binding pockets for target molecules or designing multi-recognition units within Zn(II) complexes.

Future research should also explore integrating Zn(II) complexes with complementary imaging modalities, such as magnetic resonance imaging or positron emission tomography. Such multimodal approaches could provide a more comprehensive understanding of disease states by enabling both the detection of biomolecules and visualization of their spatial distribution within tissues or organs. To translate the promising in vitro performance of Zn(II)-based probes into effective *in vivo* applications, several challenges must be addressed, including biocompatibility, stability under physiological conditions, and efficient delivery to target sites. Conjugation of Zn(II) complexes with specific targeting moieties can facilitate selective delivery to particular organelles or diseased cells. Fine-tuning the biocompatibility of these complexes through the use of biocompatible ligands or chemical modifications that minimize cytotoxicity while preserving detection capabilities is essential for safe and effective *in vivo* use. Overall, these advancements will significantly enhance the sensitivity and accuracy of biomolecule detection, ultimately enabling more precise diagnosis and improved therapeutic monitoring.

Conflict of interest

The authors declare no conflict of interest.

Acknowledgment

One of the authors (Dr. J. Annaraj) acknowledged DST-FIST-MKU, RUSA MKU (File No. 002/RUSA/MKU/2020-2021) for the financial support.

Open Access Article. Published on 10 June 2026. Downloaded on 6/10/2026 10:50:53 PM.
This article is licensed under a Creative Commons Attribution 3.0 Unported Licence.

Sensors & Diagnostics Accepted Manuscript

View Article Online
DOI: 10.1039/D6SD00010J

References

1. S. Ma, G. Chen, J. Xu, Y. Liu, G. Li, T. Chen, Y. Li and T.D. James, *Coord. Chem. Rev*., 2021, **427**, 213553.
2. S. Theiner, K. Loehr, G. Koellensperger, L. Mueller and N. Jakubowski, *J. Anal. At. Spectrom.*, 2020, **35**, 1784–1813.
3. M. Wu, Z. Zhang, J. Yong, P.M. Schenk, D. Tian, Z.P. Xu and R. Zhang, *Top. Curr. Chem.*, 2022, **380**, 29.
4. H. Kobayashi, M. Ogawa, R. Alford, P.L. Choyke and Y. Urano, *Chem. Rev.*, 2010, **110** 2620–2640.
5. B. Mohan, N. M. Kunhumon and S. Shanmugaraju, *Sens. Diagn.*, 2023, **2**, 1158-1175.
6. R. Diana and B. Panunzi, *Molecules*, 2020, **25**, 4984.
7. P. A. Gale, *Chem. Soc. Rev.*, 2010, **39**, 3746–3771.
8. C. Caltagirone and P. A. Gale, *Chem. Soc. Rev.*, 2009, **38**, 520–563.
9. J. L. Sessler, P. A. Gale and W. S. Cho, Royal Society of Chemistry, Cambridge, 2006.
10. P. D. Beer and P. A. Gale, *Angew. Chem., Int. Ed.*, 2001, **40**, 486–516.
11. S. Kubik, *Chem. Soc. Rev.*, 2010, **39**, 3648–3663.
12. A. V. Gourine, E. Llaudet, N. Dale and K. M. Spyer, *Nature*, 2005, **436**, 108–111.
13. F. Westheimer, *Science*, 1987, **235**, 1173–1178.
14. T. M. Du, H. S. Yang and X. F. Niu, *Mater. Today Chem.*, 2021, **22**, 100579.
15. K. G. Clarke, Bioprocess Engineering: An Introductory Engineering and Life Science Approach, Woodhead Publisher, 2013.
16. J. Dong, F. Ye, J. Lin, H. He and Z. Song, *Mitochondrial Comm.*, 2023, **1**, 2-12.
17. T. Tian, X. Y. Chu, Y. Yang, X. Zhang, Y.M. Liu, J. Gao, B. G. Ma and H. Y. Zhang, *Life*, 2019, 9, 43.
18. A. Shaikh, T. Berndt and R. Kumar, *Pediatr. Nephrol.*, 2008, **23**, 1203–1210.
19. W. G. Junger, *Nat. Rev. Immunol.*, 2011, **11**, 201–212.
20. S. K. Kim, D. H. Lee, J.-I. Hong and J. Yoon, *Acc. Chem. Res.*, 2009, **42**, 23-31.
21. A. E. Hargrove, S. Nieto, T. Zhang, J. L. Sessler and E. V. Anslyn, *Chem. Rev.*, 2011, **111**, 6603-6782.
22. G. J. Lee and J. Marks, *Pediatr. Nephrol.*, 2015, **30**, 363–371.
23. N. M. Hansen, R. Felix, S. Bisaz and H. Fleisch, *Acta. Gen. Subj.*, 1976, **451**, 549–559.
24. M. Crook and R. Swaminathan, *Ann. Clin. Biochem.*, 1996, **33**, 376–396.
25. J. R. Knowles, *Annu. Rev. Biochem.*, 1980, **49** 877–919.

Open Access Article. Published on 10 June 2026. Downloaded on 6/10/2026 10:50:53 PM.
This article is licensed under a Creative Commons Attribution 3.0 Unported Licence.

Sensors & Diagnostics Accepted Manuscript

View Article Online
DOI: 10.1039/D6SD00010J

26. R. D. Fields and B. Stevens, *Trends Neurosci.*, 2000, **23**, 625–633.
27. X. Shen, G. Mizuguchi, A. Hamiche and C. Wu, *Nature*, 2000, **406**, 541–544.
28. Z. Xu, N. J. Singh, J. Lim, J. Pan, H. N. Kim, S. Park, K. S. Kim and J. Yoon, *J. Am. Chem. Soc.*, 2009, **131**, 15528–15533.
29. C. Zhu, Y. Zhao, M. Yan, Y. Huang, J. Yan, W. Bai and A. Chen, *Anal. Bioanal. Chem.*, 2016, **408**, 4151–4158.
30. J. A. Cruz-Aguado, Y. Chen, Z. Zhang, N. H. Elowe, M. A. Brook and J. D. Brennan, *J. Am. Chem. Soc.*, 2004, **126**, 6878–6879.
31. Q. S. Gu, T. Li, T. Liu, G. Yu, G. J. Mao, F. Xu and C. Y. Li, *Chemosensors*, 2023, **11**, 417.
32. J. Kaur and P. K. Singh. *Trends Anal Chem.*, 2022, **146**, 116483.
33. G. Theiler, F. Quehenberger, F. Rainer, M. Neubauer, M. Stettin and C. Robier, *Rheumatol. Int.*, 2014, **34**, 137–9.
34. F. W. L. Tsui, *Curr. Rheumatol. Rep.*, 2012, **14**, 155–60.
35. A. E. Timms, Y. Zhang, R. G. G. Russell, M. A. Brown, *Rheumatology*, 2002, **41**, 725–729.
36. C. J. Williams and A. K. Rosenthal. *Best. Pract. Res. Clin. Rheumatol.*, 2021, **35**, 101718.
37. E. Lespessailles, H. Toumi, *Int J Mol Sci.*, 2022, **23**, 10733.
38. S. Anbu, A. Paul, G. J. Stasiuk and A. J. L Pombeiro, *Coord. Chem. Rev.*, 2021, **431**, 213744
39. C. A. Weatherly, S. Du, C. Parpia, P. T. Santos, A. L. Hartman and D. W. Armstrong, *ACS Chem. Neurosci.*, 2017, **8**, 1251-1261.
40. K. Micskei, T. Patonay, L. Caglioti and G. Pályi, *Biodiversity*, 2010, **7**, 1660-1669.
41. G.F. Cahill, Jr., *Annu. Rev. Nutr.*, 2006, **26**, 1–22.
42. P. J. Reeds, *J. Nutr.*, 2000, 130, 1835S-1840S.
43. Y. Hou, Y. Yin and G. Wu, *Exp. Biol. Med.*, 2015, **240**, 997-1007.
44. Y. Hou and G. Wu, *Adv. Nutr.*, 2018, **9**, 849-851.
45. R. M. Canet-Aviles, M. A. Wilson, D. W. Miller, R. Ahmad, C. Mclendon and S. Bandyopadhyay, *Proc. Natl. Acad. Sci. U. S.A.*, 2004, **101**, 9103–9108.
46. T. Rehman, M. A. Shabbir, M. Inam-Ur-Raheem, M. F. Manzoor, N. Ahmad, Z. W. Liu, M. H. Ahmad, A. Siddeeg, M. Abid and R. M. Aadil, *Food Sci. Nutr.*, 2020, **8**, 4696–4707.
47. L. L. Zhu, T. G. Zhang, Y. Y. Ma and W. Y. Lin, *Sens. Actuator B: Chem.*, 2020, **305**, 127202.

Open Access Article. Published on 10 June 2026. Downloaded on 6/10/2026 10:50:53 PM.
This article is licensed under a Creative Commons Attribution 3.0 Unported Licence.

Sensors & Diagnostics Accepted Manuscript

View Article Online
DOI: 10.1039/D6SD00010J

48. M. Travaglio, F. Michopoulos, Y. Yu, R. Popovic, E. Foster, M. Coen and L. M. Martins, *Dis. Model Mech.*, 2023, **16**, dmm049727.
49. M. L. Pavao, R. Ferin, A. Lima and J. Baptista, *Adv. Clin. Chem.*, 2022, **109**, 75–127.
50. A. Pastore, A. Alisi, G. D. Giovamberardino, A. Crudele, S. Ceccarelli, N. Panera, C. Dionisi-Vici and V. Nobili, *Int. J. Mol. Sci.*, 2014, **15**, 21202–21214.
51. Y. Fan, X. Yang, J. Zhao, X. Sun, W. Xie, Y. Huang, G. Li, Y. Hao and Z. Zhang, *Arthritis Res Ther.*, 2019, **21**, 123.
52. T. Nagendraraj, S. Vishnu Priya, J. Annaraj and S. Sagadevan, *Coord. Chem. Rev.*, 2023, **495**, 215368.
53. A. E. Thalacker-Mercer and M. E. Gheller, *J. Nutr.*, 2020, **150**, 2588S-2592S.
54. A. L. Jones, M. D. Hulett and C. R. Parish, *Immunol. Cell Biol.*, 2005, **83**, 106–118.
55. M. Holeček, *Nutrients*, 2020, **12**, 848.
56. J. A. Pedroso, T. T. Zampieri and J. Donato Jr., *Nutrients*, 2015, *7*, 3914-3937.
57. Y. Duan, F. Li, Y. Li, Y. Tang, X. Kong, Z. Feng, T. G. Anthony, M. Watford, Y. Hou, G. Wu and Y. Yin. *Amino Acids*, 2016, **48**, 41-51.
58. Y. Martínez, X. Li, G. Liu, P. Bin, W. Yan, D. Más, M. Valdivié, C. A. Hu, W. Ren and Y. Yin, *Amino Acids*, 2017, **49**, 2091-2098.
59. W. B. Hanley, *Am. J. Med.*, 2004, **117**, 590.
60. M. Holeček, *Nutrients*, 2022, **14**, 1987.
61. Y. P. Chen, Y. F. Cheng, X. H. Li, W. L. Yang, C. Wen, S. Zhuang and Y. M. Zhou, *Poult. Sci.*, 2017, **96**, 405–413.
62. F. Kheiri and M. Alibeyghi, *Italian J. Anim. Sci.*, 2017, **16**, 580-587.
63. W. Wang, X. Zeng, X. Mao, G. Wu and S. Qiao, *J. Nutr.*, 2010, **140**, 981–986.
64. Y. Chen, H. Zhang, Y. Cheng, Y. Li, C. Wen and Y. Zhou, *Br. J. Nutr.*, 2018, **119**, 1254–1262.
65. A. Hase, S. E. Jung and M. aan het Rot, *Pharmacol. Biochem. Behav.*, 2015, **133**, 1-6.
66. P. A. Frey, A. D. Hegeman and G. H. Reed, *Chem. Rev.*, 2006, **106**, 3302.
67. M. S. Rogers, E. M. Tyler, N. Akyumani, C. R. Kurtis, R. K. Spooner, S. E. Deacon, S. Tamber, S. J. Firbank, K. Mahmoud, P. F. Knowles, S. E. Phillips, M. J. McPherson and D. M. Dooley, *Biochemistry*, 2007, **46**, 4606.
68. V. R. Kaila, M. I. Verkhovsky and M. Wikström, *Chem. Rev.*, 2010, **110**, 7062-7081.
69. S. Koide and S, S. Sidhu, *ACS Chem. Biol.*, 2009, **4**, 325-334.
70. J. E. Sperringer, A. Addington and S. M. Hutson. *Neurochem. Res.*, 2017, **42**, 1697–709.
71. L. E. Rojo, J. A. Fernández, A. A. Maccioni, J. M. Jimenez and R. B. Maccioni, *Arch. Med. Res.*, 2008, **39**, 1-16.
72. P. Kamoun, *Med. Hypotheses*, 2001, **57**, 389-392.

Open Access Article. Published on 10 June 2026. Downloaded on 6/10/2026 10:50:53 PM.
This article is licensed under a Creative Commons Attribution 3.0 Unported Licence.

Sensors & Diagnostics Accepted Manuscript

View Article Online
DOI: 10.1039/D6SD00010J

73. C. Q. Chen, H. Xin, Y. Z. Zhu, *Acta Pharmacol. Sin.*, 2007, **28**, 1709–1716.
74. L. Li and P. K. Moore, *Biochem. Soc. Trans.*, 2007, **35**,1138–1141.
75. F. Sami, M. Faizan, A. Faraz, H. Siddiqui, M. Yusuf and S. Hayat, *Nitric oxide*, 2018, **73**, 22–38.
76. P. Ahmad, A. A. Abdel Latef, A. Hashem, E. F. Abd_Allah, S. Gucel and L. S. P. Tran, *Front. Plant Sci.*, 2016, **7**, 347.
77. M. A. Rahman, A. H. Kabir, Y. Song, S. H. Lee, M. Hasanuzzaman and K. W. Lee. *Antioxidants*, 2021, 10, 1556.
78. M. J. Hill, 8-Nitrates and Nitrites in food and water in relation to human disease, Nitrates and Nitrites in Food and Water, Woodhead Publishing Limited, England, 1st edn, 1996.
79. N. S. Bryan, *Free Radical Biol. Med.*, 2006, **41**, 691–701.
80. T. Fazio, J. N. Damico, J. W. Howard, R. H. White and J. O. Watts, *J. Agric. Food Chem.*, 1971, **19**, 250–253.
81. F. R. Greer and M. Shannon, *Pediatrics*, 2005, **116**, 784-786.
82. World Health Organization, in Guidelines for Drinking Water Quality: Incorporating 1st and 2nd Addenda, Recommendations, WHO Press, Geneva, Switzerland, 3rd edn, 1 2008.
83. National Institutes of Health. Zinc—Fact Sheet for Health Professionals. Available online: https://ods.od.nih.gov/factsheets/Zinc-HealthProfessional/
84. L. A. Finney and T. V. O'Halloran, *Science*, 2003, **300**, 931–936.
85. I. Turel and J. Kljun, *Curr. Top. Med. Chem.*, 2011, **11**, 2661–2687.
86. C. Pettinari, A. Lorenzotti, M. Pellei and C. Santini, *Polyhedron*, 1997, **16**, 3435–3445.
87. S. Adhikari, T. Bhattacharjee, R. J. Butcher, M. Porchia, M. De Franco, C. Marzano, V. Gandin and F. Tisato, *Inorg. Chim. Acta.*, 2019, **498**, 119098.
88. M. Porchia, M. Pellei, F. Del Bello and C. Santini, *Molecules*, 2020, **25**, 5814.
89. W. N. Lipscomb and N. Sträter, *Chem. Rev.*, 1996, **96**, 2375–2434.
90. J. E. Coleman, *Annu. Rev. Biochem.*, 1992, **61**, 897–946.
91. T. Koike and E. Kimura, *J. Am. Chem. Soc.*, 1991, **113**, 8935–8941.
92. E. Kimura, S. Aoki, T. Koike and M. Shiro, *J. Am. Chem. Soc.*, 1997, **119**, 3068–3076.
93. E. Kimura, T. Shiota, T. Koike and M. Shiro, *J. Am. Chem. Soc.*, 1990, **112**, 5805–5811.
94. T. Koike, S. Kajitani, I. Nakamura, E. Kimura and M. Shiro, *J. Am. Chem. Soc.*, 1995, **117**, 1210–1219.
95. H. S. Jung, P. Verwilst, W. Y. Kim and J. S. Kim, *Chem. Soc. Rev.*, 2016, 45, 1242-1256.
96. L. J. Fan and W. E. Jones Jr., *J. Phys. Chem. B.*, 2006, **110**, 7777-82.
97. P. Y. Fu, S. Z. Yi, M. Pan and C. Y. Su, *Acc. Mater. Res.*, 2023, **4**, 939–952.

Open Access Article. Published on 10 June 2026. Downloaded on 6/10/2026 10:50:53 PM.
This article is licensed under a Creative Commons Attribution 3.0 Unported Licence.

Sensors & Diagnostics Accepted Manuscript

View Article Online
DOI: 10.1039/D6SD00010J

98. X. Xin, W. Shi, Y. Zhao, G. Zhao and Y. Li, *Chem. Phys*, 2023, **570**, 111882.
99. X. Li, H. Ma, J. Qian, T. Cao, Z. Teng, K. Iqbal, W. Qin and H. Guo, *Talanta*, 2019, **194**, 717-722.
100. M. K. Goshisht, G. K. Patra and N. Tripathi, *Mater. Adv.*, 2022, **3**, 2612–2669.
101. B. Musikavanhu, S. Muthusamy, D. Zhu, Z. Xue, Q. Yu, C. N. Chiyumba, J. Mack, T. Nyokong, S. Wang and L. Zhao, *Spectrochim. Acta Part A Mol. Biomol. Spectrosc.*, 2022, 264 120338.
102. B. Musikavanhu, Y. Liang, Z. Xue, L. Feng and L. Zhao, *Molecules*, 2023, **28**, 6960.
103. J. C. Qin, J. Yan, B. D. Wang and Z. Y. Yang, *Tetrahedron Lett.*, 2016, **57**, 1935-1939.
104. R. W. Ramette and E. B. Sandell, *J. Am. Chem. Soc.*, 1956, 78 4872-4878.
105. N. Kumar, V. Bhalla and M. Kumar, *Analyst*, 2014, **139**, 543-558.
106. A. Afrin, A. Jayaraj, M. S. Gayathria and P. Chinna Ayya Swamy, *Sens. Diagn.*, 2023, **2**, 988.
107. K. Ostrowska, K. M. Stadnicka, M. Gryl, O. Klimas, M. Z. Brela, P. Goszczycki, M. Liberka, J. Grolik and A. Węgrzyn, *Cryst. Growth Des.*, 2022, **22**, 1571−1582.
108. P. Srujana, P. Sudhakar and T. P. Radhakrishnan, *J. Mater. Chem. C*, 2018, **6**, 9314-9329.
109. C. Chang, F. Wang, T. Wei and X. Chen, *Ind. Eng. Chem. Res.*, 2017, **56**, 31, 8797–8805.
110. A. Gogoi, S. Mukherjee, A. Ramesh, and G. Das, *RSC Adv.*, 2015, **5**, 63634-63640.
111. D. Rajasekaran, K. Venkatachalam and V. Periasamy, *Spectrochim Acta A Mol. Biomol. Spectrosc.*, 2020, **242**, 118730.
112. D. Singh, S. Tomar, S. Singh, G. Chaudhary, A. P. Singh and R. Gupta, *J. Photochem. Photobiol. A: Chem.*, 2023, **435**, 114334.
113. A. Gomathi, M. Vasanthi, P. Viswanthamurthi, S. Suresh and R. Nandhakumar, *ChemistrySelect*, 2018, **3**, 11809-11815.
114. S. Lohar, S. Pal, M. Mukherjee, A. Maji, N. Demitrib and P. Chattopadhyay, *RSC Adv.*, 2017, **7**, 25528-25534.
115. J. Wang, B. Liu, X. Liu, M. J. Panzner, C. Wesdemiotisa and Y. Pang, *Dalton Trans.*, 2014, **43**, 14142.
116. G. Asaithambi, V. Periasamy and N. Karuppannan, *J. Photochem. Photobiol. A: Chem.*, 2019, **370**, 75-83.
117. K. Mawai, S. Nathani, P. Roy, U. P. Singh and K. Ghosh, *Dalton Trans.*, 2018, **47**, 6421-6434.

Open Access Article. Published on 10 June 2026. Downloaded on 6/10/2026 10:50:53 PM.
This article is licensed under a Creative Commons Attribution 3.0 Unported Licence.

Sensors & Diagnostics Accepted Manuscript

View Article Online
DOI: 10.1039/D6SD00010J

118. Y. Xu, H. Wang, J. Zhao, X. Yang, M. Pei, G. Zhanga and Y. Zhang, *New J. Chem.*, 2019, **43**, 14320-14326.

119. S. Suganya, S. Velmathi, P. Venkatesan, S. P. Wu and M. S. Boobalan, *Inorg. Chem. Front.*, 2015, **2**, 649–656.

120. S. Yang, Y. Huang, A. Lu, Z. Wang and H. Li. *Molecules*, 2023, **28**, 4166.

121. O. Anitha, S. Ghorai, T. Thiruppathiraja, H. Amir, A. Murugan, R. Natarajan, S. Lakshmipathi, C. Viswanathan, M. Jothi and B. Murugesapandian, *Talanta*, 2024, **273** 125900.

122. B. Naskar, R. Modak, D. K. Maiti, M. G. B. Drew, A. Bauzá, A. Frontera, C. D. Mukhopadhyay, S. Mishra, K. D. Sahae and S. Goswami, *Dalton Trans.*, 2017, **46**, 9498-9510.

123. A. S. Murugan, N. Vidhyalakshmi, U. Ramesh and J. Annaraj, *Sens. Actuators B Chem.*, 2019, **281**, 507-513.

124. Y. Upadhyay, T. Anand, L. T. Babu, P. Paira, G. Crisponi, S. K. Ashok Kumar, R. Kumar and S. K. Sahoo, *Dalton Trans.*, 2018, **47**, 742-749.

125. G. Sivaraman, T. Anand and D. Chellappa, *Anal. Methods*, 2014, **6**, 2343-2348.

126. X. Zhang, J. Liu, J. Wang, L. Han, S. Ma, M. Zhao and G. Xi, *J. Photochem. Photobiol. B, Biol.*, 2021, **223**, 112279.

127. W. Z. Xue, X. F. Han, X. L. Zhao, W. N. Wu, Y. Wang, Z. Q. Xu, Y. C. Fan and Z. H. Xu, *Spectrochim Acta A Mol BiomolSpectrosc.*, 2021, **263**, 120169.

128. C. Patra, C. Sen, A. D. Mahapatra, D. Chattopadhyay, A. Mahapatra and C. Sinha, *J. Photochem. Photobiol. A: Chem.*, 2017, **341**, 97-107.

129. Megha, V. Kumar, P. Kaur and K. Singh, *Anal. Chim. Acta*, 2023, **1240**, 340758.

130. R. K. Pathak, K. Tabbasum, A. Rai, D. Panda and C. P. Rao, *Anal. Chem.*, 2012, **84**, 5117–5123.

131. R. K. Pathak, V. K. Hinge, A. Rai, D. Panda and C. P. Rao, *Inorg. Chem.*, 2012, **51**, 4994−5005.

132. S. Khatua, S. H. Choi, J. Lee, K. Kim, Y. Do and D. G. Churchill, *Inorg. Chem.*, 2009, **48**, 2993-2999.

133. S. Chakraborty, S. Lohar, K. Dhara, R. Ghosh, S. Dam, E. Zangrando and P. Chattopadhyay, *Dalton Trans.*, 2020, **49**, 8991-9001.

134. J. H. Kang, J. Han, H. Lee, M. H. Lim, K. T. Kim and C. Kim, *Dyes Pigm.*, 2018, **152**, 131–138.

135. W. H. Chen, Y. Xing and Y. Pang, *Org. Lett.*, 2011, **13**, 1362–1365.

Open Access Article. Published on 10 June 2026. Downloaded on 6/10/2026 10:50:53 PM.
This article is licensed under a Creative Commons Attribution 3.0 Unported Licence.

Sensors & Diagnostics Accepted Manuscript

View Article Online
DOI: 10.1039/D6SD00010J

136. J. Wang, X. Liua and Y. Pang, *J. Mater. Chem. B*, 2014, **2**, 6634.
137. J. Wang, W. Chen, X. Liu, C. Wesdemiotisa and Y. Pang, *J. Mater. Chem. B*, 2014, **2**, 3349-3354.
138. S. Y. Jiao, K. Li, X. Wang, Z. Huang, L. Pua and X. Q. Yu, *Analyst*, 2015, **140**, 174-181.
139. H. N. Lee, Z. Xu, S. K. Kim, K. M. K. Swamy, Y. Kim, S. J. Kim and J. Yoon, *J. Am. Chem. Soc.*, 2007, 129, 3828–3829.
140. J. F. Zhang, S. Kim, J. H. Han, S. J. Lee, T. Pradhan, Q. Y. Cao, S. J. Lee, C. Kang and J. S. Kim, *Org. Lett.*, 2011, **13**, 5294–5297.
141. A. J. Moro, P. J. Cywinski, S. Körstena and G. J. Mohrac, *Chem. Commun.*, 2010, **46**, 1085–1087.
142. B. Roy, A. S. Raoa and K. H. Ahn, *Org. Biomol. Chem.*, 2011, **9**, 7774-7779.
143. A. S. Rao, D. Kim, H. Nam, H. Jo, K. H. Kim, C. Ban and K. H. Ahn, *Chem. Commun.*, 2012, **48**, 3206–3208.
144. J. H. Lee, A. R. Jeong, J. H. Jung, C. M. Park and J. I. Hong, *J. Org. Chem.*, 2011, **76**, 417–423.
145. H. N. Lee, K. M. K. Swamy, S. K. Kim, J. Y. Kwon, Y. Kim, S. J. Kim, Y. J, Yoon and J. Yoon, *Org. Lett.*, 2007, **9**, 243–246.
146. F. Huanga and G. Feng, *RSC Adv.*, 2014, **4**, 484-487.
147. A. Ojida, S. Park, Y. Mito-oka and I. Hamachi, *Tetrahedron Lett.*, 2002, **43**, 6193–6195.
148. Q. C. Xu, H. J. Lv, Z. Q. Lv, M. Liu, Y.J. Li, X. F. Wang, Y. Zhangac and G. W. Xing, *RSC Adv.*, 2014, **4**, 47788-47792.
149. P. Das, N. B. Chandar, S. Chourey, H. Agarwalla, B. Ganguly and A. Das, *Inorg. Chem.*, 2013, **52**, 11034–11041.
150. H. Singh, S. Sreedharan, R. Tiwari, C. Walther, C. Smythe, S. K. Pramanik, J. A. Thomas and A. Das, *Cryst. Growth Des.*, 2018, **18**, 7199–7206.
151. U. Tamima, S. Sarkar, M. R. Islam, A. Shil, K. H. Kim, Y. J. Reo, Y. W. Jun, H. Banna, S. Lee and K. H. Ahn. *Angew. Chem. Int. Ed.*, 2023, **62**, e202300580.
152. I. J. Bazany-Rodríguez, M. K. Salomón-Flores, J. M. Bautista-Renedo, N. González-Rivas and A. Dorazco-González, *Inorg. Chem.*, 2020, **59**, 7739–7751.
153. A. Ojida, H. Nonaka, Y. Miyahara, S. Tamaru, K. Sada and I. Hamachi, *Angew. Chem. Int. Ed. Engl.*, 2006, **45**, 5518-21.

Open Access Article. Published on 10 June 2026. Downloaded on 6/10/2026 10:50:53 PM.
This article is licensed under a Creative Commons Attribution 3.0 Unported Licence.

Sensors & Diagnostics Accepted Manuscript

View Article Online
DOI: 10.1039/D5SD00010J

154. A. Ojida, I. Takashima, T. Kohira, H. Nonaka and I. Hamachi, *J. Am. Chem. Soc.*, 2008, **130**, 12095–12101.

155. Z. Zhu, L. Xu, H. Li, X. Zhou, J. Qina and C. Yang, *Chem. Commun.*, 2014, **50**, 7060-7062.

156. K. A. Jolliffe, *Acc. Chem. Res.*, 2017, **50**, 2254–2263.

157. J. R. Lin, C. J. Chu, P. Venkatesan and S. P. Wu, *Sens. Actuators B*, 2015, **207**, 563–570.

158. S. Yang, W. Feng and G. Feng, *Anal. Chim. Acta*, 2018, **1034**, 119-127.

159. C. M. López-Alled, S. J. Park, D. J. Lee, L. C. Murfin, G. Kociok-Köhn, J. L. Hann, J. Wenk, T. D. James, H. M. Kim and S. E. Lewis, *Chem. Commun.*, 2021, **57**, 10608-10611.

160. Q. Xu, X. Wang, G. Xing and Y. Zhang, *RSC Adv.*, 2013, **3**, 15834-15841.

161. Y. Suzuki, M. Masuko, T. Hashimoto and T. Hayashita, *New J. Chem.*, 2023, **47**, 7035-7040.

162. X. Peng, Y. Xu, S. Sun, Y. Wua and J. Fan, *Org. Biomol. Chem.*, 2007, **5**, 226–228.

163. R. R. Zhao, Q. L. Xu, Y. Yang, J. Cao, Y. Zhou, R. Xu and J. F. Zhang, *Tetrahedron Lett.*, 2016, **57**, 5022-5025.

164. A. K. Purohit, H. K. Kisan, S. Sahu and P. K. Kar, *J. Mol. Struct.*, 2021, **1243**, 130868.

165. P. Das, A. Ghosh, M. K. Kesharwani, V. Ramu, B. Ganguly and A. Das, *Eur. J. Inorg. Chem.*, 2011, **2011,** 3050-3058.

166. M. Liu, X. Zhang, L. Wang, W. Sun, Z. Xie and J. Wang, *J. Mol. Struct.*, 2024, **1303**, 137558.

167. D. Chao and S. Ni, S*ci. Rep.*, 2016, **6**, 26477.

168. T. W. Hsu, H. C. Hsu, H. Y. Chan and J. M. Fang, *J. Org. Chem.*, 2020, **85**, 12747–12753.

169. J. Harathi, R. Selva Kumar, S. K. Ashok Kumar, D. Saravanakumar, S. Senthilkumar and K. Thenmozhi, *Sens. Actuators B Chem.*, 2023, **390**, 133967.

170. W. Fang, C. Liu, F. Yu, Y. Liu, Z. Li, L. Chen, X. Bao and T. Tu, *ACS Appl. Mater. Interfaces*, 2016, **8**, 20583–20590.

171. L. Shi, P. Hu, Y. Rena and G. Feng, *Chem. Commun.*, 2013, **49**, 11704 -11706.

172. P. Hu, S. Yanga and G. Feng, *Org. Biomol. Chem.*, 2014, **12**, 3701-3706.

173. X. H. Huang, Y. Lu, Y. B. He and Z. H. Chen, *Eur. J. Org. Chem.*, 2010, **2010**, 1921–1927.

174. Y. Mikata, A. Ugai, R. Ohnishi and H. Konno, *Inorg. Chem.*, 2013, **52**, 10223–10225.

Open Access Article. Published on 10 June 2026. Downloaded on 6/10/2026 10:50:53 PM.
This article is licensed under a Creative Commons Attribution 3.0 Unported Licence.

Sensors & Diagnostics Accepted Manuscript

View Article Online
DOI: 10.1039/D6SD00010J

175. Y. Mikata, R. Ohnishi, R. Nishijima and H. Konno, *Inorg. Chem.*, 2016, **55**, 11440–11446.

176. L. M. Mesquita, V. André, C. V. Esteves, T. Palmeira, M. N. Berberan-Santos, P. Mateus, and R. Delgado, Inorg. Chem., 2016, **55**, 2212–2219.

177. H. Song and Z. Zhang, *Dyes Pigm.*, 2019, **165**, 172-181.

178. S. Saravana Kumar, R. Selva Kumar and S.K. Ashok Kumar, *Inorg. Chim. Acta*, 2020, **502**, 119348.

179. M. Pushina, S. Farshbaf, W. Mochida, M. Kanakubo, R. Nishiyabu, Y. Kubo and P. Anzenbacher, *Chem. Eur. J.*, 2021, **27**, 11344-11351.

180. R. V. Velázquez-Castillo, M. K. Salomón-Flores, A. O. Viviano-Posadas, I. J. Bazany-Rodríguez, C. Bustos-Brito, J. M. Bautista-Renedo, N. González-Rivas, L. D. Rosales-Vázquez and A. Dorazco-González, *Dyes Pigm.*, 2021, **196**, 109827.

181. K. Du, S. Niu, L. Qiao, Y. Dou, Q. Zhu, X. Chen and P. Zhang, *RSC Adv.*, 2017, **7**, 40615-40620.

182. O. G. Tsay, S. T. Manjare, H. Kim, K. M. Lee, Y. S. Lee and D. G. Churchill, *Inorg. Chem.*, 2013, **52**, 10052−10061.

183. S. J. Butler, *Chem. Eur. J.*, 2014, **20**, 15768 – 15774.

184. A. K. Mahapatra, S. K. Manna, C. D. Mukhopadhyay and D. Mandal, *Sens. Actuators B Chem.*, 2014, **200**, 123–131.

185. J. Wen, Z. Geng, Y. Yin, Z. Zhang and Z. Wang, *Dalton Trans.*, 2011, **40**, 1984–1989.

186. P. Mahato, A. Ghosh, S. K. Mishra, A. Shrivastav, S. Mishra and A. Das, *Inorg. Chem.*, 2011, **50**, 4162–4170.

187.P. Mahato, A. Ghosh, S. K. Mishra, A. Shrivastav, S. Mishra and A. Das, *Chem. Commun.*, 2010, **46**, 9134–9136.

188. M. An, B. Y. Kim, H. Seo, A. Helal and H. S. Kim, Spectrochim Acta A Mol Biomol Spectrosc., 2016, **169**, 87–94.

189. B. B. Shi, Y. M. Zhang, T. B. Wei, Q. Lin, H. Yao, P. Zhang and X. M. You, *Sens. Actuators B Chem.*, 2014, **190**, 555-561.

190. D. Bansala and R. Gupta, *Dalton Trans.*, 2019, **48**, 14737-14747.

191. J. Oh and J. I. Hong, *J. Org. Chem.*, 2019, **84**, 15797–15804.

192. S. Yang, G. Feng and N. H. Williams, *Org. Biomol. Chem.*, 2012, **10**, 5606-5612.

193. D. A. Jose, S. Mishra, A. Ghosh, A. Shrivastav, S. K. Mishra and A. Das, *Org. Lett.*, 2007 **9**, 1979–1982.

194. Z. Li, W. Zhang, X. Liu, C. Liu, M. Yu and L. Wei, *RSC Adv.*, 2015, **5**, 25229-25235.

Open Access Article. Published on 10 June 2026. Downloaded on 6/10/2026 10:50:53 PM.
This article is licensed under a Creative Commons Attribution 3.0 Unported Licence.

Sensors & Diagnostics Accepted Manuscript

View Article Online
DOI: 10.1039/D6SD00010J

195. M. Shellaiah, N. Thirumalaivasan, B. Aazaad, K. Awasthi, K. W. Sun, S. P. Wu, M. C. Lin and N. Ohta, *Chemosensors*, 2022, **10**, 381.

196. Y. Chen, F. Zhao, J. Tian, L. Jiang, K. Lu, Y. Jiang, H. Li, S. Yu, X. Yu and L. Pu, *J. Org. Chem.*, 2021, **86**, 9603−9609.

197. F. Zhao, Y. Du, J. Tian, D. Shi, Y. Wang, L. Hu, S. Yu, X. Yu and L. Pu, *Eur. J. Org. Chem.*, 2018, **2018**, 1891-1895.

198. Y. Y. Zhu, X. D. Wu, S. X. Gu and L. Pu, *J. Am. Chem. Soc.*, 2019, **141**, 175–181.

199. J. Du, Z. Huang, X. Q. Yu and L. Pu, *Chem. Commun.*, 2013, **49**, 5399-5401.

200. Q. Y. Yu, C. W. Wei, X. J. Wang, S. Q. Gao, X. Y. Tong and Y. W. Lin, *J. Biol. Inorg. Chem.*, 2023, **28**, 205–211.

201. M. Strianese, D. Guarnieri, M. Lamberti, A. Landi, A. Peluso and C. Pellecchia, *Inorg. Chem.*, 2020, **59**, 15977–15986.

202. P. Liu, X. F. Han, W. N. Wu, Y. Wang, Y. C. Fan, X. L. Zhao and Z. H. Xu, *J. Mol. Struct.*, 2022, **1249**, 131629.

203. J. Y. Yun, J. B. Chae, M. Kim, M. H. Lim and C. Kim, *Photochem. Photobiol. Sci.*, 2019, **18**, 166–176.

204. H. Fu, H. Liu, L. Zhao, B. Xiao, T. Fan and Y. Jiang, *Tetrahedron*, 2019, **75**, 130710.

205. J. M. Jung, J. J. Lee, E. Nam, M. H. Lim, C. Kim and R. G. Harrison, *Spectrochim Acta A Mol. Biomol. Spectrosc.*, 2017, **178**, 203–211.

206. D. Yun, J. B. Chae, H. So, H. Lee, K. T. Kim and C. Kim, *New J. Chem.*, 2020, **44**, 442-449.

207. S. M. Hwang, D. Yun, H. Lee, M. Kim, M. H. Lim, K. T. Kim and C. Kim, *Dyes Pigm.*, 2019, **165**, 264-272.

208. H. Liu, Y. Tan, Q. Dai, H. Liang, J. Song, J. Qu and W. Y. Wong, *Dyes Pigm.*, 2018, **158**, 312-318.

209. M. Strianese, S. Brenna, G. A. Ardizzoia, D. Guarnieri, M. Lamberti, I. D'Auria and C. Pellecchia, *Dalton Trans.*, 2021, **50**, 17075–17085.

210. R. Kaushik, P. Kumar, A. Ghosh, N. Gupta, D. Kaur, S. Arorac and D. A. Jose, *RSC Adv.*, 2015, **5**, 79309-79316.

211. Z. Liu, C. Peng, Y. Wang, M. Peia and G. Zhang, *Org. Biomol. Chem.*, 2016, **14**, 4260-4266.

212. J. Mou, H. Qi, R. Xiang, S. Xu, J. Liu, S. Meng, N. Chen, Y. Xue and D. Pei, *New J. Chem.*, 2021, **45**, 2958-2966.

213. G. D. Luker and K. E. Luker, *J. Nucl. Med.*, 2008, **49**, 1–4.

Open Access Article. Published on 10 June 2026. Downloaded on 6/10/2026 10:50:53 PM.
This article is licensed under a Creative Commons Attribution 3.0 Unported Licence.

Sensors & Diagnostics Accepted Manuscript

View Article Online
DOI: 10.1039/D6SD00010J

214. A. Refaat, M. L. Yap, G. Pietersz, A. P. G. Walsh, J. Zeller, B. del Rosal, X. Wang and K. Pete, *J. Nanobiotechnol.*, 2022, **20**, 450.

215. Q. S. Gu, T. Li, T. Liu, G. Yu, G. J. Mao, F. Xu and C. Y. Li, *Chemosensors*, 2023, **11**, 417.

216. M. J. Hou, J. T. Chen, W. L. Jiang, G. F. Zeng, J. Zhan, G. J. Mao and C. Y. Li, *Sens. Actuators B Chem.*, 2022, **369**, 132286.

217. Z. Zhang, P. Chen and Y. Sun, *Molecules*, 2023, **28**, 5360.

218. F. Lv, B. Cao, Y. Cui and T. Liu, *Molecules*, 2012, **17**, 6348-6361.

219. Z. Chen, X. Mu, Z. Han, S. Yang, C. Zhang, Z. Guo, Y. Bai and W. He, *J. Am. Chem. Soc.*, 2019, **141**, 17973–17977.

220. Y. Shi, F. Huo, Y. Yue and C. Yin, *Front. Chem. Sci. Eng.*, 2022, **16**, 64–71.

Open Access Article. Published on 10 June 2026. Downloaded on 6/10/2026 10:50:53 PM.
This article is licensed under a Creative Commons Attribution 3.0 Unported Licence.

Sensors & Diagnostics Accepted Manuscript

Data Availability Statement

View Article Online
DOI: 10.1039/D6SD00010J

No Data Collected or Analyzed.

Open Access Article. Published on 10 June 2026. Downloaded on 6/10/2026 10:50:53 PM.
This article is licensed under a Creative Commons Attribution 3.0 Unported Licence.

Sensors & Diagnostics Accepted Manuscript